VAPOR PHASE HOMOGENEOUS NUCLEATION AND THE THERMODYNAMIC PROPERTIES OF SMALL CLUSTERS OF ARGON ATOMS

Thesis by

David Jackson McGinty

In Partial Fulfillment of the Requirements

For the Degree of

Doctor of Philosophy

California Institute of Technology

Pasadena, California

1972

(Submitted March 9, 1972)

To Sally

and

My Parents

ACKNOWLEDGEMENTS

I have been very fortunate in having received help from numerous individuals during my tenure at Caltech. I am especially grateful to Professor G. Wilse Robinson, who provided advice, support, and inspiration without which this work would not have been completed. I am indebted to Dr. Robert P. Futrelle for invaluable help at all stages of the project and to Dr. Paul L. Fehder for suggesting the study of nucleation and helping me to get started in my research. I thank Mrs. Adria Larson for typing this thesis and, more generally, for being a great secretary. Most of all, I am grateful to my wife, Sally, who has been extremely patient and unselfish during the past five years.

ABSTRACT

Two methods have been developed for calculating the thermodynamic properties of the small clusters of atoms believed important in the phenomenon of vapor phase homogeneous nucleation. Clusters of up to 100 argon atoms have been considered. The interactions among atoms are represented by the Lennard-Jones pairwise additive potential function and all degrees of freedom are explicitly included.

In the first method, the microcrystal model is used and the independent-cluster partition function is evaluated in the same way as one would evaluate that for a polyatomic molecule in the simplest approximation: the harmonic, rigid-rotator, and perfect-gas approximations are used to calculate the vibrational, rotational, and translational contributions to the partition function. The steady-state rate of formation of nuclei as a function of degree of supersaturation has been calculated and is found to have a behavior similar to that expected from the classical, "liquid-drop" model.

The importance of using several stable configurations of a cluster in calculating its properties from the microcrystal model is examined in detail. It is shown that the single-configuration approximation that has been used extensively in recent work can lead to serious errors. Methods for selecting configurations that will minimize these errors are suggested.

In the second method, molecular dynamics computer simulation calculations are used. In these calculations the classical equations of motion for the atoms in a cluster are numerically integrated to yield time records of the atomic position and velocity coordinates. Values

of the independent-cluster thermodynamic functions are calculated from these coordinate data and are compared with those obtained from the microcrystal model. The comparison indicates surprising agreement for values of the Gibbs free energy of formation. The transition between "solid-like" and "fluid-like" diffusion in the clusters occurs gradually; no semblance of a phase transition is noted. The radial variation of density indicates that nearly all the atoms of a cluster exist in the "surface" region; the radial distribution of potential energy indicates that the environment inside the clusters is quite different from that inside the bulk liquid or solid phases.

The largest error in the molecular dynamics results is statistical error in the temperature. An expression for this error has been derived in terms of the kinetic-energy autocorrelation function. We have shown that this and other correlation functions can be computed from the molecular dynamics data very rapidly using a method based on the Fast Fourier Transform.

Finally, several very fundamental problems have been discovered in the classical, liquid-drop theory of nucleation. These problems are discussed in the context of a rigorous approach to nucleation theory that is based on the Frenkel-Band theory of noninteracting physical clusters.

TABLE OF CONTENTS

not included.

PART I: THE THEORY OF VAPOR PHASE HOMOGENEOUS NUCLEATION

A. Introduction

It is well known that a pure supersaturated vapor can exist in a metastable state. If the degree of supersaturation is not too high, the lifetime of the metastable state will be quite long and the vapor will appear stable. As one increases the level of supersaturation of the vapor, the lifetime of the metastable state decreases and the vapor eventually condenses. The point at which condensation occurs is a reproducible characteristic of the vapor and is referred to as the "critical" level of supersaturation. Nucleation experiments are generally designed to measure this critical supersaturation over a range of temperatures; nucleation theory attempts to predict the critical supersaturation and, more generally, to understand the details of the nucleation process.

In this part of the thesis a general overview of nucleation theory will be presented. We begin in Section B with a purely thermodynamic explanation for the metastability of supersaturated vapors, which is due originally to Gibbs.[1] The explanation is of great conceptual value but it does not lead to a quantitatively significant understanding of nucleation. In particular, it does not enable one to calculate the critical supersaturation level of a vapor.

In order to calculate this quantity and to obtain a more detailed understanding of nucleation, it is necessary to consider the kinetics of the interactions among "clusters" of molecules in the vapor. In the kinetic theory of nucleation, described in Section C, a supersaturated vapor is treated as a gaseous mixture of clusters and the time dependence of the cluster concentrations is determined using the methods of

chemical kinetics. Solution of the rate equations that describe the nucleation process requires that one know the critical concentrations of the clusters in the supersaturated vapor. The calculation of these concentrations is a problem in equilibrium thermodynamics or statistical mechanics, and it has proved to be the most difficult aspect of the theory.

Two general approaches to the calculation have been developed. The classical approach uses the Gibbs surface theory[1] to evaluate the "liquid-drop" model for clusters and to determine their thermodynamic properties. The classical approach is discussed in some detail in Sections D and E. Section D contains a brief outline of pertinent aspects of the surface theory and in Section E the classical evaluation of the liquid-drop model is followed. The purpose of these two sections is to show exactly how the classical expression for the standard Gibbs free energy of formation of a cluster is derived. The derivation is periodically interrupted by "NOTE's" in which the approximations and assumptions involved in the derivation are discussed. These annotations may appear somewhat laborious but it is the feeling of the author that the significance and even the existence of the approximations and assumptions are not generally realized by many of those working in the field. As a consequence, much of the theory that appears in the literature is either ambiguous and confusing or just plain incorrect. In addition to difficulties with the classical derivation that are easily corrected, we find a number of very fundamental problems with the liquid-drop model that we believe cannot be rectified.

The second approach to the calculation of cluster concentrations is based on the statistical mechanical theory of physical clusters. In

Section F we present a rigorous development of that theory and use it as a basis for a new, descriptive approach to nucleation. The approach enables us to determine just what is involved, on the molecular level, when a nucleus is formed in a supersaturated vapor. Numerical evaluation of cluster concentrations from physical cluster theory requires computation of the "independent-cluster partition functions," which has only recently been made practical by the availability of high-speed computers. Development of methods for accomplishing this computation is the object of most of the research reported in Parts II and III of this thesis.

B. A Phenomenological Approach to Nucleation

Why does a supersaturated vapor not condense? The reason is that the vapor is supersaturated with respect to bulk liquid with a planar surface, but it is unsaturated with respect to the very small droplets that must be formed at the initial stages of the condensation process. The small droplets tend to evaporate rather than to grow into macroscopic drops.

The problem can be understood on a more quantitative basis if we consider an approximate calculation of the work required to form one of the small droplets in the vapor. According to an argument that will be examined in more detail later, this work can be approximated by the following expression,

$$W = n(\mu_\ell - \mu_v) + \sigma\, Bn^{2/3} \quad , \tag{1}$$

where n is the number of molecules in the droplet, μ_v is the chemical potential of the vapor, μ_ℓ is the chemical potential of bulk liquid at the

temperature and pressure of the vapor, σ is the surface tension, and B is a positive constant. The first term $n\Delta\mu$ in the expression is negative because the vapor is supersaturated and its chemical potential is higher than that of the bulk liquid; the second term is positive. A maximum therefore exists in the function as shown in Fig. 1.

The droplet whose work of formation is maximum is called the nucleus. It exists in unstable equilibrium with the vapor: droplets smaller than the nucleus tend thermodynamically to evaporate while those larger than the nucleus tend to grow. Formation of the nucleus is therefore regarded as the barrier to nucleation--if a nucleus is formed in the vapor, condensation is likely to follow.

Thermodynamically a supersaturated vapor will be metastable as long as the work of formation of the nucleus is positive. In practice, however, metastable states for which the barrier to nucleation is low are not observed since fluctuations carry the system over the barrier in a very short time. A purely thermodynamic theory is not, therefore, capable of predicting the observed critical supersaturation. A kinetic theory is required to accomplish this prediction.

C. The Kinetic Theory of Nucleation

In the kinetic theory one treats a supersaturated vapor as a gaseous mixture of clusters and uncombined molecules that interact according to a series of reactions resembling those for a chemical polymerization:

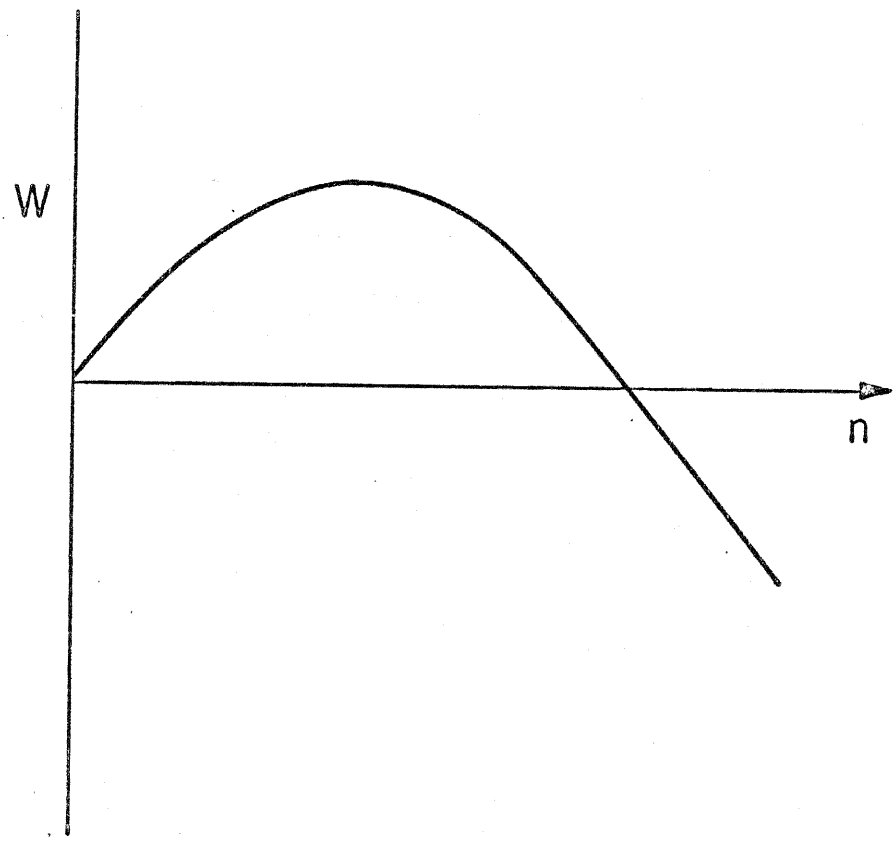

Figure 1. The work required to form a droplet in a supersaturated vapor as a function of the size of the droplet.

$$
\begin{aligned}
A_1 + A_1 &\underset{k_{-1}}{\overset{k_1}{\rightleftharpoons}} A_2 \\
A_2 + A_1 &\underset{k_{-2}}{\overset{k_2}{\rightleftharpoons}} A_3 \\
&\vdots \\
A_m + A_1 &\underset{k_{-m}}{\overset{k_m}{\rightleftharpoons}} A_{m+1} \\
&\vdots
\end{aligned}
\qquad (2)
$$

where A_m represents a cluster of m molecules. Reactions between "polymers" are generally ignored because collisions between them are relatively infrequent. For the series of reactions one can write a set of coupled differential rate equations that can, in principle, be solved for the time dependence of the cluster concentrations. The equations are as follows:

$$
\begin{aligned}
dC_2 &= k_1C_1^2 - k_{-1}C_2 - k_2C_1C_2 + k_{-2}C_3 , \\
dC_3 &= k_2C_1C_2 - k_{-2}C_3 - k_3C_1C_3 + k_{-3}C_4 , \\
&\vdots \\
dC_m &= k_{m-1}C_1C_{m-1} - k_{-(m-1)}C_m - k_mC_1C_m + k_{-m}C_{m+1} \\
&\vdots
\end{aligned}
\qquad (3)
$$

where C_m is the number of m-molecule clusters per unit volume.

To solve the equations, the following two sets of data are required:

1. The initial concentration of clusters, i.e., the concentrations in the equilibrium metastable state corresponding to the supersaturated vapor, and
2. the rate constants, k_1, k_{-1}, etc.

Estimation of the Rate Constants

Rate constants for the forward reactions are estimated by assuming that all collisions between a cluster and a monomer result in reaction (accommodation coefficient of unity). From the kinetic theory of gases, the rate of the reaction

$$A_n + A_1 \xrightarrow{k_n} A_{n+1} \tag{4}$$

is therefore simply[2]

$$\text{Forward rate} = k_n C_1 C_n = \left(\frac{8\pi kT}{\mu_n}\right)^{\frac{1}{2}} D_n^2 C_1 C_n \,. \tag{5}$$

Here μ_n is the reduced mass $m_1 m_n/(m_1 + m_n)$ and D_n is the collision diameter of the two particles. Thus

$$k_n = \left(\frac{8\pi kT}{\mu_n}\right)^{\frac{1}{2}} D_n^2 \,. \tag{6}$$

The reverse rate for the reaction is determined using the principle of detailed balance.[3] According to that principle the forward and reverse rates of each of the reactions in Eq. (3) are equal when the system is at equilibrium. If we denote equilibrium concentrations by a superscript "e", then

$$k_n C_n^e C_1^e = k_{-n} C_{n+1}^e \tag{7}$$

and

$$k_{-n} = k_n \frac{C_n^e C_1^e}{C_{n+1}^e} \quad . \tag{8}$$

The rate constants are therefore easily estimated in terms of the equilibrium concentrations C_n^e; and the only data that are actually needed for solution of the rate equations are these concentrations.

D. The Gibbs Surface Theory[1]

In discussing the surface theory we consider the system illustrated in Fig. 2 that contains two nearly homogeneous regions, one liquid (ℓ) and the other vapor (v), separated by a nonhomogeneous film (σ). To enable a precise treatment of the two-phase system, Gibbs divided the volume of the system by a geometrical dividing surface that passes through points within the nonhomogeneous film that have similar environments. The exact location of the surface is arbitrary. For a particular dividing surface the volume becomes

$$V = V_\ell + V_v \ , \tag{9}$$

where V_ℓ is the volume inside the surface and V_v is the remaining volume. The total number of molecules in the system is also divided, according to the expression

$$N = N_\ell + N_v + N_\sigma \ . \tag{10}$$

Here N_v is the number of atoms that would be in V_v if the density of the vapor were constant up to the dividing surface, N_ℓ is the number that would be in V_ℓ if that volume contained homogeneous liquid at the temperature and chemical potential of the vapor, and N_σ is essentially a correction factor to make the two sides of the equation equal. Similar

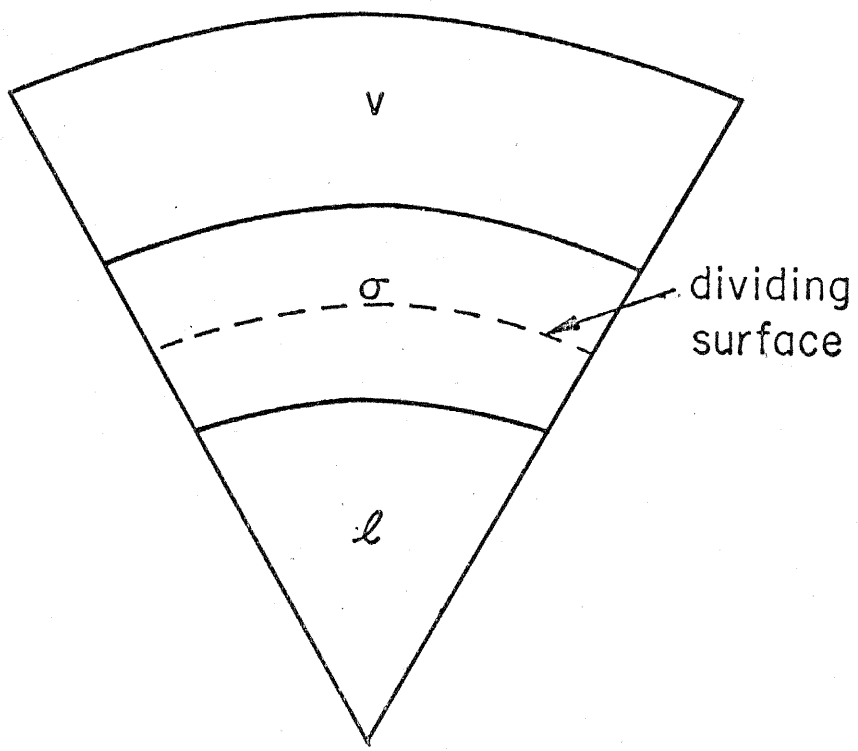

Figure 2. Section of a two-phase system that is partitioned by a dividing surface. The regions v and ℓ are homogeneous phases and the region σ includes the inhomogeneous transition region.

divisions are made for each of the other extensive variables: the energy becomes

$$E = E_\ell + E_V + E_\sigma \ , \tag{11}$$

and the entropy becomes

$$\mathcal{S} = \mathcal{S}_\ell + \mathcal{S}_V + \mathcal{S}_\sigma \ . \tag{12}$$

NOTE 1: The division of the extensive variables of the system is achieved on mathematical rather than physical grounds. A consequence of this abstract approach is that the surface theory is largely independent of a model for the two-phase system. The theory is therefore quite general, but it is incapable of providing information about the structure of the system.

According to Gibbs, the energy of an equilibrium state of the system is completely determined by the variables $\mathcal{S}$, N, V_ℓ, V_V, and the area S and the principal curvatures c_1 and c_2 of the dividing surface: the fundamental equation of the system is $E(\mathcal{S}, N, V_\ell, V_V, S, c_1, c_2)$. Again, according to Gibbs the dependence of E on c_1 and c_2 vanishes for a particular choice of the dividing surface, which we call the surface of tension. For this choice of the dividing surface the individual terms in Eq. (11) can be written as follows:

$$E_\sigma = T\mathcal{S}_\sigma + \mu N_\sigma + \sigma S \ , \tag{13}$$

$$E_\ell = T\mathcal{S}_\ell + \mu N_\ell - P_\ell V_\ell \ , \tag{14}$$

$$E_V = T\mathcal{S}_V + \mu N_V - P_V V_V \ . \tag{15}$$

Here σ is the surface tension, $\sigma = (\partial E/\partial S)_{\mathcal{S}, N, V_\ell, V_V, c_1, c_2}$, T is the temperature, μ the chemical potential, P_ℓ the pressure of bulk liquid at temperature T and chemical potential μ, and P_V is the pressure of the vapor.

NOTE 2: For surfaces with radii of curvature that are large compared with the thickness of the nonhomogeneous surface film, Gibbs argues that the surface of tension lies within the nonhomogeneous film (Ref. 1, pp. 225-228). This argument establishes an important connection between the abstractly defined variables of the surface theory and the physical structure of the system. Gibbs notes, however, that the argument does not apply to surfaces of very high curvature such as those of the microscopic droplets important in nucleation (Ref. 1, pp. 253-255). For these droplets the position of the surface of tension cannot be located with respect to the physical inhomogeneity by purely thermodynamic means. Thus, the surface of tension might be located outside the nonhomogeneous film. Connection between the abstract variables and the physical structure is not, therefore, established for the small droplets. Indeed, Gibbs notes that, "vanishing of the radius of the somewhat arbitrarily determined dividing surface [surface of tension] may not necessarily involve the vanishing of the physical heterogeneity" (Ref. 1, p. 255).

It is now possible to compute the work of formation of a liquid drop in a supersaturated vapor. The Helmholtz free energy of the initial state (pure vapor) is

$$F^i = N\mu_v^o - P_v^o V \,. \tag{16}$$

The free energy of the final state, which contains a liquid drop in equilibrium with ambient vapor, is

$$\begin{aligned} F^f &= F_\ell^f + F_v^f + F_\sigma^f \\ &= N_\ell \mu_\ell - P_\ell V_\ell + N_v \mu_v - P_v V_v + N_\sigma \mu_\sigma + \sigma S \,. \end{aligned} \tag{17}$$

We now assume that the volume is large enough so that the pressure and chemical potential of the vapor remain approximately constant during the process, i.e.,

$$P_v = P_v^o \,, \tag{18a}$$

and

$$\mu_v = \mu_v^o \quad ; \tag{18b}$$

and we note that since the final state is at equilibrium,

$$\mu_\ell = \mu_v = \mu_\sigma \,. \tag{19}$$

The change in free energy, which is the work required to form the drop, is then

$$\Delta F = W = -V_\ell (P_\ell - P_v) + \sigma S \ , \tag{20}$$

which can be simplified using the Kelvin equation, $P_\ell - P_v = 2\sigma/R$, to yield

$$\Delta F = W = \frac{1}{3}\sigma S \ . \tag{21}$$

NOTE 3: The effect of the assumptions $P_v = P_v^o$ and $\mu_v = \mu_v^o$ should be examined. The changes that actually occur in the pressure and chemical potential are most certainly small, but then so is the free energy change that we are calculating! We can estimate the effect by treating the vapor as an ideal gas of pure monomers and assume that the drop corresponds to a cluster of n molecules. Then the number of particles in the vapor decreases from N to N-n when the drop is formed and the volume available to the vapor changes from V to $(V - V_\ell)$. The change in pressure is then

$$\Delta P = (P_v - P_v^o) = -nkT/V + P_v V_\ell / V \ ; \tag{22}$$

and the change in chemical potential is

$$\Delta\mu = (\mu_v - \mu_v^o) = -nkT/N + kTV_\ell / V \ , \tag{23}$$

where the relation

$$\mu_v(T, P) = \mu_o(T) + kT \ln P \tag{24}$$

for an ideal gas has been used. If the above corrections in P_v and μ_v are included in the derivation of ΔF, one finds that the effects due to ΔP and $\Delta\mu$ exactly cancel, yielding the same result as with the approximations in Eq. (18).

E. The Liquid-Drop Model

The equilibrium cluster concentrations in a supersaturated vapor can be determined from the Gibbs free energy of formation of the clusters. We consider the reaction

$$nA_1 \rightleftharpoons A_n \ , \tag{25}$$

and note that if the clusters are treated as perfect gas particles, the change in free energy for the reaction is

$$\Delta G_n(T, P, X_1, X_n) = \Delta G_n^{\dagger}(T, P) + kT \ln [X_n/X_1^n] , \tag{26}$$

where X_n is a mole fraction and P is the total pressure of the vapor. At equilibrium $\Delta G_n = 0$ and

$$X_n = X_1^n \exp[-\Delta G_n^{\dagger}(T, P)/kT] . \tag{27}$$

In the liquid-drop approach the result for ΔF in Eq. (20) that was determined from the Gibbs surface theory is used to evaluate $\Delta G_n^{\dagger}$. The classical derivation is traced in the next few paragraphs.

STEP 1: The familiar expression $(\partial \mu_\ell / \partial P)_T = v_\ell$, where μ_ℓ is the chemical potential and v_ℓ is the volume per molecule of bulk liquid, can be integrated between P_v and P_ℓ to yield

$$\mu_\ell(T, P_\ell) - \mu_\ell(T, P_v) = v_\ell(P_\ell - P_v). \tag{28}$$

In performing this integration the liquid is assumed incompressible.

STEP 2: As a consequence of Eq. (19), $\mu_\ell(T, P_\ell) = \mu_v(T, P_v)$ and Eq. (27) becomes

$$\mu_v(T, P_v) - \mu_\ell(T, P_v) = v_\ell(P_\ell - P_v) . \tag{29}$$

STEP 3: According to the definition of N_ℓ in Section C,

$$V_\ell = N_\ell v_\ell , \tag{30}$$

where v_ℓ is the molecular volume of bulk liquid at the temperature and chemical potential of the vapor.

STEP 4: Substitution into Eq. (20) leads to the following expression:

$$\Delta F = N_\ell [\mu_\ell(T, P_v) - \mu_v(T, P_v)] + BN_\ell^{2/3}\sigma, \tag{31}$$

where $B = (36\, v_\ell^2\, \pi)^{1/3}$.

STEP 5: To evaluate the difference $\mu_\ell(T, P_v) - \mu_v(T, P_v)$ in Eq. (31), we consider the cyclic operation illustrated in Fig. 3. Along the path I → II → III, the liquid is isothermally expanded to the equilibrium vapor pressure P_e, the liquid is then converted to vapor at that pressure, and finally the vapor is isothermally compressed to the original pressure P_v. The change in chemical potential for each process is as follows:

$$\Delta\mu_I = v_\ell(P_e - P_v) \tag{32}$$

$$\Delta\mu_{II} = 0 \tag{33}$$

$$\Delta\mu_{III} = kT\, \ell n\,(P_v/P_e). \tag{34}$$

The term $\Delta\mu_I$ is generally ignored because it is much smaller in magnitude than $\Delta\mu_{III}$, leading to

$$\Delta\mu_{IV} = -[\mu_\ell(T, P_v) - \mu_v(T, P_v)] = kT\, \ell n(P_v/P_e). \tag{35}$$

Substitution into Eq. (30) yields

$$\Delta F = -N_\ell kT\, \ell n\,(P_v/P_e) + BN_\ell^{2/3}\sigma\,. \tag{36}$$

STEP 6: Under the assumption that $P_v = P_v^o$ in Eq. (18),

$$\Delta(PV) = 0, \tag{37}$$

and

$$\Delta G = \Delta F\,, \tag{38}$$

for the formation of a nucleus.

NOTE 4: In NOTE 3 we found that in the approximation that the vapor can be treated as a perfect gas of monomers, the effect on ΔF of changes in pressure and chemical potential cancel. We now use the same approximation to estimate the actual change $\Delta(PV)$ and hence the validity of Eq. (38). By the same reasoning used in NOTE 3, we find that

$$\Delta(PV) = \Delta G - \Delta F = -nkT. \tag{39}$$

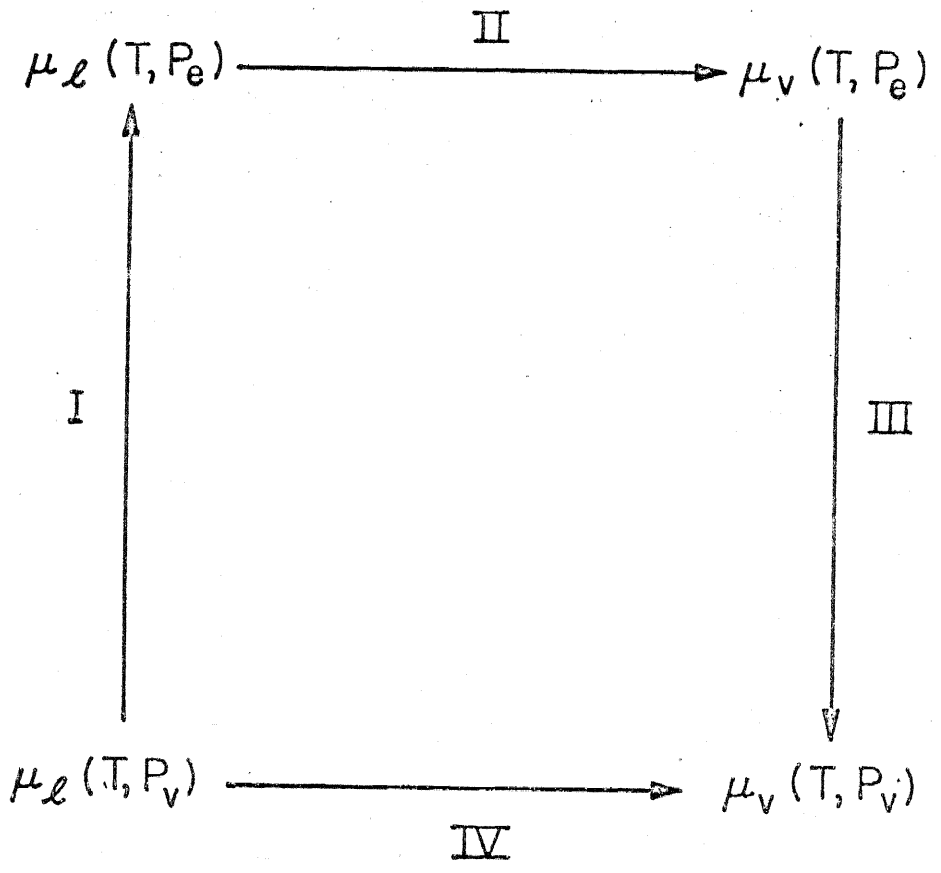

Figure 3. Thermodynamic cycle used in the classical evaluation of the liquid-drop model.

This difference is of the same order of magnitude as the total kinetic energy of the molecules in the nucleus, which is (3/2)nkT. Clearly Eq. (38) is not very good and a more exact derivation than the classical one would include the effect of the change $\Delta(PV)$.

STEP 7: We next assume that N_ℓ equals the number of molecules $\underline{n}$ in the cluster that corresponds to the drop,

$$n = N_\ell \, . \tag{40}$$

Equation (33) then becomes

$$\Delta G = -nkT \, \ell n \, (P_v/P_e) + Bn^{2/3}\sigma \, . \tag{41}$$

NOTE 5: As discussed earlier (NOTES 1 and 2), the variable N_ℓ is an abstract quantity. It is not the number of molecules that actually exist inside the volume V_ℓ, it is the number that would exist there if the volume contained homogeneous liquid at the temperature and chemical potential of the ambient vapor. Furthermore, the volume V_ℓ is not necessarily related to that of the physical inhomogeneity. The variable $\underline{n}$, therefore, has no physical significance and, in particular, it is not equal to the size of the cluster that most nearly corresponds to the drop.

The error associated with Eq. (40) is quite fundamental. It results from the fact that Gibbs did not base his surface theory on a physical model. Consequently, there is no purely thermodynamic way to get molecular level information, such as the average number of molecules inside V_ℓ, from the theory.

STEP 8: In the final step it is assumed that the reaction by which the nucleus is formed in a vapor is that of Eq. (25). Thus ΔG in Eq. (41) refers to the change in free energy for that reaction. In the classical derivation ΔG is incorrectly equated to the standard change in free energy for the reaction, $\Delta G_n^\dagger$ in Eq. (26). Thus

$$\Delta G_n^\dagger (T, P_v) = \Delta G \tag{42}$$

and

$$\Delta G_n^\dagger (T, P_v) = -nkT \, \ell n(P_v/P_e) + Bn^{2/3}\sigma \, . \tag{43}$$

NOTE 6: Under the assumption made in STEP 8 that the formation of a nucleus in a supersaturated vapor corresponds to the reaction $nA_1 \rightarrow A_n$, ΔG in Eq. (41) equals the change in free energy for that reaction, which is ΔG_n, not $\Delta G_n^\dagger$ as assumed in Eq. (42). Thus the correct

expression is

$$\Delta G_n = -nkT \ln (P_v/P_e) + Bn^{2/3}\sigma. \qquad (44)$$

But $\Delta G_n = \Delta G_n^\dagger + kT \ln [X_n/X_1^n]$; and for the formation of a nucleus, $X_n = 1/N$ and $X_1 = n_1/N \sim 1$. Thus $\Delta G_n^\dagger$ can be evaluated from Eq. (44) to be

$$\Delta G_n^\dagger = -nkT \ln(P_v/P_e) + Bn^{2/3}\sigma + kT \ln N. \qquad (45)$$

NOTE 7: The assumption that the process by which a nucleus is formed in the supersaturated vapor is represented by the reaction $nA_1 \rightarrow A_n$ is quite fundamental to the liquid-drop approach. This assumption, which we do not consider justified, is discussed in some detail at the end of the next section.

NOTE 8: As noted by Long, [4] any derivation of $\Delta G_n^\dagger$ based on the liquid-drop model is valid only for the nucleus. This n cluster is the only one to which the basic expression $\Delta F = 1/3\ \sigma A$ applies.

NOTE 9: A practical problem associated with the liquid-drop model is that the surface tension is not known for other than plane surfaces. The problem was recognized by Gibbs who states, "the fundamental equation of a surface of discontinuity can hardly be regarded as capable of experimental determination, except for plane surfaces" (Ref. 1, p. 257). When the classical formula for $\Delta G_n^\dagger$ in Eq. (43) is actually evaluated, values of the surface tension for plane surfaces are used and the dependence on droplet radius is ignored.

F. Rigorous Calculation of Cluster Concentrations

In this section a rigorous approach to the calculation of cluster concentrations in the equilibrium states of a system is presented. This approach is based on the Frenkel-Band theory of noninteracting physical clusters. [5] We show how the various equilibrium states can be identified and describe the nucleation process in terms of the motion of the system through these states. In particular, the process by which a nucleas is formed in a supersaturated vapor is expressed in a precise manner.

Definition of a Cluster

Consider a specific configuration of a system of N atoms in a volume V. If we regard pairs of molecules that are separated by less than some distance R_o, which is of the order of the range of intermolecular forces ($\sim 3\sigma$ for the Lennard-Jones potential), as "interacting pairs" and imagine them connected by bonds, then the configuration will appear divided into clusters of molecules that are bonded together.

Decomposition of the Partition Function

Each possible distribution of molecules among clusters is described by a value of the N-dimensional vector

$$\underset{\sim}{n} = (n_1, n_2, \ldots, n_N), \tag{46}$$

where n_i is an integer that denotes the number of i-molecule clusters in the distribution. Allowed values of $\underset{\sim}{n}$ are consistent with the equation

$$\sum_{i=1}^{N} i n_i = N . \tag{47}$$

The canonical ensemble partition function for the system of N atoms is

$$Q = \frac{1}{N!}\left(\frac{2\pi mkT}{h^2}\right)^{3N/2} \int_V \exp[-U(\underset{\sim}{r}_1, \ldots, \underset{\sim}{r}_N)/kT] d\underset{\sim}{r}_1 \ldots d\underset{\sim}{r}_N, \tag{48}$$

where U is the potential energy. The integral in Eq. (48) can be transformed into a sum of integrals each covering a region of configuration space that corresponds to a specific value of $\underset{\sim}{n}$. Q becomes a sum of "single-distribution partition functions:"

$$Q = \sum_{\{\underset{\sim}{n}\}} Q_{\underset{\sim}{n}} , \tag{49}$$

where $Q_{\underset{\sim}{n}}$ contains the contribution to Q from configurations consistent

with a specific value of $\underset{\sim}{n}$.

The probability of a given distribution $\underset{\sim}{n}$ is proportional to $Q_{\underset{\sim}{n}}$:

$$P_{\underset{\sim}{n}} = Q_{\underset{\sim}{n}} / Q. \tag{50}$$

The Independent-Cluster Approximation

The "independent-cluster" approximation enables us to write the single-distribution partition functions in Eq.(49) in a particularly simple form. The approximation has two parts:[6]

(1) The interactions between molecules in different clusters are ignored.

(2) "Cluster interference" is ignored. In $Q_{\underset{\sim}{n}}$, configurations in which clusters overlap are excluded because they are not consistent with the specific distribution $\underset{\sim}{n}$; in the approximate evaluation of $Q_{\underset{\sim}{n}}$, these configurations are included.

The approximation leads to the following simple expression for $Q_{\underset{\sim}{n}}$:

$$Q_{\underset{\sim}{n}} = \prod_{i=1}^{N} [q_i^{n_i}/n_i!], \tag{50}$$

where q_i is an "independent-cluster partition function,"

$$q_i = \frac{V}{i!}\left(\frac{2\pi\, mkT}{h^2}\right)^{3i/2} \int_{C_i} \exp[-U(\underset{\sim}{r}_{ij})/kT]\, d\underset{\sim}{r}_{ij}\,, \tag{51}$$

and $\underset{\sim}{r}_{ij}$ represents the set of relative position coordinates for the i atoms and $d\underset{\sim}{r}_{ij}$ is the product of their differential elements. The term C_i indicates that the integration spans all relative positions of the atoms that are consistent with their being in the same cluster. In Parts II and III methods for evaluating the q_i will be presented.

The Equilibrium States of the System

Equilibrium states of the system correspond to extrema of the function $Q_{\underset{\sim}{n}}$ vs. $\underset{\sim}{n}$: a stable state corresponds to an absolute maximum, a metastable state to a local maximum, and an unstable state to a minimum. The number of extrema that the function has depends on the temperature and density of the system. The number can be inferred from the behavior of the Gibbs free energy of formation $\Delta G_n^\dagger$ as a function of n.

Figures 4-6 show three shapes of the function $\Delta G_n^\dagger$ vs. n that are possible. Beneath each of these plots, the corresponding behavior expected of $Q_{\underset{\sim}{n}}$ vs. $\underset{\sim}{n}$ is schematically illustrated. The function is plotted along a "reaction coordinate" that traces the most probably path for the system between vapor-like states on the left and condensed states on the right. Position along the path is most simply indicated by the variable i(max), which is the size of the largest cluster in a distribution. i(max) increases from 1 to N along the path.

Figure 4 refers to low density and high temperature systems. $\Delta G_n^\dagger$ increases monotonically with n and the size of the largest clusters in $\underset{\sim}{n}_{eq}$ is microscopic. The distribution $\underset{\sim}{n}_{eq}$ corresponds to an unsaturated vapor; the vector has the following form

$$\underset{\sim}{n}_{eq} = \{n_1, n_2, \ldots, n_{i(max)}, 0, 0, \ldots\} . \qquad (52)$$

The population numbers decrease monotonically for $i \leq i(max)$, i.e., $n_1 > n_2 > \ldots > n_{i(max)}$, and they are zero for $i > i(max)$.

Figure 6 refers to high density and low temperature systems for which $\Delta G_n^\dagger$ decreases monotonically with n. The size of the largest

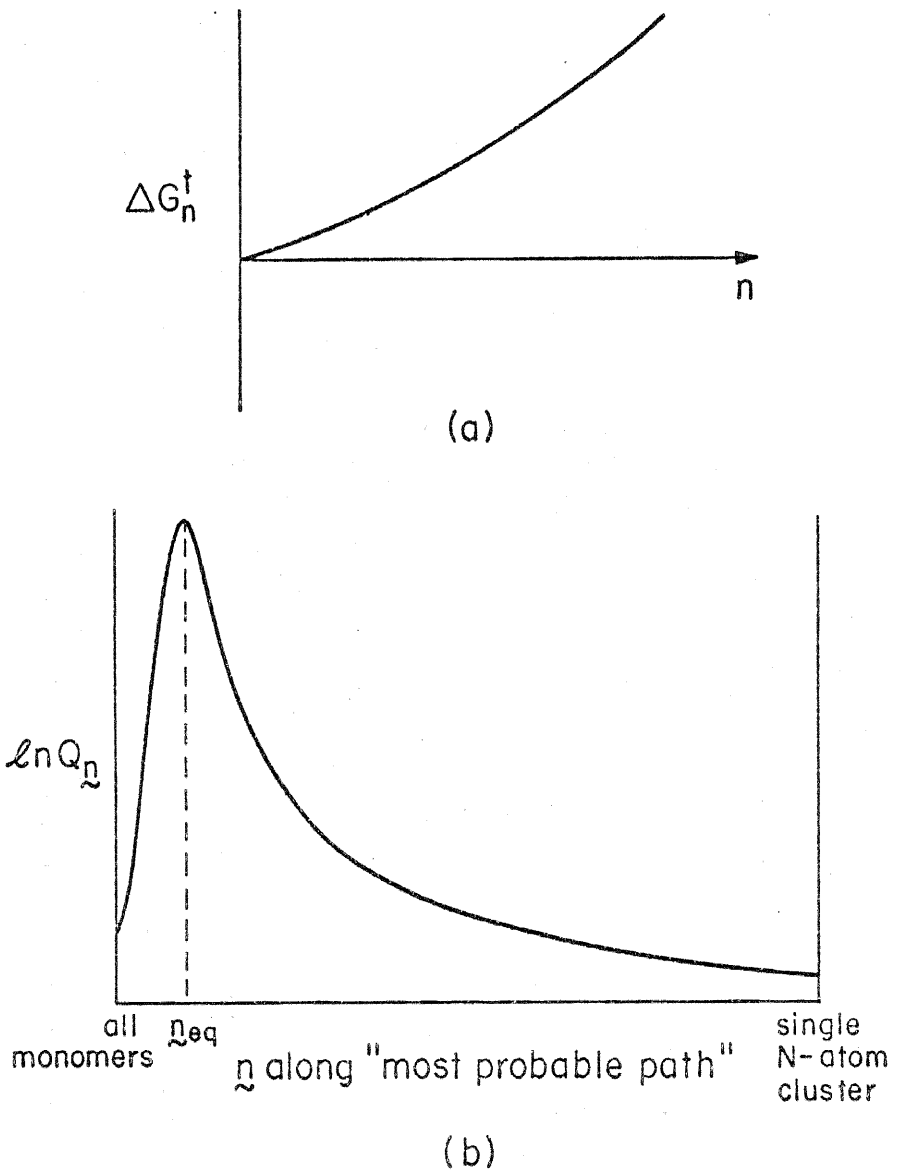

Figure 4: (a) The shape of the function $\Delta G_n^\dagger$ vs. n for a low density or high temperature system, and (b) the corresponding shape of the function $\ell n Q_{\hat{n}}$ vs. $\hat{n}$ along the "most probable path." The value of i(max) increases monotonically along this path as larger and larger clusters appear in the distributions. Both illustrations are highly schematic.

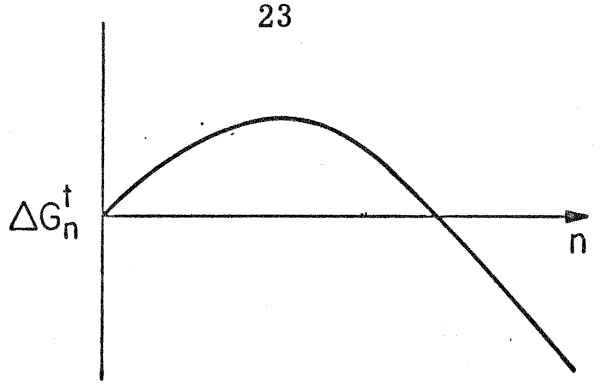

(a)

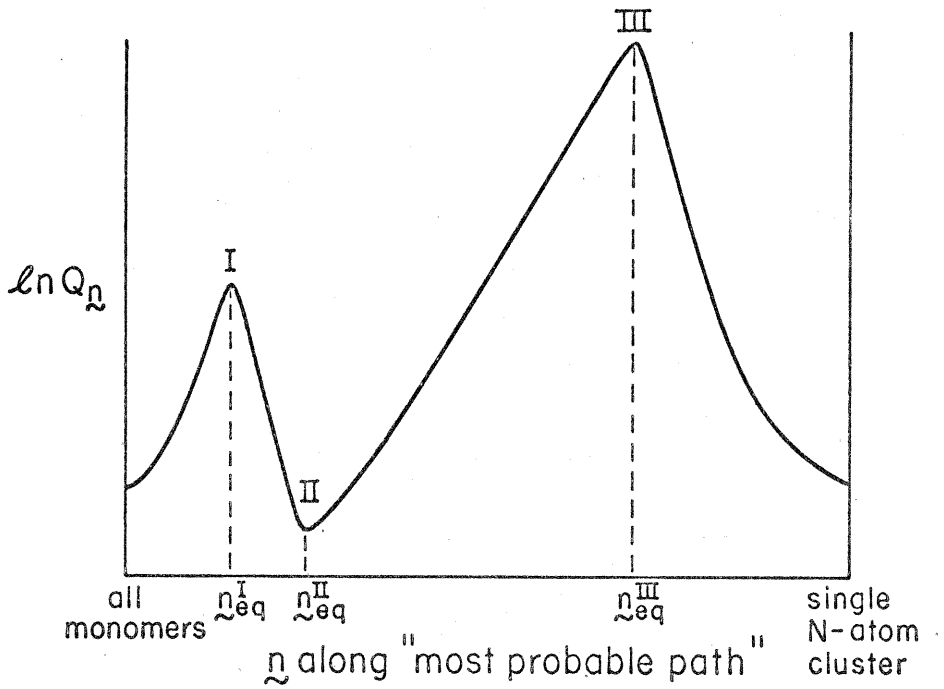

(b)

Figure 5: (a) The shape of $\Delta G_n^\dagger$ vs. n for a system in which the density and temperature are such that s metastable supersaturated vapor can exist, and (b) the corresponding shape of the function $\ell n\, Q_{\hat{n}}$ vs. $\hat{n}$ along the "most probable path." Both illustrations are highly schematic.

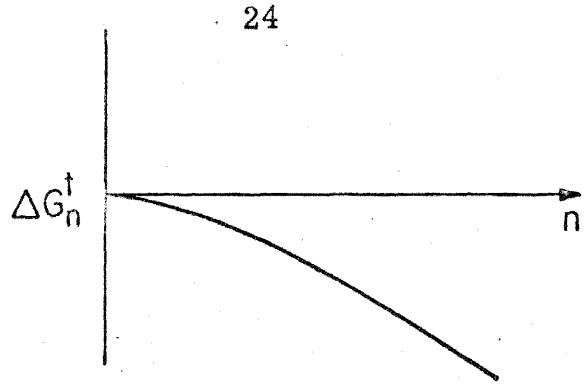

(a)

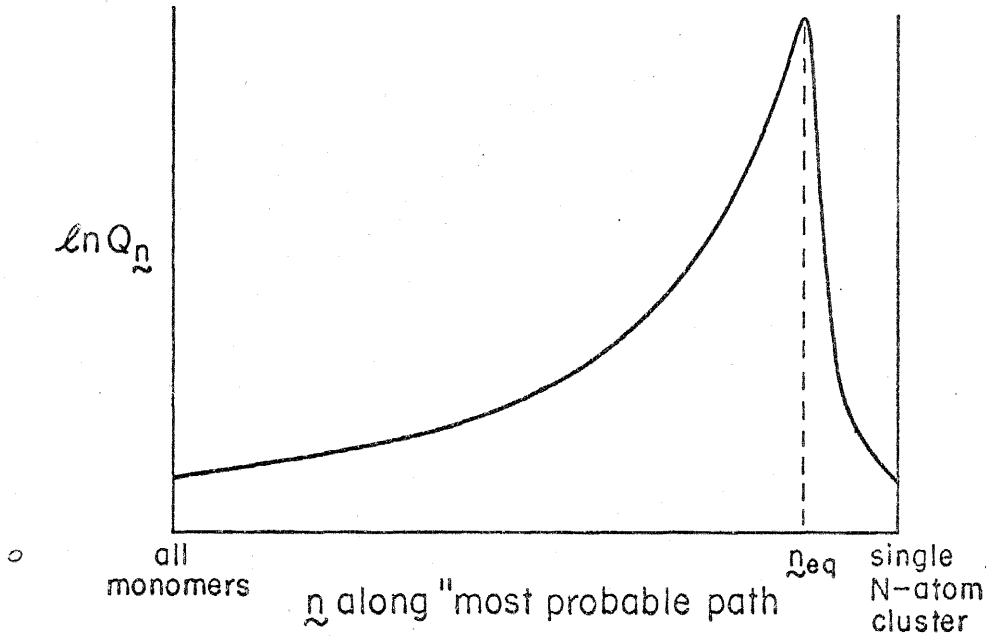

(b)

Figure 6: (a) The shape of $\Delta G_n^\dagger$ vs. n for a high density or low temperature system, and (b) the corresponding shape of the function $\ell n\, Q_{\underset{\sim}{n}}$ vs. $\underset{\sim}{n}$ along the most probable path. Both illustrations are highly schematic.

cluster in $\underset{\sim}{n}_{eq}$ is comparable in magnitude to N. The distribution corresponds to a volume of liquid in stable equilibrium with ambient vapor and the vector $\underset{\sim}{n}_{eq}$ has the form

$$\underset{\sim}{n}_{eq} = \{n_1, n_2, \ldots, 0, 0, \ldots, n_{i(max)} = 1, 0, 0, \ldots\}. \quad (53)$$

Here the population numbers decrease to zero as in Eq. (5), there is a gap in which all population numbers are zero, and then there is a single nonzero value of unity that is followed by more zeros.

In Fig. 5 the free energy curve has the familiar shape associated with nucleation theory; it has a maximum that marks the size of the nucleus. The function $Q_{\underset{\sim}{n}}$ vs. $\underset{\sim}{n}$ has two maxima and one minimum. Distribution $\underset{\sim}{n}^{I}_{eq}$ has the same form as that in Eq. (52) and corresponds to the metastable, supersaturated vapor. Distribution $\underset{\sim}{n}^{III}_{eq}$ has the same form as that in Eq. (53) and corresponds to the condensed state. Distribution $\underset{\sim}{n}^{II}_{eq}$ corresponds to the transition state in which the nucleus exists in unstable equilibrium with ambient vapor. That distribution also has the form of Eq. (53); in $\underset{\sim}{n}^{II}_{eq}$ however, i(max) is the size of the nucleus and is small, typically on the order of 100 molecules.

Nucleation

Referring to Fig. 5b, a nucleation experiment corresponds to preparing the system with an initial distribution approximately equal to $\underset{\sim}{n}^{I}_{eq}$ and measuring the time required for the system to pass through the transition state II. The rate of formation of the transition state r_t is proportional to the ratio of probabilities of the two states:

$$r_t \propto P_{\underset{\sim}{n}^{II}_{eq}} / P_{\underset{\sim}{n}^{I}_{eq}} = Q_{\underset{\sim}{n}^{II}_{eq}} / Q_{\underset{\sim}{n}^{I}_{eq}} . \quad (54)$$

This expression assumes a more familiar form if we note that the Helmholtz free energy of a system constrained to maintain a particular distribution $\underset{\sim}{n}$ is

$$F_{\underset{\sim}{n}} = -kT \ln Q_{\underset{\sim}{n}} . \tag{55}$$

Equation (54) is therefore equivalent to the following expression:

$$r_t \propto e^{-\Delta F/kT} , \tag{56}$$

where

$$\Delta F = F_{\underset{\sim}{n}^{II}_{eq}} - F_{\underset{\sim}{n}^{I}_{eq}} . \tag{57}$$

The lifetime of the metastable state is proportional to r_t^{-1} and will be very long if ΔF is large. As the level of supersaturation of the vapor increases, the values of ΔF and the lifetime decrease. The supersaturation level at which the lifetime becomes short, on the time scale of the experiment, is the critical supersaturation.

Evaluation of the Distribution of Clusters in the Metastable State

As shown in Section C, knowledge of the distribution of clusters in the metastable state is necessary for solution of the rate equations that describe nucleation. To determine this distribution we maximize $Q_{\underset{\sim}{n}}$ [Eq. (50)], treated as a function of the n_i, subject to the following constraints:

1. $\underset{\sim}{n}$ contains no macroscopic clusters,
2. $\sum_{i=1}^{N} i n_i = N$, and
3. the n_i are integers.

The last constraint is usually ignored, leading to a distribution that

contains fractions of clusters and that is not, therefore, physically realizable.

An approximate method for computing the concentrations is based on the method of Lagrange undetermined multipliers in which the n_i are treated as continuous variables. That method yields the following expression, which is incorrectly used in most treatments of nucleation theory:

$$n_i = n_1^i q_i / q_1^i, \qquad i = 1, \ldots, N. \tag{58}$$

Our approximate solution for the n_i, in terms of n_1, is

$$n_i = \text{int}[n_1^i q_i / q_1^i], \qquad i = 1, \ldots, N, \tag{59}$$

where the operator "int" extracts the largest integer value. The actual values of the n_i can be determined by an iterative process. An estimate of n_1 is used to evaluate the n_i and the value of the sum $\sum_{i=1}^{N} i n_i$ is computed. If the sum is larger than N, the estimate of n_1 is decreased; if it is smaller than N, the estimate is increased. This process is repeated until the value of the sum converges to N.

There are no nuclei in $\hat{n}_{eq}^I$. A distribution that contains a nucleus cannot correspond to a maximum in $Q_{\hat{n}}$ because a more stable distribution with a higher value of $Q_{\hat{n}}$ could always be formed by adding a monomer to the nucleus.

NOTE 10: The classical Becker-Doring solution of the nucleation rate equations[7] is based on an initial distribution $n(t_0)$ for which the integer constraint on the n_i does not hold. The solution is based on a distribution of the system that cannot in fact occur. In particular, that solution assumes that the concentration of nuclei in the initial distribution is nonzero; and it equates the rate of formation of nuclei to the product of that concentration with a frequency factor derived from kinetic theory. If the correct set of initial cluster concentrations were used, this simple approximation would not work because the initial concentration of nuclei would be zero. The Becker-Doring approach does not constitute a valid solution of the nucleation rate equations.

A Fundamental Problem with the Liquid-Drop Approach

The basic idea behind the liquid-drop approach is to use the Gibbs surface theory result $\Delta F = \frac{1}{3}\sigma A$, which is the difference in free energy between the two equilibrium states I and II in Fig. 5b, to evaluate the standard Gibbs free energy change $\Delta G_n^\dagger$ for the reaction $nA_1 \rightarrow A_n$. The approach is justified only if the change that results from going between the two equilibrium states is also represented by the above reaction. We do not believe this to be the case.

There are many reactions among the clusters in the distribution $\underset{\sim}{n}^I_{eq}$ that lead to a distribution containing a nucleus. For example, the following reactions are among those possible for the formation of such a distribution:

$$nA_1 \rightarrow A_n \tag{60A}$$

$$(n-2)A_1 + A_2 \rightarrow A_n \tag{60B}$$

$$(n-3)A_1 + A_5 \rightarrow A_2 + A_n \,. \tag{60C}$$

Only one reaction will lead to the distribution $\underset{\sim}{n}^{II}_{eq}$, and that reaction can be determined only if one knows the distributions $\underset{\sim}{n}^I_{eq}$ and $\underset{\sim}{n}^{II}_{eq}$. We have not as yet used the method outlined earlier in this section to determine the actual equilibrium distributions in a specific system so we cannot state with certainty that the correct reaction does not correspond to that in Eq. (60A); but we see no justification for the assumption that this is the correct reaction. Indeed, it appears that in the most favorable reaction, a nucleus is formed from the less stable, larger clusters instead of from n monomers.

Comment on the Translation-Rotation Controversy[8]

In what is known as the "translation-rotation controversy" it is claimed that the classical expression for $\Delta G_n^\dagger$ in Eq. (43) does not contain contributions from the translational or rotational degrees of freedom of the nucleus. Several arguments have been presented that lead to correction factors of widely differing magnitudes. We believe that all these arguments are based on an incorrect understanding of the process to which the Gibbs result $\Delta F = \frac{1}{3}\sigma A$ refers. An assumption common to all the arguments is that the process is the formation of a stationary drop. This assumption is not made by Gibbs in his derivation of the surface theory and we see no necessity for introducing it.

The actual process is quite simply a transition between states I and II in Fig. 5b, and the free energy difference is

$$\Delta F = \tfrac{1}{3}\sigma A = F_{\underset{\sim}{n}^{II}_{eq}} - F_{\underset{\sim}{n}^{I}_{eq}} , \qquad (61)$$

where $F_{\underset{\sim}{n}}$ is defined by Eq. (57). The process is not, however, easily represented by a simple reaction among clusters unless the distributions $\underset{\sim}{n}^{I}_{eq}$ and $\underset{\sim}{n}^{II}_{eq}$ are known. If the distributions were known, one could write down the statistical mechanical equivalent of ΔF in terms of independent-cluster partition functions. This equivalent would constitute a rigorous, molecular-level interpretation of the expression $\Delta F = \frac{1}{3}\sigma A$.

The Gibbs result, therefore, refers to the formation of a cluster that is free to translate and to rotate; and if an expression for $\Delta G_n^\dagger$ could be derived from this result, there would be no need to add in corrections for the translational or rotational degrees of freedom.

REFERENCES

1. J. W. Gibbs, The Scientific Papers (Dover Publications, New York, 1961), Vol. I, pp. 219-258.
2. N. Davidson, Statistical Mechanics (McGraw-Hill, New York, 1962), p. 164.
3. R. H. Fowler, Statistical Mechanics (Cambridge University Press, Cambridge, 1929), Chap. 17.
4. A. B. Long, Rev. Geophys. 7, 595 (1969).
5. J. Frenkel, J. Chem. Phys. 7, 538 (1939); W. Band, ibid. 7, 324, 927 (1939).
6. F. H. Stillinger, ibid. 38, 1486 (1963); H. Reiss, J. Stat. Phys. 2, 83 (1970).
7. R. Becker and W. Döring, Ann. Phys. 24, 719 (1935); J. Katz, J. Stat. Phys. 2, 137 (1970).
8. J. Lothe and G. M. Pound, J. Chem. Phys. 48, 1849 (1968); H. Reiss, J. L. Katz, and E. R. Cohen, ibid. 48, 5553 (1968).

PART II: THE MICROCRYSTAL MODEL FOR CLUSTERS

A. Introductory Remarks

This section contains two papers that describe our work with the microcrystal model for clusters. In this model a cluster is treated as a small crystallite and its thermodynamic properties are determined in exactly the same way that one would determine those of a polyatomic molecule in the simplest approximation: the harmonic, rigid-rotator, and perfect-gas approximations are used to evaluate the vibrational, rotational, and translational contributions to the cluster partition function.

In the first paper, which has been published [J. Chem. Phys. 55, 580 (1971)], results of calculations with clusters of 2 to 100 argon atoms are presented. This work was the first complete (all degrees of freedom) calculation of the cluster thermodynamic properties using a molecular level model. In the paper we discuss in detail the approximations involved in our calculation and present results for the cluster thermodynamic functions and the steady-state rate of nucleation.

In the second paper, which has been accepted for publication in Chemical Physics Letters, we discuss the importance of using several stable configurations of a cluster in calculating its properties with the microcrystal model. We show that the "single-configuration" approximation that was used in previous work can lead to serious errors. We also discuss methods by which the error can be minimized in future calculations.

B. Paper No. 1

Vapor Phase Homogeneous Nucleation and the Thermodynamic Properties of Small Clusters of Argon Atoms

ABSTRACT

The steady state rate of homogeneous nucleation in a vapor of Lennard-Jones spheres has been calculated using statistical mechanical techniques to compute the equilibrium concentrations of clusters in the vapor. All degrees of freedom of the clusters are explicitly considered. The harmonic approximation is used in the calculation of vibrational contributions to the cluster partition functions and the rigid body approximation is used in the calculation of rotational contributions. The Gibbs free energy of cluster formation as a function of cluster size is calculated and its dependence on temperature is examined. Size effects on the vibrational free energy are found to be mainly energetic rather than entropic. The rate of nucleation as a function of pressure is calculated at four temperatures and found to have a behavior similar to what would be expected from "liquid-drop" model calculations.

INTRODUCTION

Our theoretical understanding of homogeneous nucleation from the vapor phase is based almost entirely on the mechanism proposed by Farkas[1] in which the formation of condensed phase occurs by the growth of small clusters of molecules into droplets or crystals. The supersaturated vapor is treated as a gaseous mixture of these clusters with uncombined molecules; and the growth and decay processes of the clusters are limited to the gain or loss of single molecules. A general kinetic description of this system, yielding time-dependent concentrations for each of the clusters for a given set of initial concentrations, is not yet possible. Such a general description is, however, not entirely relevant at present since experimental measurement of these time-dependent concentrations is itself not yet possible.

The quantity that is in fact measured is the "critical" supersaturation, the degree of saturation at which the vapor collapses from metastability. To calculate this "critical" value, an equilibrium theory of rates is used. The metastable vapor is modeled as an equilibrium state of the system, which is formally established by constraining the set of possible reactions between clusters such that the formation of clusters larger than some size m is prohibited. The value of m is chosen to be slightly larger than the size of the cluster whose Gibbs free energy of formation from the monomer is maximum. The allowed reactions for the model system are thus

$$
\begin{aligned}
A_1 + A_1 &\rightleftharpoons A_2 \\
A_2 + A_1 &\rightleftharpoons A_3 \\
&\vdots \\
A_{m-1} + A_1 &\rightleftharpoons A_m \\
A_m + A_1 &\rightarrow \text{no reaction.}
\end{aligned}
\qquad (1)
$$

The rate of nucleation is equated to the initial rate of formation of A_m and is expressed in terms of the equilibrium cluster concentrations and the rate constants for the reactions of Eq. (1). The "critical" supersaturation is identified as the supersaturation value at which the rate of nucleation becomes "large". In practice this identification can be made with little ambiguity since the calculated rate increases quite drastically from a very small to a very large value as the supersaturation is increased through the "critical" value. This value is apparently relatively insensitive to the exact values used for the rate constants, and most of the effort in the development of the model has been directed toward calculation of the equilibrium cluster concentrations.

The classical "liquid-drop" model approach to this calculation is an extrapolation of Gibbs' thermodynamic theory of surfaces to microscopic clusters of molecules. Remarkable agreement with experiment has been obtained in this way,[2] but the resulting theory is not generally regarded as valid since the extrapolation is not consistent with the assumptions on which the surface theory is based. Indeed, Gibbs' model for a surface as an interface separating two homogeneous phases is clearly not applicable to small clusters of less

than 100 molecules, which are believed most important in determining the rate of nucleation, since a homogeneous region does not in fact exist anywhere inside such clusters.

In this paper, the equilibrium distribution of clusters is calculated using statistical mechanical techniques. No use is made of thermodynamic surface theory so the results are independent of those of the "liquid drop" model and not subject to many of the criticisms directed at that model.

THE METHOD

We treat the clusters themselves as "molecules" and the supersaturated vapor as a perfect gas of these "molecules". The partition function for this system is given by

$$Q = \prod_i \frac{q_i^{n_i}}{n_i!} \quad , \tag{2}$$

where n_i is the number of clusters of size i and q_i is a cluster partition function. The Hamiltonian for a given cluster is assumed separable in the usual manner

$$H_i = H_{i,tr} + H_{i,vib} + H_{i,rot} \, ,$$

where $H_{i,tr}$, $H_{i,vib}$, and $H_{i,rot}$ are the translational, vibrational, and rotational contributions to the Hamiltonian, respectively. The importance of vibration-rotation interaction, which is ignored in this separation, is discussed later in the paper. The cluster partition function can thus be expressed as a product,

$$q_i = q_{i,tr}\, q_{i,vib}\, q_{i,rot} \, .$$

The factors of the cluster partition function are evaluated from standard statistical mechanical formulas, using the harmonic approximation for the computation of $q_{i,\,vib}$ and the rigid rotator approximation for the computation of $q_{i,\,rot}$. Thermodynamic functions for the system are then calculated from the partition function Q and the equilibrium cluster concentrations are obtained from these functions using standard thermodynamic techniques.

The clusters considered in these calculations are composed of Lennard-Jones 12-6 spheres. The potential energy of a cluster of n atoms is therefore given by

$$V = \sum_{i=1}^{n} \sum_{j>i}^{n} 4\epsilon \left\{ \left(\frac{\sigma}{r_{ij}} \right)^{12} - \left(\frac{\sigma}{r_{ij}} \right)^{6} \right\} , \qquad (3)$$

where r_{ij} is the distance between atoms i and j, and the values of σ and ϵ used are those specific for argon:[3] $\sigma = 3.405$ Å and $\epsilon/k_B = 119.8°K$, where k_B is Boltzmann's constant. How well the Lennard-Jones pairwise potential represents the actual interactions among argon atoms does not concern us here; our purpose is to study in detail the characteristics of a simple, yet realistic, model of a supersaturated vapor.

THE CALCULATION

A. The Statistical Mechanical Formulas

The formulas used in calculating the contributions to the cluster partition function are, for a cluster of i atoms, as follows:

$$q_{i,\,tr}(T, P_i) = \frac{n_i k_B T}{P_i} \left(\frac{2\pi m_i k_B T}{h^2} \right)^{\frac{3}{2}} \qquad (4)$$

$$q_{i,\,vib}(T) = e^{-V_0/k_BT} \prod_{j=1}^{N_{i,\,vib}} \left(\frac{e^{-h\nu_j/2k_BT}}{1 - e^{-h\nu_j/k_BT}} \right) \tag{5}$$

$$q_{i,\,rot}(T) = \begin{cases} \dfrac{8\pi^2 I k_B T}{\sigma_r h^2} & , \; i = 2 \\ \dfrac{\pi^{\frac{1}{2}}}{\sigma_r} \left(\dfrac{8\pi^2 k_B T}{h^2} \right)^{\frac{3}{2}} (I_A I_B I_C)^{\frac{1}{2}} & , \; i > 2 \end{cases} \tag{6}$$

where P_i = partial pressure of i-atom clusters,

k_B = Boltzmann's constant,

m = mass of single atom of the cluster,

h = Planck's constant,

V_0 = equilibrium potential energy of cluster,

ν_j = the j^{th} normal frequency of vibration,

$N_{i,\,vib}$ = number of vibrational degrees of freedom: equals unity for the dimer and (3i - 6) for all other stable clusters,

I = moment of inertia of two-atom cluster,

σ_r = rotational symmetry number,

I_A, I_B, I_C = principle axis moments of inertia.

B. The Selection of "Nonequilibrium" Clusters

Each "nonequilibrium" cluster is a subset of an infinite lattice of atoms having either the hexagonal-close-packed (hcp) or the cubic-close-packed (ccp) structure. All nearest-neighbor distances in these clusters are $2^{1/6}\sigma$, the potential minimum distance for the Lennard-Jones 12-6 pair potential. Two sets of "nonequilibrium" clusters were used in this work.

The first (Set A) is composed of "spherical" clusters constructed by filling successive neighbor shells about an atom in a ccp lattice and is identical to that considered by Burton.[4]

The second (Set B) was selected in a somewhat more complicated manner aimed at creating a more complete sequence of clusters. Three series of clusters of 2 to 100 atoms were created. Each of these series was derived from one of the close packed lattices by the following process:

1. Choose either the hcp or ccp infinite lattice.
2. Select two contiguous lattice sites, number them 1 and 2, and occupy each with an atom. This diatom constitutes the first cluster of the series.
3. Consider all possible 3-atom clusters that have two atoms occupying lattice sites 1 and 2 and a third atom occupying any other lattice site and select those that have the lowest potential energy. There are several such clusters having different orientations within the lattice. One of the clusters in this latter group is arbitrarily chosen as the 3-atom cluster of the series. The new lattice site is numbered 3.
4. Successively larger clusters are formed essentially by repeating step 3. That is, consider all possible n-atom clusters, $(n - 1)$ of whose atoms occupy lattice sites numbered 1 through $(n - 1)$; select those that have the lowest potential energy; and arbitrarily choose the n-atom cluster from this latter group.

One series was derived from a ccp lattice and two, corresponding to two different outcomes of the arbitrary choice in step 3, were taken from an hcp lattice.

C. Creation of Equilibrium Clusters

Each equilibrium cluster was formed by "relaxing" one of the "nonequilibrium" clusters described above so that the potential energy of the cluster was an extremum. The equilibrium was accomplished on an IBM 360/75 computer with an iterative routine in which, at each step, each atom of a cluster was moved in the direction of the force on that atom and a distance proportional to this force. The forces were then recalculated and another iteration performed. The proportionality factor that was used was 10^{-13} sec. The process was terminated when the average of the magnitudes of the forces on the atoms became less than 1.5×10^{-10} dynes/atom. This force was found to be small enough so that the calculated normal mode frequencies did not change significantly when the value was decreased.

Two sets (1 and 2) of equilibrium clusters were created from the clusters in the two "nonequilibrium" sets (A and B). Set 1 was obtained directly by equilibrating each of the "nonequilibrium" clusters of Set A. The clusters of Set 2 were obtained from the three series of "nonequilibrium" clusters in Set B by first equilibrating the three clusters with a given value of n, and then selecting the one with the lowest equilibrium potential energy.

D. The Normal Mode Analysis

The normal mode analysis involves diagonalization of the "force constant" matrix whose elements are, for a n-atom cluster, the $(3n)^2$ second derivations of the cluster's equilibrium potential energy.[5] These elements are evaluated by inserting equilibrium coordinate values of the atoms in the cluster into analytic expressions for the second derivatives.

The normal frequencies of oscillation ν_j are obtained from the eigenvalues ω_j^2 of this matrix through the relation $2\pi\nu_j = \omega_j$. The diagonalization was accomplished with the 360/75 computer using the Givens-Householder technique.[6] All variables in the computer program were single precision except those into which sums were accumulated, which were double precision. The effect of round-off error was checked by diagonalizing the "force constant" matrix for the 55-atom "spherical" cluster using a program in which all variables were double precision. The eigenvalues were found to differ insignificantly from those obtained with the single precision program. Eigenvectors were not calculated for most clusters.

E. Unstable Clusters

An unstable cluster is indicated by a negative eigenvalue of the "force constant" matrix corresponding to a normal coordinate whose "restoring force" is negative. When indicated, this instability was verified and a stable cluster obtained by adding a very small amount of kinetic energy to the unstable equilibrium cluster and following the subsequent motion of the atoms using a molecular dynamics routine.[7] This kinetic energy was equally distributed among the atoms by giving each atom an initial velocity of the appropriate magnitude and of random direction. The molecular dynamics technique, which has been widely used in the study of dense fluids, allows one to calculate the classical "trajectories" for many-particle systems by numerically integrating the equations of motion. The algorithm due to Verlet[8] was used in this work.

RESULTS

"Spherical" (Set 1) clusters with 13, 19, 43, 55, 79, and 87 atoms were studied. The 13-atom cluster of this series had previously been found to be unstable by Burton,[4] and this was verified in our calculations. The "collapsed" cluster belongs to the D_{5d} point group and is identical to the pentagonal structure discussed by Benson and Shuttleworth.[9] We also found the 55-atom cluster to be unstable, "collapsing" to another D_{5d} structure. The "collapse" was accomplished by adding 2×10^{-18} ergs of kinetic energy per atom (equivalent to 0.01°K) to the cluster in unstable equilibrium and by following the classical motion of the atoms using the molecular dynamics routine discussed above. The transfer of potential energy to kinetic energy that accompanies the transition to a more stable configuration is shown in Fig. (1). Potential energies for the equilibrium clusters of Set 1 are listed in Table I.

Table II contains the potential energies for the clusters of Set 2. A 14-atom cluster was not included in the set because the three equilibrium clusters of this size formed in the manner described above were all unstable. Stable 14-atom clusters were not formed from these unstable clusters because it was felt that the amount of computer time required would not have been warranted. The 19-atom cluster of Set 2 is identical to that of Set 1.

The dependence of some of the cluster thermodynamic functions on n is shown in Figs. (2) - (4). The vibrational entropy and free energy calculated from $q_{i,vib}$ are plotted in Figs. (2) and (3), and the total (all degrees of freedom) Gibbs free energy is plotted in Fig. (4).

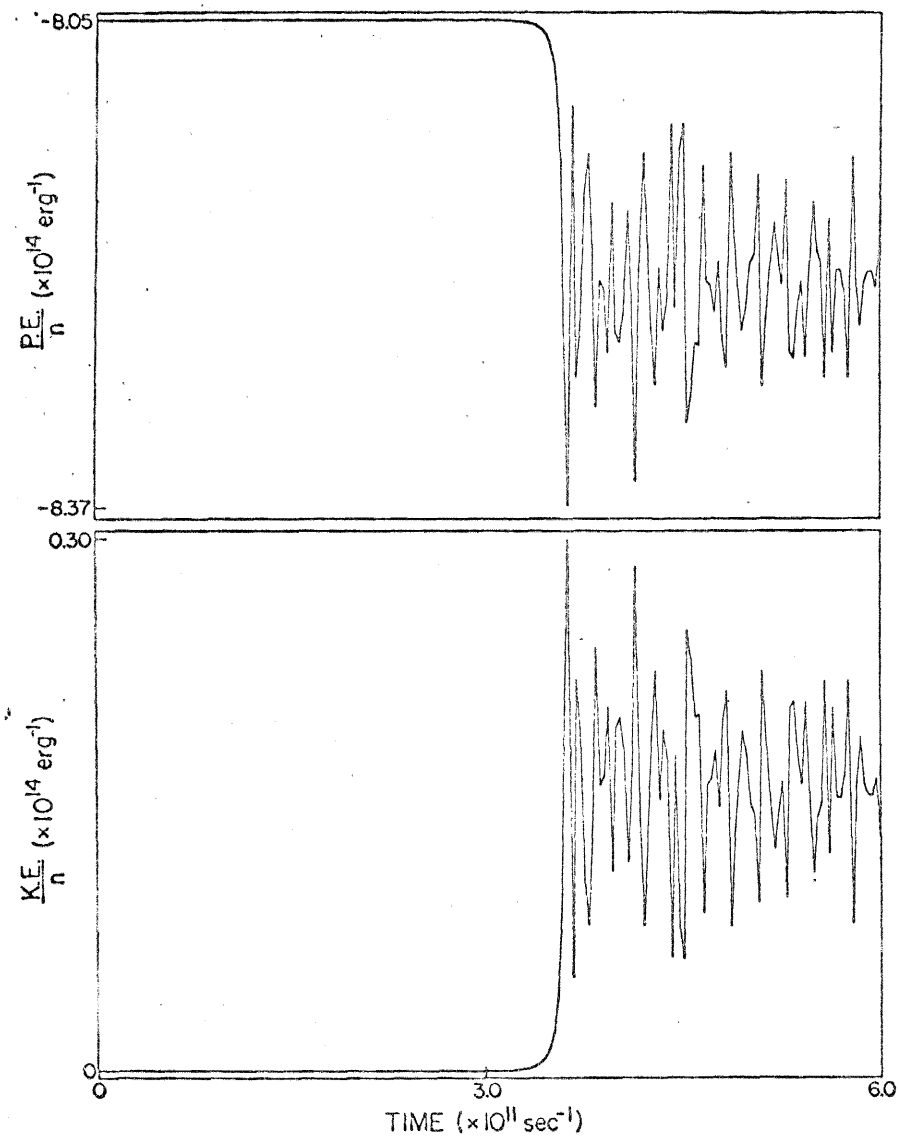

Figure 1. Potential energy per atom and kinetic energy per atom vs time for 55-atom "spherical" cluster as it "collapsed" from its unstable initial configuration. Cluster remained in the unstable configuration for about 3×10^{-11} sec after the addition of energy at time t = 0; it then "collapsed" with a transfer of potential energy to kinetic energy. The final temperature of the cluster was ~1.5 °K. Fluctuations in the energies after about 4.5×10^{-11} sec are as expected from an equilibrium cluster at this temperature.

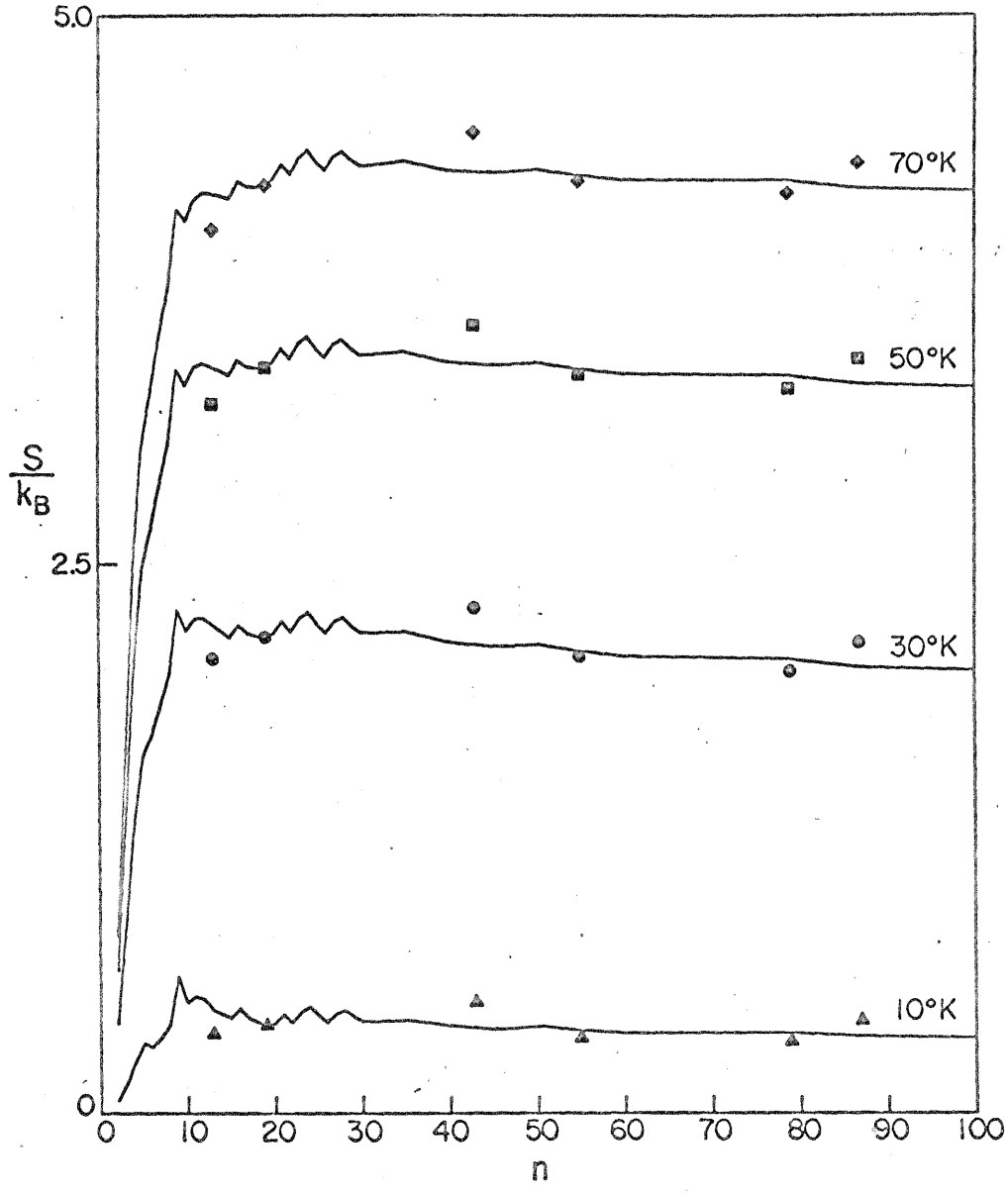

Figure 2. Dependence of the per-atom entropy on cluster size. Values for the Set 2 clusters are connected by solid lines: ——; and the Set 1 cluster values are marked as follows: ◆, 70 °K; ■, 50 °K; ●, 30 °K; ▲, 10 °K.

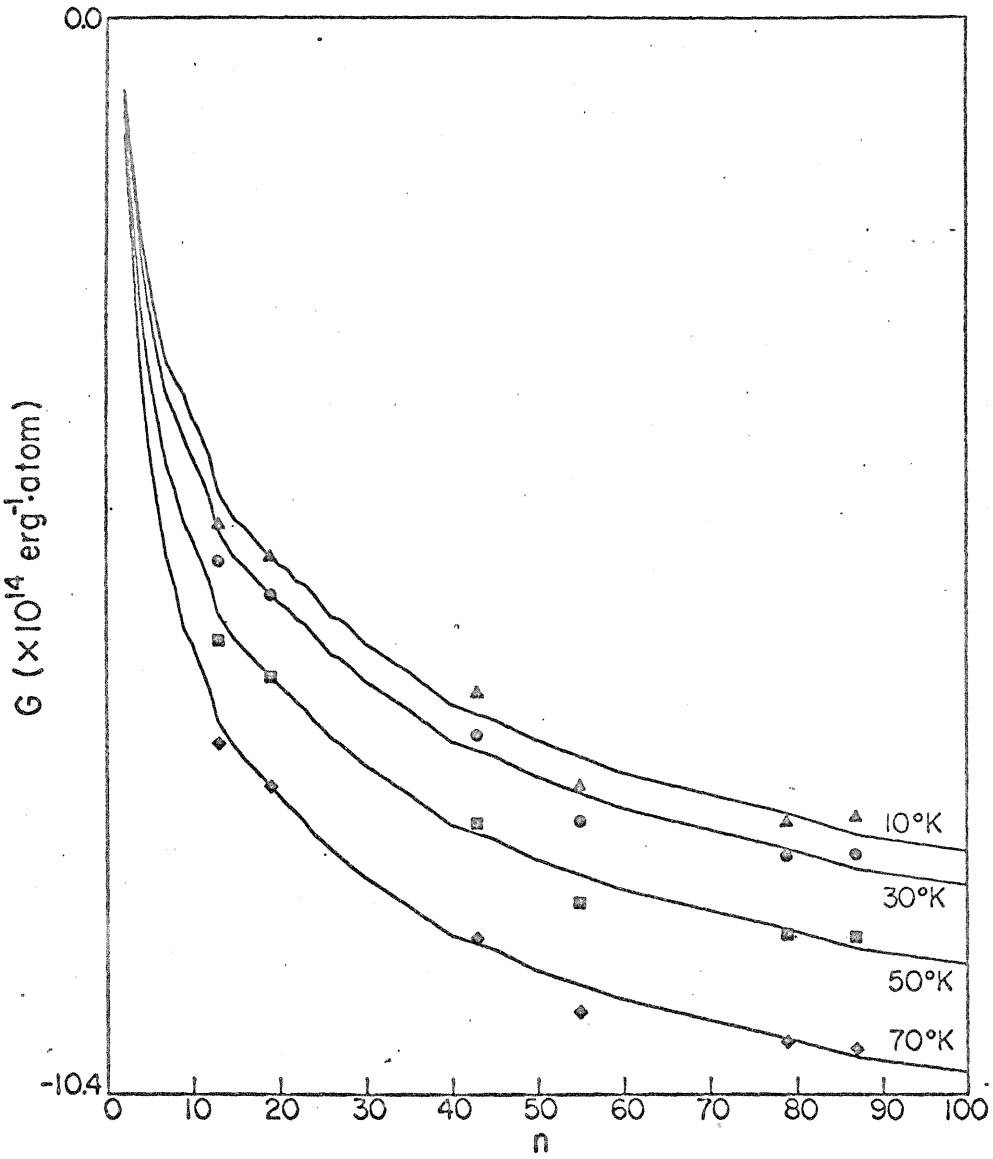

Figure 3. The vibrational Gibbs free energy per atom in clusters of size n. Set 2 clusters: ——; Set 1 clusters: ◆, 70 °K; ■, 50 °K; ●, 30 °K; ▲, 10 °K.

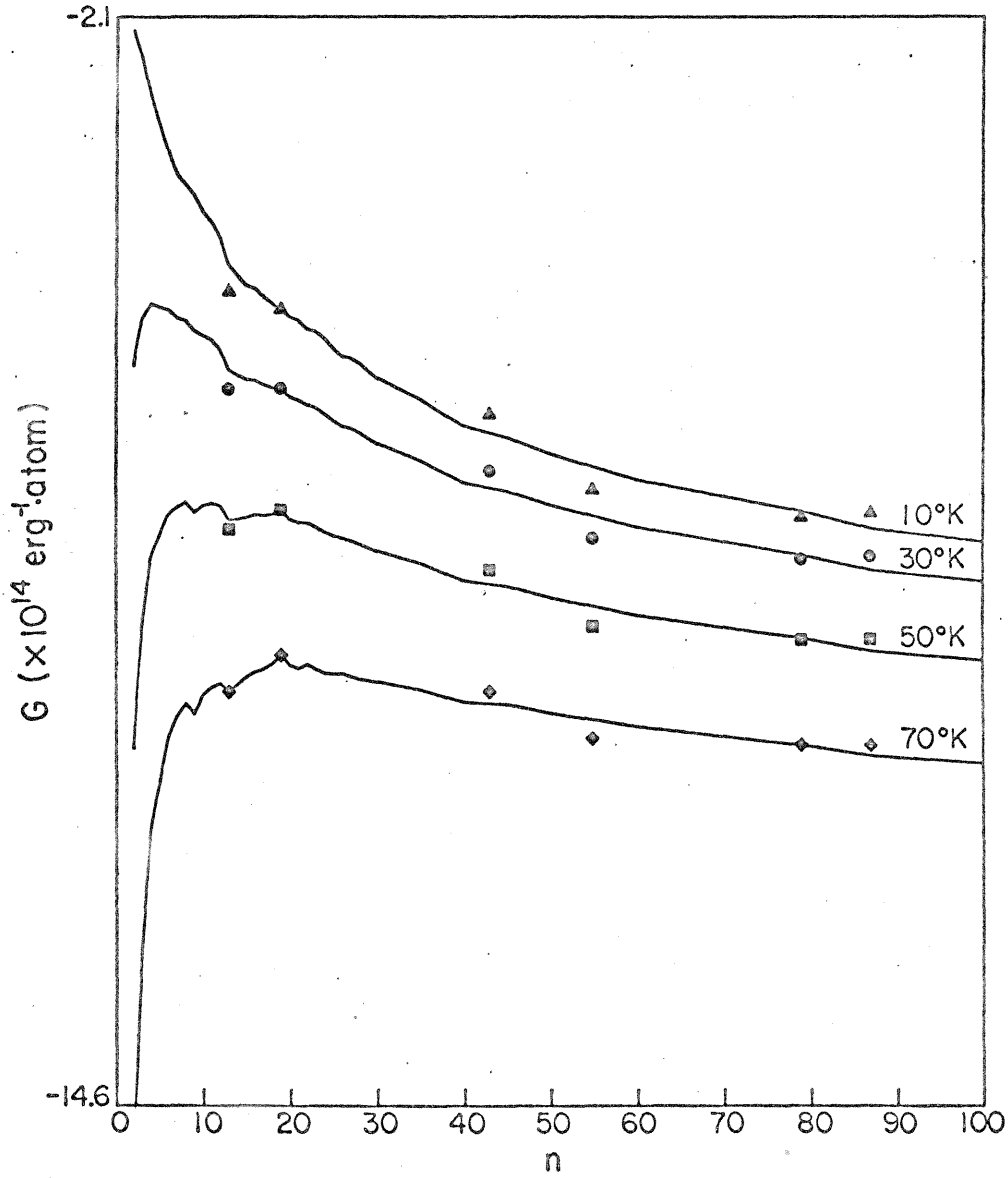

Figure 4. Total (all degrees of freedom) Gibbs free energy per atom for clusters of n atoms. Set 2 clusters: ——; Set 1 clusters: ◆, 70 °K; ■, 50 °K; ●, 30 °K; ▲, 10 °K.

The concentration of clusters of size n, relative to that of the monomer, is calculated from the Gibbs free energy of formation of the cluster by the equilibrium requirement that

$$\Delta G(n, T, P, X_n, X_1) = 0 , \tag{7}$$

where X_n is the mole fraction of clusters of size n, and P is the total pressure in the vapor. From equilibrium thermodynamics,

$$\Delta G(n, T, P, X_n, X_1) = \Delta G^{\dagger}(n, T, P) + k_B T \ln \frac{X_n}{X_1^n} , \tag{8}$$

where

$$\Delta G^{\dagger}(n, T, P) = \Delta G^{0}(n, T) + (1 - n) k_B T \ln P ; \tag{9}$$

and

$$\Delta G^{0}(n, T) = G^{0}(n, T) - n G^{0}(1, T)$$

is the standard Gibbs free energy of formation for an n-atom cluster. For later use in conjunction with the classical nucleation rate equation, we make the approximation that $(X_n/X_1^n) \sim (c_n/c_1)$, where c_n is the concentration of clusters of size n. This is a very good approximation, being based on the fact that virtually all the atoms in the vapor exist as monomers. The standard free energies are computed from the factors in the partition function, Eqs. (4)-(6), using the relations

$$G^{0}(n, T) = -k_B T \ln \left[\frac{1}{n_n} q_{n, tr}(T, 1\,\text{atm}) q_{n, rot}(T) q_{n, vib}(T) \right] \tag{10}$$

and

$$G^{0}(1, T) = -k_B T \ln \left[\frac{1}{n_1} q_{1, tr}(T, 1\,\text{atm}) \right] , \tag{11}$$

where n_n is the number of n-atom clusters and n_1 is the number of monomers. The standard Gibbs free energy of formation as a function of cluster size n is plotted in Fig. 5 for four different temperatures, and the values are tabulated in Tables I and II. The solid line in each

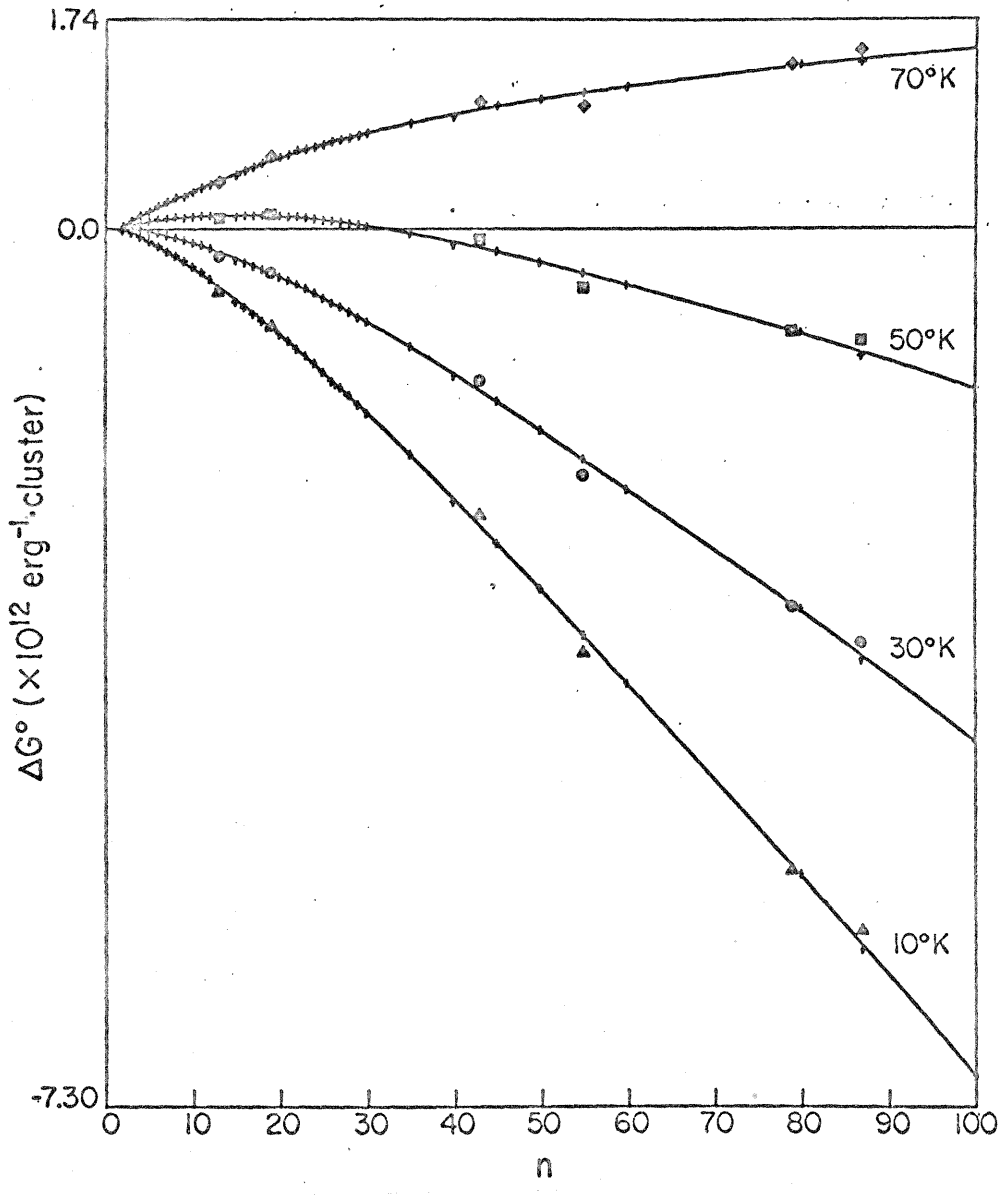

Figure 5. Standard Gibbs free energy of formation for clusters of n atoms. Set 2 clusters: +; polynomial fit of values for Set 2 clusters: ——; Set 1 clusters: ◆, 70 °K; ■, 50 °K; ●, 30 °K; ▲, 10 °K.

of these plots represents an analytic expression for $\Delta G^0(n, T)$ that was used in the calculation of the rate of nucleation. The expression was obtained by making, at each of four temperatures, a least-squares fit of the Set 2 standard free energy of formation data to a fourth-degree polynomial

$$\Delta G^0(n, T) = \sum_{i=1}^{5} C_i(T) n^{(i-1)}, \tag{12}$$

where the $C_i(T)$ are the polynomial coefficients. These coefficients are tabulated in Table III. The dependence of the curve $\Delta G^\dagger(n, T, P)$ vs n on pressure is shown in Fig. 6 for a temperature of 50 °K. The solid lines indicate values of an analytic expression for $\Delta G^\dagger$ that was obtained using the polynomial representation of ΔG^0.

The steady state rate of nucleation was calculated as a function of pressure at four temperatures using the following equation from "classical" nucleation theory[10]:

$$J(P;T) = \frac{P}{\sqrt{2\pi mkT}} S(n^*) c_1 \left[\frac{\Delta G^\dagger(n^*, P;T)}{3\pi k_B T n^{*2}} \right]^{\frac{1}{2}} \exp \left[\frac{-\Delta G^\dagger(n^*, P;T)}{k_B T} \right], \tag{13}$$

where n^* is the size, $S(n^*)$ the surface area (approximated as spherical), and $\Delta G^\dagger(n^*, P;T)$ the Gibbs free energy of formation for the cluster with the largest free energy of formation and hence the one having the lowest concentration. For each temperature this rate was calculated over the range of pressure where $2 \leq n^* \leq 100$. At each such pressure, n^* and $\Delta G^\dagger(n^*, P;T)$ were found by maximizing Eq. (9) and $J(P;T)$ was then computed from Eq. (13).

The variations of n^*, $\Delta G^\dagger(n^*)$, and J with pressure at 50 °K are shown in the plots of Figs. 7-9, respectively, and the results of the

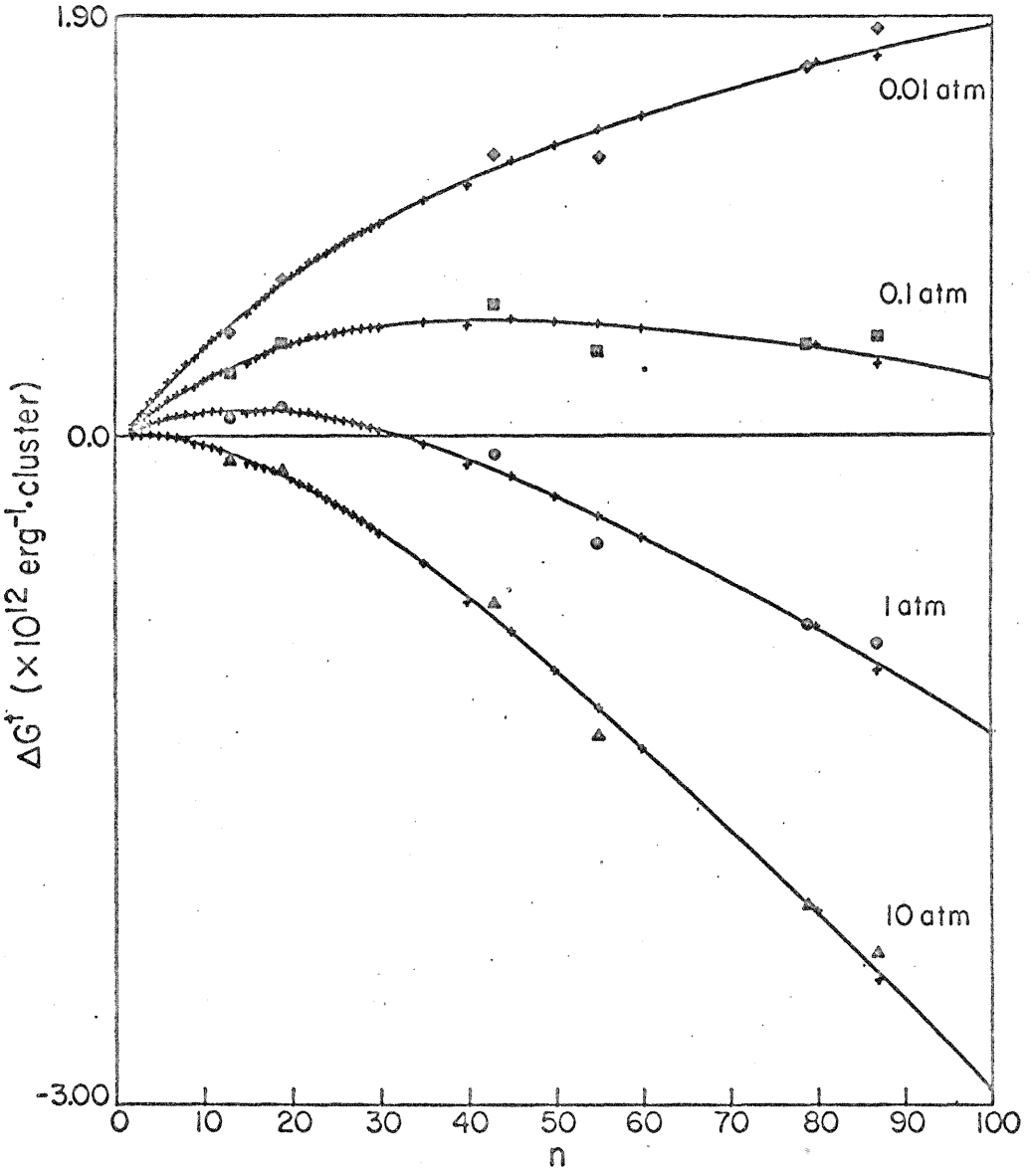

Figure 6. Gibbs free energy of formation, $\Delta G^{\dagger}(n, P;T) = \Delta G^{0}(n;T) + (1-n)k_{B}T \ln P$, at 50 °K for clusters of n atoms. Set 2 clusters: +; analytic expression using polynomial expression for ΔG^{0}: ——; Set 1 clusters: ◆, 0.01 atm.; ■, 0.1 atm.; ●, 1 atm.; ▲, 10 atm.

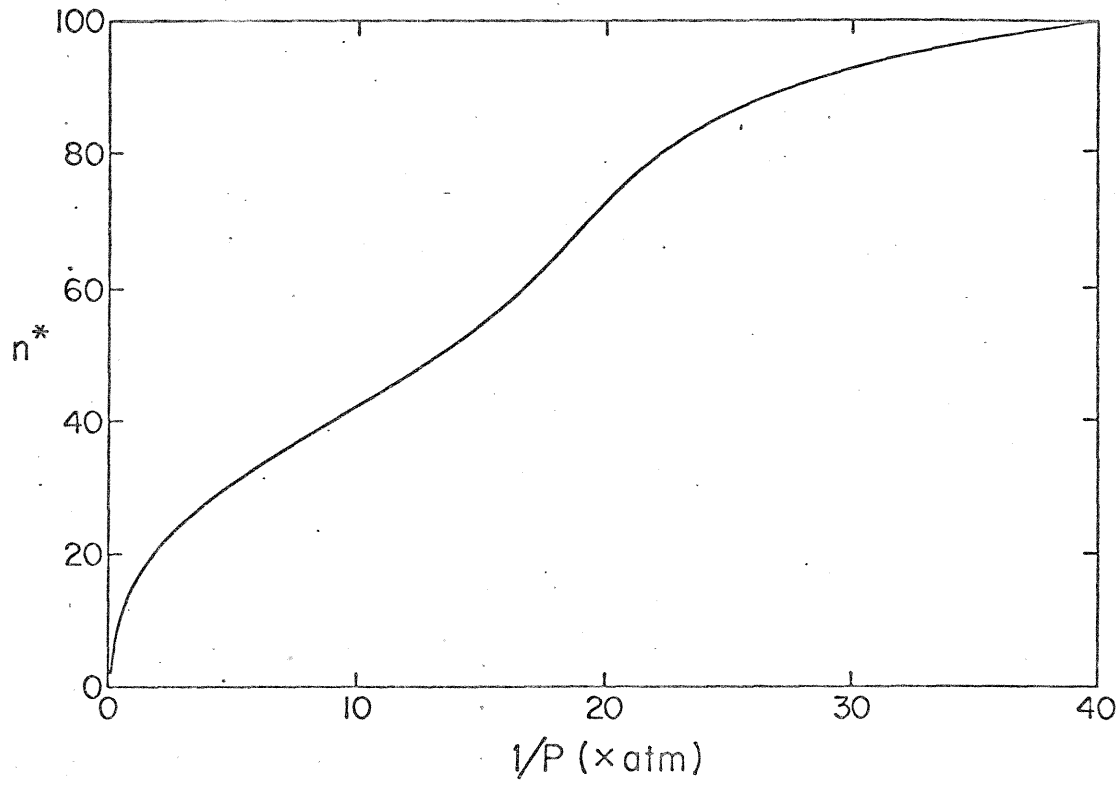

Figure 7. The dependence on pressure of the size of the cluster that at 50 °K has the largest free energy of formation $\Delta G^{\dagger}$ and, hence, the lowest "equilibrium" concentration in the supersaturated vapor. Formation of clusters of this size is, according to the classical rate theory, the rate-determining step in the nucleation process.

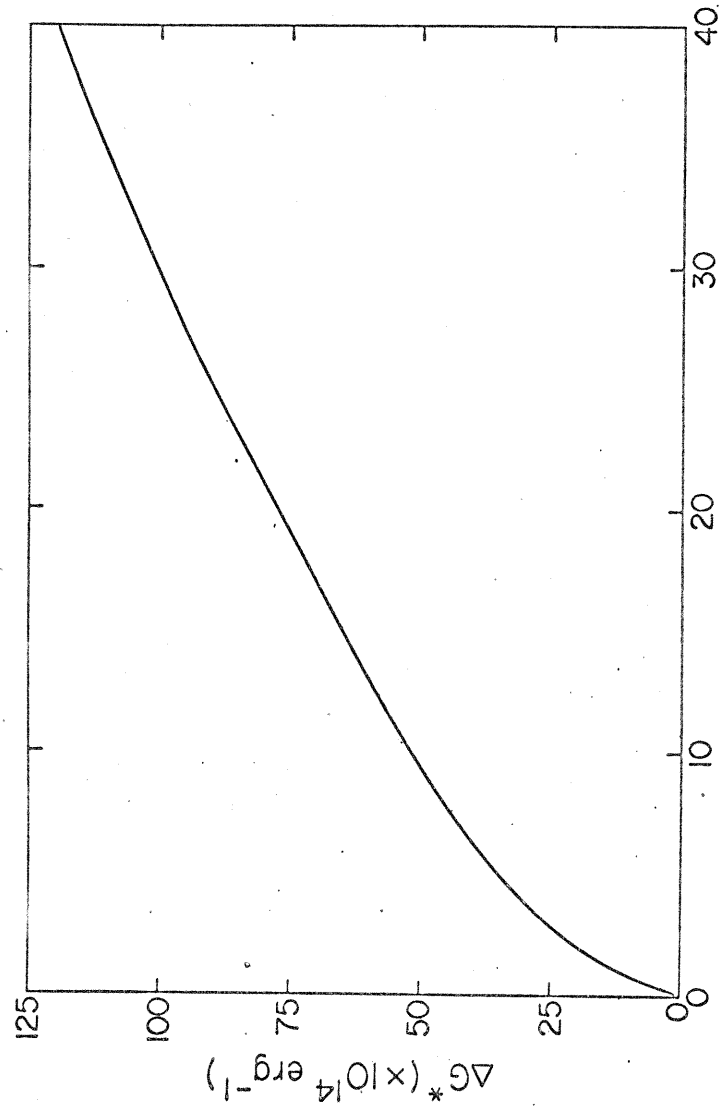

Figure 8. The maximum value of $\Delta G^{\dagger}$ at 50 °K vs pressure.

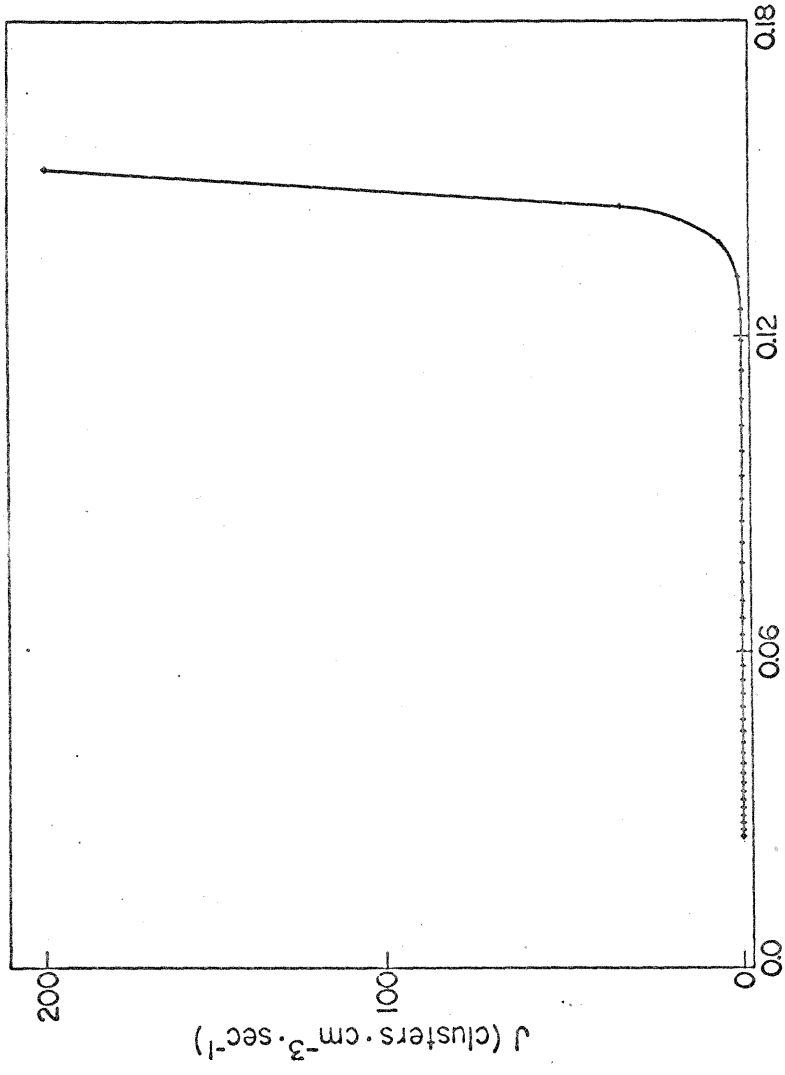

Figure 9. The steady state rate of homogeneous nucleation at 50 °K vs pressure. The rate was calculated using Eq. (14) from the "classical" rate theory theory and the values of n* and $\Delta G^{\dagger}(n^*)$ calculated in this paper.

rate calculation are summarized in Table IV. The "critical" pressure P_c was arbitrarily defined as the pressure at which the rate of nucleation is 1 cluster/($cm^3 \cdot sec$).

DISCUSSION

In this work, a cluster has been modeled as a microcrystal; that is, it has been assumed that the atoms of a cluster possess an ordered structure similar to that in a crystal. This model is realistic at temperatures below the "melting" point of the cluster, which, according to the classical Thompson equation[11]

$$T_r = T_\infty \left(1 - \frac{2\sigma_s v_m}{r\Delta H}\right) ,$$

occurs at a temperature below that for the bulk solid. In this equation, T_r is the "melting" point for a cluster of radius r, T_∞ is that for the bulk solid, σ_s is the surface tension for the solid, v_m is the volume per molecule in the solid, and ΔH is the heat of fusion per molecule. Since T_r increases with r, the temperature range over which the model is reasonable increases with cluster size.

Our evaluation of the thermodynamic functions for the microcrystal cluster is only approximate. The most serious approximation by far we believe is that of ignoring the effect on the vibrational energy levels of anharmonicity in the potential energy function. For low vibrational energies this effect could be included as a perturbation of the harmonic approximation energy levels. The vibrational energy could then, however, no longer be considered as a sum of the energies of the independent normal modes of the cluster and a simple equation like Eq. (5) could not be used to evaluate $q_{i,\,vib}$. The effect becomes much more dramatic at higher energies where fluid-like motion becomes important and the structure of real clusters ceases to resemble that of our model. The importance of anharmonicity is indicated by a comparison of the time average "vibrational"

potential energies $\langle V \rangle$ of two "classical", nonrotating clusters, one harmonic and the other "exact", at the same temperature. By the equipartition of energy theorem[12] it is known that $\langle V \rangle$ for a harmonic cluster of i atoms with a nonlinear configuration is

$$\langle V \rangle = (3i - 6)\frac{kT}{2} \quad ,$$

where $(3i - 6)$ is the number of normal modes. The "exact" value of $\langle V \rangle$ is obtained from molecular dynamic calculations performed as described above. These calculations are "exact" in the sense that the complete Lennard-Jones pairwise potential is used. All time averages are taken over intervals of 8×10^{-11} sec or longer.[13] Table V contains values for the two sets of energies at three different temperatures for a 30-atom cluster. The effect of anharmonicity is indicated by the difference between $\langle V \rangle_{harmonic}$ and $\langle V \rangle_{exact}$. This difference, which increases quite rapidly from about 5% of $\langle V \rangle_{harmonic}$ at 30 °K to 85% of this value at 50 °K, suggests that for a 30-atom cluster the harmonic approximation is useful up to temperatures of about 30 °K but is not very good at temperatures much higher than this value.

Another approximation is the neglect of vibration-rotation coupling. This coupling can, in a first approximation, be resolved into two parts[5]: (1) changes in the vibrational energy levels due to Coriolis interaction; and (2) changes in the rotational energy levels due to the fact that the average values of the moments of inertia in a vibrating cluster are not equal to the values calculated from the equilibrium positions of the atoms. The magnitude of each of these effects was estimated for a 30-atom cluster using data from a molecular dynamics calculation at 30 °K.

To estimate the magnitude of the Coriolis interaction, the time average Coriolis force per particle

$$\langle F_{\text{Coriolis}} \rangle = \langle \frac{1}{N} \sum_{i=1}^{N} (2m_i \underset{\sim}{v}_i \times \underset{\sim}{\omega}) \rangle \ ,$$

was computed and compared with the time average total force per particle. The value of ω used in the calculation corresponded to a rotational temperature [defined in terms of the average rotational kinetic energy by $\langle KE_{rot} \rangle = (3/2)k_B T_{rot}$] of approximately 50 °K. The average Coriolis force was found to be only 0.6% of the average total force. This small relative size of the Coriolis force suggests that its effect on the thermodynamic functions should be small, especially when compared with that of the anharmonicity described above.

The second part of the vibration-rotation coupling can be approximately included in the calculation of the thermodynamic functions by using the time average moment-of-inertia product $\langle I_A I_B I_C \rangle$ in the evaluation of $q_{i,\,rot}$ from Eq. (6). The value of this average in a 30-atom cluster at 30 °K was computed from the molecular dynamics data and found to be 12% larger than the equilibrium moment-of-inertia product. The increase in $q_{30,\,rot}$ that results from using this value of $\langle I_A I_B I_C \rangle$ in Eq. (6) is 6%. This increase, however, is reflected as a decrease of only 0.4% in the rotational Gibbs free energy ($G_{rot} = -k_B T \ln q_{rot}$). Neglecting this part of the coupling appears, therefore, not to be a bad approximation.

A third approximation involves neglecting the effect of centrifugal distortion, which acts to increase the moments of inertia of a rotating cluster and thereby changes the rotational energy levels. To estimate the importance of this effect, the 30-atom cluster of Set 2 was re-equilibrated with a centrifugal force acting on each atom. The force was equivalent to

that expected if the rotational temperature of the cluster were 100°K. Inclusion of this force caused a change of only 0.2% in the moment of inertia product $I_A I_B I_C$, which is much smaller than the effect of the second type of vibration-rotation coupling discussed above. Centrifugal distortion is therefore not expected to have an important effect on the thermodynamic functions.

The above arguments suggest that the approximations involved in our calculation of thermodynamic functions for a microcrystal are dominated in importance by the neglect of anharmonic effects on the vibrational energy levels and not the effects of vibration-rotation coupling and centrifugal distortion. Qualitatively, the reasons for this are: (1) for clusters large enough to be important in determining the rate of nucleation, the moments of inertia are large and the probable rotational velocities small; and (2) for these same clusters, contributions of the rotational degrees of freedom to the thermodynamic functions are small relative to those from the vibrational degrees of freedom.

The preceding discussion has concerned the evaluation of the partition function for a single configuration of a cluster. We now consider the approximation involved in our use of such a "single-configuration" partition function to represent a cluster partition function. For clusters of all but the smallest size, we know that there is more than one stable configuration, each corresponding to a different local minimum in the clusters potential energy function. The partition function of the cluster contains large contributions from the regions of phase space in the neighborhood of each of these minima. If there are m_i stable configurations for a cluster of i-atoms, the vibrational partition function of the cluster can be written as

$$q_{i,\,vib} = \sum_{k=1}^{m_i} q_{i,\,vib}^{(k)} \qquad (14)$$

where $q_{i,\,vib}^{(k)}$ is a "single-configurational" partition function containing the contribution to $q_{i,\,vib}$ from the region of phase space in the neighborhood of the k^{th} potential minimum. By using only one configuration p, we make the approximation that $q_{i,\,vib} \cong q_{i,\,vib}^{(p)}$.

The importance of the "single-configuration" approximation in the calculation of cluster thermodynamic functions is difficult to estimate because of our lack of knowledge concerning the number and distribution of the single-configuration partition functions for a given sized cluster. An idea of its importance can, however, be obtained by noting in Figs. 2 and 3 the differences in entropy and free energy per atom between clusters of the same size but different configurations (the Set 1 and Set 2 clusters of size 13, 55, 79, and 87 have different configurations). Differences of up to about 2% in free energy and 8% in entropy are noted. These are large enough relative to the magnitude of the fine structure in the functions to suggest that much of this fine structure may be an artifact of the "single-configuration" approximation rather than physically significant characteristics of the multi-configurational functions. For this reason, we do not consider the detailed structure in vibrational entropy and free energy suggested by the six data points in Set 1 to have the physical significance suggested by Burton.[4] We believe that only gross features of the single-configurational functions as, for example, represented by the polynomial expression for $\Delta G^{o}(n;T)$, are significant.

In the plot of vibrational entropy per atom in Fig. 2, it is noted that the Set 2 values at a given temperature change very slowly for $n > 9$. This indicates that, for microcrystal clusters of all but very small size, changing the ratio of the "surface" of the cluster to its "volume" has a remarkably small effect on the vibrational entropy per atom of the cluster. The Set 1 data are generally consistent with this conclusion although the small number of data points makes the identification of the gross characteristics of the functions difficult. The effect of varying the "surface" to "volume" ratio on the vibrational free energy per atom is clearly important, however, as shown by the plots of Fig. 3. The characteristics of the entropy function indicate that these "size" effects in the free energy are primarily energetic rather than entropic.

The great importance of nonvibrational degrees of freedom in the cluster free energy is indicated by the plot of the total Gibbs free energy per atom in Fig. 4. A maximum is noted that occurs at decreasing values of n as the temperature is decreased. The shape of the curve is radically different from that of the vibrational free energy per atom, although the curves do approach each other a large n, where the nonvibrational degrees of freedom are relatively unimportant.

The Gibbs free energy of formation as a function of n plotted in Fig. 5 and 6 has the qualitative features expected from considerations based on the "liquid-drop" model. The value of n at which the maximum of the curve occurs decreases as the degree of supersaturation of the vapor is increased, i.e., as the temperature is decreased or the pressure increased. As pointed out by Long, [14] however,

calculations of ΔG based on the "liquid-drop" model are strictly valid only for the one cluster, known as the "nucleus", that can exist in phase equilibrium with the vapor, and the values of ΔG for other clusters can only be obtained from the model by methods which are not entirely thermodynamic in nature. This limitation does not apply to the values of ΔG reported here, because we have treated clusters as "molecules", not as droplets of the liquid phase. The complete ΔG vs n curves of Figs. 5 and 6 are therefore valid.

The rate of nucleation we calculate also behaves like that computed using the "liquid-drop" model: it increases from very small to very large values over a narrow range of supersaturation. This increase is shown by the plot of the rate as a function of pressure in Fig. (9). The critical supersaturation ratios $S_c = P_c/P_e$, where P_e is the equilibrium vapor pressure,[15] were found to increase very rapidly as the temperature was decreased (see Table IV). This behavior is attributed mainly to the decreasing collision frequency within the vapor that accompanies the decreasing temperature. The collision frequency is so low at 10°K that the rate of nucleation reaches only 3.6×10^{-5} clusters/($cm^3 \cdot sec$) "at a pressure where" n* becomes 2.

Values for cluster thermodynamic functions reported in this paper are expected to approximate closely those for real clusters only at low temperatures where the microcrystal model is realistic and the approximations involved in the evaluation of the functions are good. Even at temperatures above the "melting" point of clusters, however, the calculations can be of use in a "first approximation" in much the same way that cell theory has been used in studying the liquid state.

More generally, calculations of the type reported here are the first step in the development of understanding of clusters on an atomic or molecular level. An approach on this level is necessary, we believe, in order to avoid problems such as the "translation-rotation" paradox[16] that have resulted from uncertainties concerning the exact nature of droplets used in the "liquid-drop" model.

FUTURE WORK

Work is nearly completed on the development of a much more realistic model for argon atom clusters. Molecular dynamics calculations have been performed for a number of different sized clusters at temperatures up to about 75°K, and the data are being analyzed to obtain values for cluster thermodynamic functions. Results from this work will be published soon.

ACKNOWLEDGEMENTS

The author wishes to express his thanks to Professor G. Wilse Robinson for his advice and support during the course of this work, to Dr. P. L. Fehder for help with the molecular dynamics calculations, and to Dr. R. P. Futrelle for many illuminating discussions.

REFERENCES

1. L. Farkas, Z. Physik. Chem. (Leipzig) A125, 236 (1927).
2. J. L. Katz, J. Chem. Phys. 52, 4733 (1970).
3. J. O. Hirschfelder, C. F. Curtiss, and R. B. Bird, Molecular Theory of Gases and Liquids (John Wiley & Sons, Inc., New York, N. Y., 1954), p. 1110.
4. J. J. Burton, J. Chem. Phys. 52, 345 (1970).
5. G. Herzberg, Molecular Spectra and Molecular Structure (D. Van Nostrand Co., Inc., Princeton, N.J., 1945), Vol. II.
6. J. Ortega, Mathematical Methods for Digital Computers, A. Ralston and H.S. Wilf, Eds. (John Wiley & Sons, Inc., New York, N. Y., 1967), Vol. II, Chap. 4.
7. A. Rahman, Phys. Rev. 136, A405 (1964); P. L. Fehder, J. Chem. Phys. 50, 2617 (1969).
8. L. Verlet, Phys. Rev. 159, 98 (1967).
9. G. C. Benson and R. Shuttleworth, J. Chem. Phys. 19, 130 (1951).
10. J. Lothe and G. M. Pound, Nucleation, A.C. Zettlemoyer, Ed. (Dekker, New York, 1969), p. 118.
11. W. J. Dunning, ibid., p. 9.
12. N. Davidson, Statistical Mechanics (McGraw-Hill Book Co., Inc., New York, New York, 1962), Chap. 10.
13. A much more detailed discussion of these dynamics calculations will be presented in another paper.
14. A. B. Long, Rev. Geophys. 7, 595 (1969).

15. R. E. Honig and H. O. Hook, RCA Review 21, 360 (1960).

16. H. Reiss, J. L. Katz, and R. E. Cohen, J. Chem. Phys. 48, 5553 (1968); J. Lothe and G. M. Pound, ibid. 48, 1849 (1968); and references cited therein.

TABLE I. Equilibrium potential energy and standard Gibbs free energy of formation for Set 1 clusters.

n	V_n/n ($\times 10^{14}$erg)	ΔG^0 ($\times 10^{14}$ erg)			
		10.2 °K	30.0 °K	50.3 °K	70.1 °K
13	-5.6390	-52.94	-23.26	7.822	37.75
19	-6.0014	-82.00	-35.71	12.74	59.34
43	-7.4279	-239.2	-127.0	-9.166	104.1
55	-8.3967	-354.1	-205.5	-49.08	101.6
79	-8.7887	-534.6	-316.1	-85.45	136.7
87	-8.7188	-584.0	-345.5	-93.88	148.4

TABLE II. Equilibrium (0°K) potential energy and standard Gibbs free energy of formation for Set 2 clusters.

n	V_n/n ($\times 10^{14}$ erg)	ΔG^0 ($\times 10^{14}$ erg^{-1})			
		10.2 °K	30.0 °K	50.3 °K	70.1 °K
2	-0.8269	-1.043	0.179	1.575	2.993
3	-1.6538	-3.168	-0.025	3.425	6.847
4	-2.4807	-6.381	-0.615	5.539	11.54
5	-3.0112	-9.943	-1.920	6.565	14.79
6	-3.5039	-14.01	-3.236	8.121	19.10
7	-3.8995	-18.49	-5.101	8.965	22.54
8	-4.0860	-22.27	-6.610	9.810	25.64
9	-4.2192	-26.29	-8.976	9.152	26.60
10	-4.4967	-31.24	-10.94	10.30	30.74
11	-4.6727	-35.86	-12.98	10.94	33.96
12	-4.9104	-41.44	-15.80	11.00	36.78
13	-5.2759	-49.05	-20.54	9.264	37.93
15	-5.6091	-60.35	-25.92	10.14	44.84
16	-5.6671	-65.03	-27.96	10.86	48.20
17	-5.7889	-70.75	-30.83	10.97	51.18
18	-5.8996	-76.42	-33.46	11.52	54.79
19	-6.0014	-82.00	-35.71	12.74	59.34
20	-6.0813	-88.02	-39.72	10.86	59.50
21	-6.1212	-93.26	-42.67	10.29	61.21
22	-6.2563	-99.99	-46.01	10.52	64.88
23	-6.2848	-105.3	-49.24	9.483	65.94
24	-6.3773	-111.9	-53.22	8.245	67.33

TABLE II. (continued)

n	V_n/n ($\times 10^{14}$ erg)	ΔG^0 ($\times 10^{14}$ erg^{-1})			
		10,2 °K	30.0 °K	50.3 °K	70.1 °K
25	-6.5123	-119.3	-57.51	7.301	69.62
26	-6.6350	-126.7	-61.65	6.586	72.21
27	-6.6492	-132.0	-64.77	5.797	73.66
28	-6.7158	-138.6	-68.70	4.656	75.19
29	-6.8251	-146.2	-73.21	3.423	77.13
30	-6.9219	-153.7	-77.69	2.157	78.96
35	-7.2120	-188.3	-98.22	-3.634	87.35
40	-7.5675	-227.7	-123.0	-13.07	92.80
45	-7.7266	-262.2	-143.3	-18.16	102.2
50	-7.9360	-300.7	-167.5	-27.36	107.5
55	-8.1093	-339.2	-191.6	-36.21	113.4
60	-8.2813	-379.2	-217.1	-46.25	118.2
79	-8.6953	-528.6	-312.2	-83.82	136.1
80	-8.7230	-537.3	-317.9	-86.33	136.7
87	-8.9203	-599.7	-359.5	-105.8	138.6
100	-9.0877	-704.3	-426.7	-133.3	149.4

TABLE III. Coefficients in the polynomial expression for the Gibbs free energy of formation $\Delta G^{0}(n, T) = \sum_{j=1}^{5} C_j(T) n^{(j-1)}$.

T (°K)	$C_1(T)$ (10^{-14} erg)	$C_2(T)$ (10^{-14} erg)	$C_3(T)$ (10^{-16} erg)	$C_4(T)$ (10^{-18} erg)	$C_5(T)$ (10^{-20} erg)
10.2	7.682	-3.119	-10.02	9.605	-3.597
30.0	3.379	-0.7034	- 8.777	8.173	-3.002
50.3	-0.9043	1.789	- 7.322	6.524	-2.322
70.1	-4.896	4.172	- 5.875	4.894	-1.652

TABLE IV. Data for vapor whose level of supersaturation is "critical." [a]

T (°K)	P_c [b] (atm)	S_c [c]	n_c^* [d]	$\Delta G^{\dagger}(n_c^*)$ [e] (10^{-14} erg/cluster)
10.2 [f]				
30.0	3.9×10^{-4}	5.8×10^{5}	19	22
50.3	1.3×10^{-1}	3.3×10^{2}	37	44
70.1	2.5	3.3×10^{1}	70	66

[a] Defined as supersaturation at which the rate of homogeneous nucleation is 1 cluster/($cm^3 \cdot sec$).

[b] Pressure of vapor whose supersaturation is critical.

[c] "Critical" supersaturation ratio, P_c/P_e, where P_e is the equilibrium vapor pressure.

[d] Size of cluster with highest Gibbs free energy of formation and lowest "equilibrium" concentration.

[e] Gibbs free energy of formation for cluster of size n*.

[f] Rate of nucleation remains less than 1 cluster/($cm^3 \cdot sec$) for all $n^* \geq 2$.

TABLE V. Comparison of the average potential energy of a 30-atom "classical" non-rotating cluster calculated using the harmonic approximation and using an "exact" potential. Energy here is measured relative to that of the equilibrium cluster at 0 °K.

T(°K)	$\langle V \rangle_{harmonic}$ (10^{-14} erg)	$\langle V \rangle_{exact}$ (10^{-14} erg)	$\langle V \rangle_{exact} - \langle V \rangle_{harmonic}$ (10^{-14} erg)
30	17.4	18.2	0.8
37	21.4	29.8	8.4
50	29.0	53.9	24.9

C. Paper No. 2

THE SINGLE-CONFIGURATION APPROXIMATION IN THE CALCULATION OF THE THERMODYNAMIC PROPERTIES OF MICROCRYSTALLINE CLUSTERS*

DAVID J. McGINTY†

Arthur Amos Noyes Laboratory of Chemical Physics‡
California Institute of Technology
Pasadena, California 91109

ABSTRACT

The single-configuration approximation that has been used in previous calculations of the thermodynamic properties of microcrystalline clusters can lead to quite significant errors in calculated values of the thermodynamic functions. The origin of the errors and methods by which they can be minimized are discussed in this note.

---

* This work was supported in part by a grant (No. GP-12381) from the National Science Foundation.

† Woodrow Wilson Fellow, 1967-1968; NSF Predoctoral Fellow, 1969-1971.

‡ Contribution No. 4395.

I. INTRODUCTION

Recently considerable work has been done using the "microcrystal" model to study the thermodynamic properties of small clusters of atoms [1-5]. These clusters are thought to exist in significant concentrations in supersaturated vapors and to play an important role in the process of homogeneous nucleation from the vapor phase. The thermodynamic properties of the clusters are used to evaluate their equilibrium concentrations in the vapor and these concentrations are used in the "classical" theory to calculate the rate of nucleation [6].

In the model calculations the Hamiltonian of the cluster is assumed separable,

$$H = H_{vib} + H_{rot} + H_{tr}, \tag{1}$$

enabling the cluster partition function q to be written as a product,

$$q = q_{vib} q_{rot} q_{tr}. \tag{2}$$

The individual terms in the product are evaluated from standard statistical mechanical formulas using the harmonic approximation to evaluate q_{vib}, the rigid-rotator approximation to evaluate q_{rot}, and the perfect-gas approximation to evaluate q_{tr}.

In previous work with the microcrystal model, calculation of thermodynamic properties has been based on a single stable configuration of the cluster. In general, however, many stable configurations exist and the actual thermodynamic properties are

determined by all these configurations. Each stable configuration corresponds to a minimum in the potential energy function of the cluster. The cluster partition function contains large contributions from the regions of phase space in the neighborhood of each of these minima. Contributions from other regions are very small because the potential energy is large away from the minima. The partition function for a microcrystal with m stable configurations can therefore be written as a sum of m single-configuration partition functions, each containing the contribution from the region of phase space surrounding one of the minima,

$$q = \sum_{k=1}^{m} q^{(k)}. \tag{3}$$

The "single-configuration" approximation that has been used in previous calculations approximates q by one of the single-configuration partition functions $q^{(p)}$,

$$q \cong q^{(p)}, \tag{4}$$

and ignores the other (m - 1) terms in the sum. The approximate value is always smaller than the exact one since all the $q^{(k)}$'s are positive.

In order to determine the importance of this approximation, we have evaluated multiconfiguration thermodynamic functions for a number of clusters using the Lennard-Jones pair potential[7] to represent the interaction between argon atoms. The functions were

obtained by combining according to Eq. 3 single-configuration functions that were computed by previously described methods.[2] The multiconfiguration functions obtained in this way are not exact since many configurations are left out, but they are better approximations than any of the single-configuration functions.

II. RESULTS

In Fig. 1 we have plotted the Gibbs free energy of formation [8] of argon clusters from monomers at 50°K and 1 atm. as a function of cluster size. It is this function that is generally used to compute cluster concentrations in the classical theory of nucleation. All degrees of freedom are explicitly included in the computation. Multiconfiguration values of the function are connected by solid lines; the vertical bars indicate the range of our single-configuration values.

The following types of configurations were included in the calculation:

(1) "Spherical-ccp" configurations of 13, 19, 43, 55, 79, and 87 atoms and "spherical-hcp" configurations of 13, 19, and 87 atoms. These were formed by filling successive neighbor shells in a cubic-close packed (ccp) and a hexagonal-close-packed (hcp) lattice.

(2) "Grown" configurations created by an aufbau process designed to produce low energy configurations and described in reference 2.

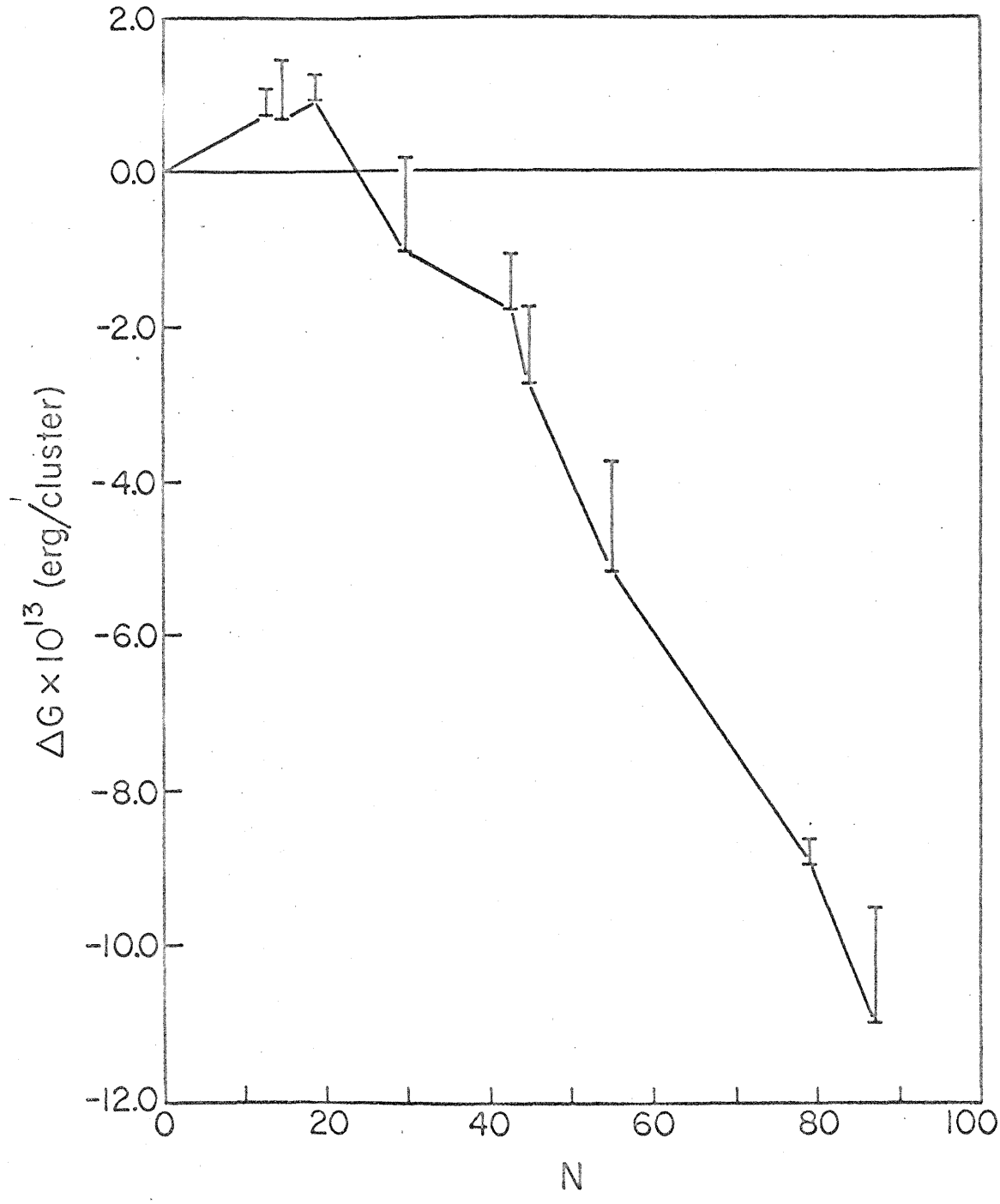

Figure 1. Gibbs free energy of formation at 50 °K and 1 atm. as a function of cluster size. The multiconfiguration values are connected by solid lines. The range of single-configuration values for each cluster is indicated by a vertical bar.

(3) "Dynamic" configurations of 15, 30, and 45 atoms formed by "relaxing" configurations that occur in molecular dynamics calculations with clusters [9].

Fig. 2 shows the temperature dependence of the difference, $[G^{(m)} - G]$, between the single-configuration Gibbs free energy (all degrees of freedom) and the multiconfiguration value. The difference is plotted for four configurations of the 19-atom cluster at 1 atm. pressure.

III. DISCUSSION

The plot in Fig. 1 indicates that the spread in single-configuration values of the free energy of formation is quite large. This spread is particularly important for the clusters in the region of the maximum of the curve since these clusters have the lowest concentrations and are most important in determining the rate of nucleation. An uncertainty of 50 to 100% exists in the single-configuration values of ΔG in this region; this translates into an uncertainty of several hundred percent in the concentrations of the clusters and in the rate of nucleation. The magnitude of this error indicates that caution must be exercised in the interpretation of results obtained using the single-configuration approximation. For example, the curve in Fig. 1 connecting multiconfiguration values suggest that ΔG is not a smooth function of N. Burton has noted the fine structure in this [1] and other thermodynamic functions [10] for clusters and has suggested that the structure has important physical significance. Our results show, however, that

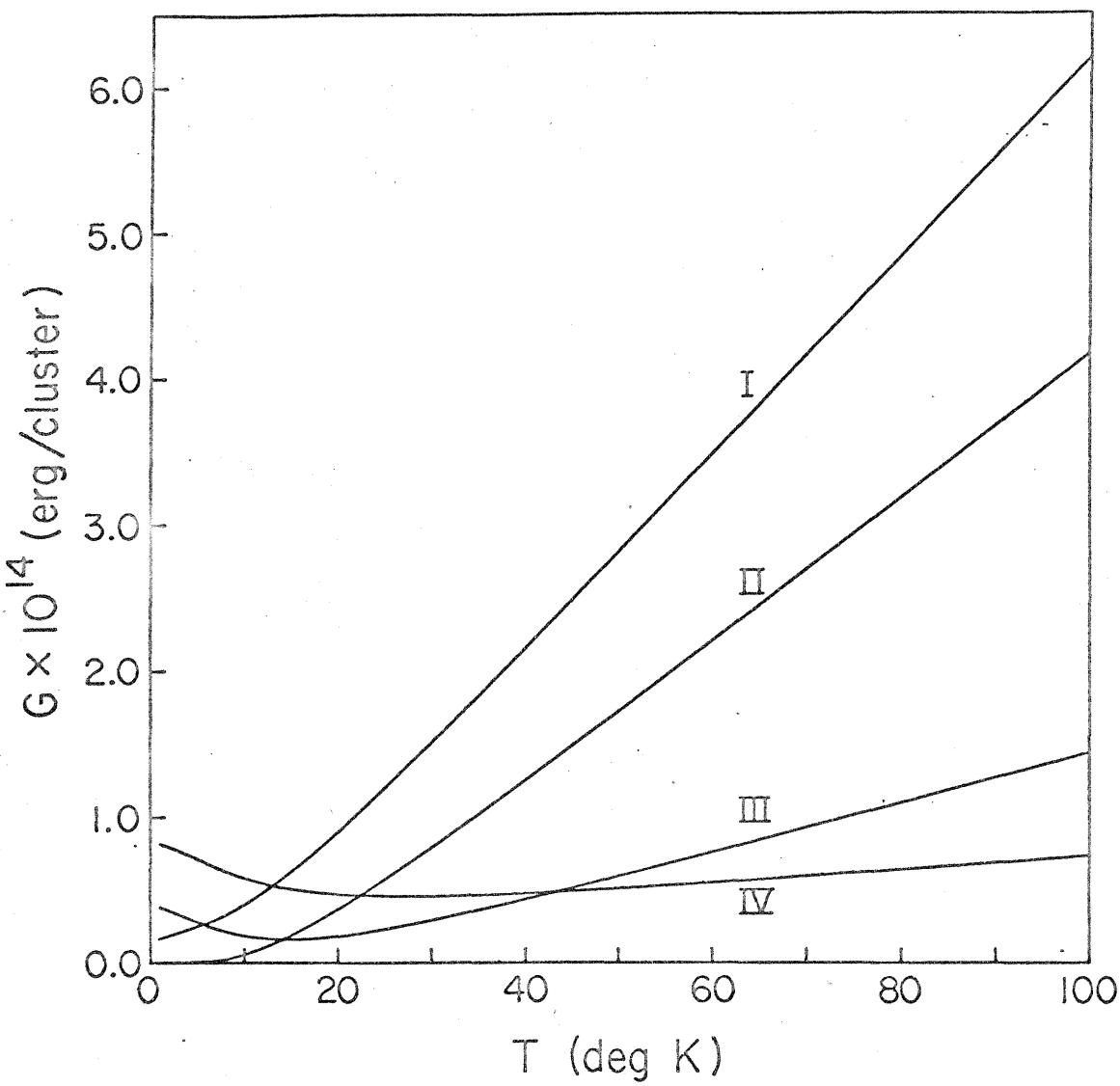

Figure 2. Temperature dependence of the difference $[G^{(m)} - G]$ at 1 atm. for four configurations of a cluster of 19 argon atoms. $G^{(m)}$ is a single-configuration free energy and G is the multi-configuration value.

the error in the single-configuration free energy has about the same magnitude as the fine structure of the function, indicating that the structure may not be a feature of the physically significant multiconfiguration function. In agreement with our earlier conclusion [2] and that of Abraham and Dave [3], we believe that the error is too large to support Burton's interpretation and that only the gross features of the single-configuration functions are physically significant.

It is interesting to note in Fig. 1 that even though most of the single-configuration free energies differ significantly from the multiconfiguration value, the free energy of the most stable (lowest in free energy) configuration does not. The free energy is dominated by the largest terms in Eq. 3, which correspond to the most stable configurations. As an example of this behavior, consider the two most stable configurations we have found for the 45-atom cluster at 50°K and the two-configuration Gibbs free energy computed from them. This free energy can be written,

$$G(T, P) = G_{tr}(T,P) - kT\ell n[q_{vib}^{(1)}q_{rot}^{(1)}] - kT\ell n\left[1 + \frac{q_{vib}^{(2)}q_{rot}^{(2)}}{q_{vib}^{(1)}q_{rot}^{(1)}}\right], \qquad (5)$$

where the translational contribution has been factored out since it is the same for all configurations. From the values $q_{vib}^{(1)}q_{rot}^{(1)} = 182 \times 10^{235}$ and $q_{vib}^{(2)}q_{rot}^{(2)} = 1.98 \times 10^{235}$, it is determined that the contribution of the more stable configuration to G(T, P) is larger than that of the second configuration by a factor of 5×10^4. It is

interesting to note also that if there were n configurations with the same stability as configuration (1), the free energy would be,

$$G(T, P) = G_{tr}(T, P) - kT\ell n[q_{vib}^{(1)} q_{rot}^{(1)}] - kT\ell n(n), \qquad (6)$$

and unless n is very large indeed, the last term is ignorable. For example, for $n = 10^{12}$ and the value of $q_{vib}^{(1)} q_{rot}^{(1)}$ quoted above, the magnitude of that term is only about 1% the magnitude of the second term. In conclusion, if the number of low-free-energy configurations is not too large, the single-configuration approximation should be very good, but only if it is based on one of the most stable configurations.

Neither the "spherical" nor the "grown" configurations that have been used in previous work with the microcrystal model yield good approximations to the multiconfiguration free energy for all clusters. At 50°K, "grown" configurations are more stable than the "spherical" ones for 19, 43, and 87-atom clusters, but "spherical" configurations are more stable for 13, 55, and 79-atom clusters. A better method of selecting configurations is clearly needed. One possible method is that of relaxing configurations that occur in molecular dynamics calculations. The method is expected to produce configurations with low free energy because these are the ones that occur with highest probability during the molecular dynamics calculations. "Dynamic" configurations were considered in this work for clusters of 15, 30, and 45 atoms; for

each of these clusters we find "dynamic" configurations that have lower free energy than any of the "grown" ones.

The temperature dependence of the single-configuration free energies for the 19-atom cluster in Fig. 2 suggests that no single configuration of the cluster is most stable at all temperatures. Configuration II ("spherical-hcp") is most stable from 0 to 15°K, III ("grown") from 15 to 43°K, and IV (also "grown") from 43 to 100°K. Configuration I is "spherical-ccp." The crossings of the single-configuration curves is due to the competition between energy (or enthalpy) and entropy for dominance in the free energy function, $G = H - TS$. At low temperature, low energy configurations tend to be most stable; and at higher temperatures, high entropy configurations tend to be most stable. In accord with these tendencies, we note that for the 19-atom cluster the single-configuration free energies at low temperature are ranked according to the equilibrium potential energies,

$$V^{II} < V^{I} < V^{III} < V^{IV}$$

and at high temperature their ranking is determined by that of the entropies,

$$S^{IV} > S^{III} > S^{II} > S^{I}.$$

It is evident that, in general, a satisfactory evaluation of the microcrystal model over a range of temperatures cannot be based on a single configuration of the cluster.

IV. CONCLUSIONS

The error in cluster free energies due to the single-configuration approximation is too large to be ignored. Future calculations with the microcrystal model should be based on a number of configurations for each cluster; and at each temperature considered, one of these should be close to the absolute minimum in free energy for the cluster. Work is needed to develop techniques for selecting these configurations; both low energy and high entropy ones must be considered. Relaxing configurations occurring in molecular dynamics calculations is one such technique that appears very promising. Estimates of the number of stable configurations as a function of cluster size and the distribution of the free energy among these configurations are also needed to determine how many configurations must be included to achieve a good approximation of the exact thermodynamic functions.

V. ACKNOWLEDGMENTS

The author gratefully acknowledges the advice and support of Professor G. Wilse Robinson and helpful discussions with Dr. R. P. Futrelle.

REFERENCES

[1] J. J. Burton, J. Chem. Phys. 52 (1970) 345 and Surface Sci. 26 (1971) 1.

[2] David J. McGinty, J. Chem. Phys. 55 (1971) 580.

[3] F. F. Abraham and J. V. Dave, J. Chem. Phys. 55 (1971) 1587 and J. Chem. Phys. 55 (1971) 4817.

[4] K. Nishioka, R. Shawyer, A. Bienenstock, and G. M. Pound, J. Chem. Phys. 55 (1971) 5082.

[5] M. R. Hoare and P. Pal, Nature Phys. Sci. 230 (1971) 250.

[6] J. Lothe and G. M. Pound, Nucleation, A. C. Zettlemoyer, Ed. (Dekker, New York, 1969), Chap. 3.

[7] The Lennard-Jones pair potential is $V(r) = 4\epsilon[(\frac{\sigma}{r})^{12} - (\frac{\sigma}{r})^{6}]$. The values of the parameters σ and ϵ for argon, $\sigma = 3.4050$ Å and $\epsilon/k_B = 119.8$ K, are from J. O. Hirschfelder, C. F. Curtiss, and R. B. Bird, Molecular Theory of Gases and Liquids (Wiley, New York, 1954), p. 1110.

[8] For a precise definition of the Gibbs free energy of a cluster and details on its calculation for a single configuration see reference 2.

[9] Details of the molecular dynamics calculations with clusters will be presented in another paper. For information about the technique as applied to the study of liquids see the following: A. Rahman, Phys. Rev. 136 (1964) 405A; L. Verlet, Phys. Rev. 159 (1967) 98.

[10] J. J. Burton, Chem. Phys. Letters 3 (1969) 594; 7 (1970) 567.

PART III: MOLECULAR DYNAMICS CALCULATIONS OF THE PROPERTIES OF CLUSTERS

A. Introductory Remarks

In this section we describe the use of molecular dynamics computer simulation calculations for the determination of the properties of clusters of argon atoms. The molecular dynamics technique has been extensively applied to the study of the fluid state in the past decade, and remarkable agreement with the experimentally determined equilibrium properties of argon has been obtained. The work reported in Paper III represents the first application of the technique to the study of clusters.

In that paper, which has not yet been submitted for publication, the computer-generated data are used to evaluate the cluster thermodynamic functions at temperatures where the clusters are fluid-like and the microcrystal model is not valid. The data were also used to determine some of the more general characteristics of the clusters with the hope of inspiring more realistic models that can be used for purely theoretical calculations of the cluster thermodynamic properties. The temperature dependence of the coefficient of self-diffusion was examined to characterize the motion of atoms in the clusters; the radial variation in density was examined to understand the average "size" of the clusters; and the radial variation of the potential energy was examined to characterize the environment inside the clusters.

Considerable effort was devoted to understanding the statistical error in the temperature and other averages calculated from the raw trajectory data. An expression for the error in temperature was derived in terms of the kinetic-energy autocorrelation function. The second paper in this section is actually a spin-off from our work with the error expression. In that paper [Chem. Phys. Letters 12, 285 (1971)] we

show that the kinetic-energy autocorrelation function and other correlation functions can be computed from molecular dynamics data very rapidly using a method based on the Fast Fourier Transform.

B. Paper No. 3

Molecular Dynamics Studies of the Properties of Small Clusters of Argon Atoms

DAVID J. McGINTY

Arthur Amos Noyes Laboratory of Chemical Physics, California Institute of Technology, Pasadena, California 91109

ABSTRACT

Molecular dynamics calculations have been performed on clusters of 15, 30, 45, 60, 80, and 100 argon atoms at temperatures of up to 70°K. Values of the independent-cluster thermodynamic functions are presented and compared with those obtained from the micro-crystal model. The comparison indicates surprising agreement for values of the Gibbs free energy of formation. The transition from solid-like to fluid-like diffusion in the clusters occurs gradually; no semblance of a phase transition is noted. The radial density functions for the clusters have maxima and minima reminiscent of those in the radial distribution function for bulk liquids. The temperature dependence of that function indicates that clusters expand quite rapidly as the temperature is increased. The radial distribution of potential energy indicates that there is no region inside the clusters where the environment resembles that in the bulk phases; the properties of the clusters are dominated by the "surface region" where nearly all the atoms exist.

I. INTRODUCTION

There has been considerable interest in the calculation of the thermodynamic properties of small clusters of molecules due primarily to the importance of these clusters in the phenomenon of vapor phase homogeneous nucleation. Much of the work has been with the classical, liquid-drop model[1] in which clusters are treated as small droplets and their properties calculated using the Gibbs surface theory. This approach is not generally regarded as valid, however, because the application of the surface theory to the small droplets important in nucleation is not consistent with assumptions on which that theory is based.

Recently, the availability of large computers has made it possible for investigators to attack the problem on the molecular level and actually to evaluate partition functions for model clusters. In the "microcrystal" model, which has been most extensively used, the clusters are treated as very small crystallites. The partition function for a microcrystal is evaluated in the same way one would evaluate that for a polyatomic molecule in the simplest approximation. The cluster Hamiltonian is assumed separable,

$$H = H_{vib} + H_{rot} + H_{tr} \tag{1}$$

enabling the cluster partition function to be written as a product,

$$q = q_{vib} q_{rot} q_{tr}. \tag{2}$$

The individual terms in the product are evaluated from standard statistical mechanical formulas using the harmonic approximation to evaluate q_{vib}, the rigid-rotator approximation to evaluate q_{rot}, and the perfect-gas approximation to evaluate q_{tr}. The exact microcrystal partition function contains contributions from all stable configurations of a cluster,[4] although most investigators have used the "single-configuration" approximation, ignoring all but one configuration for each cluster. A more approximate, Einstein technique[5] has also been used to evaluate the vibrational partition function and has enabled the study of quite large clusters.

Cluster partition functions evaluated from the microcrystal model using the harmonic approximation are exact in the low temperature limit where anharmonicities in the potential energy function are negligible. At higher temperatures, the anharmonicities become significant. Eventually, when fluid motion becomes important, the model itself becomes unrealistic. In order to study the "fluid-like" clusters in this higher temperature region, we have used molecular dynamics computer simulation calculations.[6,7] The data from these calculations have been analyzed to obtain the thermodynamic functions for clusters of up to 100 argon atoms at temperatures below 75°K.

In addition to this thermodynamic data, the molecular dynamics calculations yield very detailed information about the structure and dynamics of the clusters. We feel that this type of information about the general characteristics of clusters should be very useful in the development of new, realistic models that can be used in purely

theoretical calculations of cluster thermodynamic properties. In the present paper we shall describe the molecular dynamic calculations and discuss cluster properties that have been determined from our data.

A. The Kinetic Problem

The goal of nucleation theory is prediction of the "critical" supersaturation of a vapor, the supersaturation level at which the vapor condenses. In the calculation of this property, one treats the vapor as a gaseous mixture of clusters that interact according to the following set of reactions, which resemble those of a chemical polymerization:

$$\begin{aligned} A_1 + A_1 &\rightleftharpoons A_2 \\ A_2 + A_1 &\rightleftharpoons A_3 \\ &\vdots \\ A_m + A_1 &\rightleftharpoons A_{m+1} \end{aligned} \qquad (3)$$

where A_m represents an m-atom cluster. Reaction between "polymers" are generally ignored because collisions between them are relatively infrequent. The set of coupled differential rate equations for the set of reactions can in principle be solved to yield the time dependence of the cluster concentrations. Two sets of data are needed for the solution: (1) the rate constants for the reactions, and (2) the cluster concentrations in the initial, metastable state that corresponds to the supersaturated vapor. The rate constants for the forward reactions in Eq. 3 are estimated by assigning an approximate hard-sphere radius to each cluster and assuming that every polymer-monomer collision leads to reaction (accomodation coefficient of

unity). The principle of detailed balance along with the cluster concentrations in the metastable state are then used to determine the reverse rate constants.[8] The cluster concentrations are thus of key importance to solution of the rate equations.

The actual solution of these equations can be accomplished by numerical integration with a computer or by various approximate analytical methods. In this paper we shall be concerned only with the equilibrium problem of computing the cluster concentrations in the metastable state, which has been the object of most of the recent effort in nucleation theory. The rigorous basis for this computation will now be considered.

II. THEORY

A. Decomposition of the Partition Function

The basis for our thinking of a supersaturated vapor in terms of a gaseous mixture of clusters is a transformation of the canonical ensemble partition function for the vapor. Considering a vapor of N atoms in a volume V we focus our attention on a single configuration of the system, corresponding to a single point in the 3N-dimensional configuration space spanned by the position coordinates of the system. If we now regard pairs of atoms separated by less than some distance R_o, which is of the order of the range of interatomic forces ($\sim 3\sigma$ for the Lennard-Jones potential), as "interacting pairs" and imagine them connected by bonds, then the configuration will appear divided into clusters of atoms that are bonded together. The partitioning of atoms into clusters is illustrated for a sample configuration in Fig. 1. It is, of course, possible to use other definitions of a cluster, and any definition is acceptable as long as it enables a unique division of each configuration of the system into clusters.

Each possible distribution of atoms among clusters is described by a value of the N-dimensional vector,

$$\underset{\sim}{n} = (n_1, n_2, \cdots, n_N), \tag{4}$$

where n_i is an integer that denotes the number of i-atom clusters in the distribution. The allowed values of $\underset{\sim}{n}$ are consistent with the constraint equation

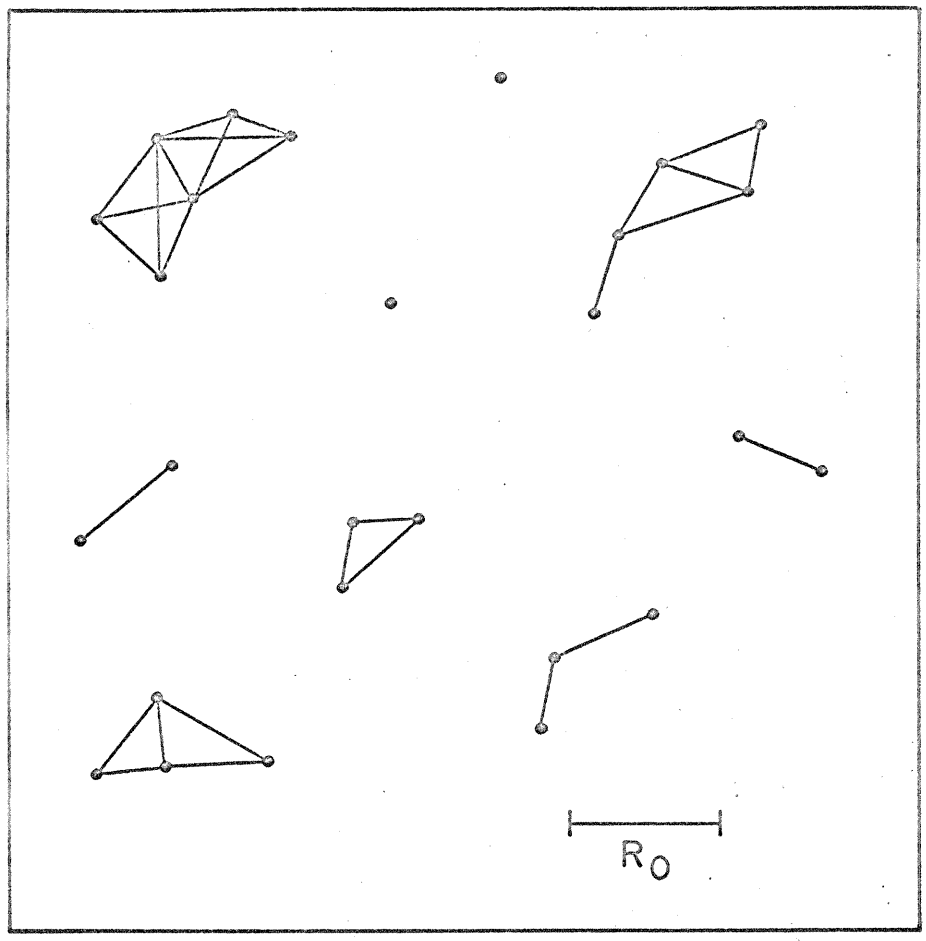

Fig. 1. The partitioning of atoms in a configuration into clusters. Each point represents the center of an atom and the bonds connect "interacting pairs."

$$\sum_{i=1}^{N} i n_i = N. \tag{5}$$

The partition function for the system of N atoms is

$$Q = \frac{1}{N!}\left(\frac{2\pi mkT}{h^2}\right)^{3N/2} \int_V \exp[-U(\underset{\sim}{r}_1, \cdots, \underset{\sim}{r}_N)/kT]\, d\underset{\sim}{r}_1 \cdots d\underset{\sim}{r}_N, \tag{6}$$

where U is the potential energy. Every configuration of the system and, hence, every point in the region of configuration space available to the system can be assigned a unique value of $\underset{\sim}{n}$. It is, therefore, possible to transform the configuration integral in Eq. (6) into a sum of integrals, each over the region of configuration space that corresponds to a specific value of $\underset{\sim}{n}$. Q then becomes a sum of "single-distribution partition functions":

$$Q = \sum_{\{\underset{\sim}{n}\}} Q_{\underset{\sim}{n}}, \tag{7}$$

where

$$Q_{\underset{\sim}{n}} = \frac{1}{N!}\left(\frac{2\pi mkT}{h^2}\right)^{3N/2} \int_{\underset{\sim}{n}} \exp[-U(\underset{\sim}{r}_1, \cdots, \underset{\sim}{r}_N)/kT]\, d\underset{\sim}{r}_1 \cdots d\underset{\sim}{r}_N \tag{8}$$

and $\{\underset{\sim}{n}\}$ is the set of all values of $\underset{\sim}{n}$ consistent with the constraint of Eq. (5). The integral covers all configurations in the distribution $\underset{\sim}{n}$.

B. The Independent-Cluster Approximation

The "independent-cluster" approximation enables us to simplify the single-distribution partition function in Eq. (8). The approximation has two parts:[9]

(1) The interactions between atoms in different clusters are ignored.

(2) "Cluster interference" is ignored. In $Q_{\underset{\sim}{n}}$ configurations in which clusters overlap are excluded because they are not consistent with the specific distribution $\underset{\sim}{n}$; in the approximate evaluation of $Q_{\underset{\sim}{n}}$, these configurations are included.

The approximation leads to the following simple expression for $Q_{\underset{\sim}{n}}$;

$$Q_{\underset{\sim}{n}} = \prod_{i=1}^{N} [q_i^{n_i}/n_i!], \tag{9}$$

where q_i is an independent-cluster partition function,

$$q_i = \frac{V}{i!}\left(\frac{2\pi\, mkT}{h^2}\right)^{3i/2} \int_{C_i} \exp\left[-U(\underset{\sim}{r}_{ij})/kT\right] d\underset{\sim}{r}_{ij}, \tag{10}$$

and $\underset{\sim}{r}_{ij}$ represents the set of relative position coordinates for the i atoms and $d\underset{\sim}{r}_{ij}$ is the product of their differential elements. The term C_i indicates that the integration spans all relative positions of the atoms that are consistent with their being in the same cluster.

C. The Equilibrium Distribution of Clusters

To determine the equilibrium distribution that corresponds to the metastable, supersaturated vapor we maximize $Q_{\hat{n}}$, treated as a function of the n_i and subject to the following constraints:

1. $\hat{n}_N$ contains no macroscopic clusters.
2. $\sum_{i=1}^{N} i n_i = N$, and
3. the n_i are integers.

This last constraint is usually ignored, leading to a distribution that contains fractions of clusters and that is not, therefore, physically realizable.

An approximate method for computing the concentrations is based on the method of Lagrange undetermined multipliers in which the n_i are treated as continuous variables. That method yields the following expression, which is incorrectly taken as the final form in most treatments of nucleation theory:

$$n_i = n_1^i \, q_i / q_1^i, \quad i = 1, \cdots, N. \tag{11}$$

Our approximate solution for the n_i, in terms of n_1, is

$$n_i = \text{int}[\, n_1^i \, q_i / q_1^i \,], \quad i = 1, \cdots, N, \tag{12}$$

where the operator "int" extracts the largest integer value. The actual values of the n_i can be determined by an iterative process. An estimate of n_1 is used to evaluate the n_i and the value of the sum

$\sum_{i=1}^{N} in_i$ is computed. If the sum is larger than N, the estimate of n_1 is reduced; if it is smaller than N, the estimate is increased. The process is repeated until the value of the sum converged to N.

D. The Computational Problem

In this paper we are concerned with evaluating the independent-cluster partition functions q_i. Our results will be expressed in terms of the more common, thermodynamic functions derived from the q_i. The Gibbs free energy expression that is equivalent to Eq. (11) is

$$\Delta G_i(T, P, X_i, X_1) = \Delta G_i^{\dagger}(T, P) + kT \ell n(X_i/X_1^i) \tag{13}$$

where

$$\Delta G_i^{\dagger}(T, P) = \Delta G_i^{\circ}(T) + (1-i)kT \ell nP \tag{14}$$

and

$$\Delta G_i^{\circ}(T) = G_i^{\circ}(T) - iG_i^{\circ}(T). \tag{15}$$

At equilibrium ΔG_i in Eq. (13) is zero. The standard free energies G_i° and G_i° are

$$G_i^{\circ}(T) = -kT \ell n\{kT(\frac{2\pi imkT}{h^2})^{3/2} q_{vib} q_{rot}\}, \tag{16}$$

and

$$G_i^{\circ}(T) = -kT \ell n\{kT(\frac{2\pi mkT}{h^2})^{3/2}\} \tag{17}$$

In these expressions P is the total pressure of the vapor and X_i is the mole fraction of i-atom clusters. In our calculation we evaluate the function $\Delta G_i^{\dagger}$ for a range of cluster sizes; these can be used in Eq. (13) to determine the mole fraction X_i. These mole fractions should,

of course, be made consistent with the integer constraint on n_i by a device equivalent to that of Eq. (12).

III. THE MOLECULAR DYNAMICS CALCULATIONS

In the molecular dynamics calculations, the classical equations of motion for the atoms in a cluster are numerically integrated to yield a time record of the position and velocity coordinates of the atoms.[6,7] Our calculations were performed using single-precision arithmetic on IBM 360/75 and 370/155 computers.

Rotationless (zero angular momentum) clusters of Lennard-Jones 12-6 spheres were studied. The interactions of all pairs of atoms in a cluster were considered so that the potential energy of a cluster of N atoms is

$$V = \sum_{i=1}^{N} \sum_{j>i}^{N} 4\epsilon \left[\left(\frac{\sigma}{r_{ij}}\right)^{12} - \left(\frac{\sigma}{r_{ij}}\right)^{6} \right], \tag{18}$$

where r_{ij} is the distance between atoms i and j. We used values of the Lennard-Jones parameters that are specific for argon:[10] $\sigma = 3.4050$Å and $\epsilon/k = 119.8$°K. According to the principle of corresponding states,[11] however, the results can easily be applied to any other substance for which the Lennard-Jones potential is applicable. The numerical integration routine due to Verlet[7] with a time increment of 10^{-14} sec was used.

To perform the calculations it is necessary to adopt an operational definition of a cluster. In particular, one must be able to distinguish an N-atom cluster from (N-1) and (N+1)-atom clusters. The definition was accomplished with a spherical boundary centered

at the center of mass of the cluster and having radius R_N. A particle was regarded as having escaped from the cluster when it passed beyond this boundary. The value of R_N depended on N in such a way that the volume per atom within the boundary was the same for all clusters; R_N was therefore proportional to $N^{1/3}$. The value of the proportionality constant that determines the actual magnitudes of the R_N was chosen rather arbitrarily. The values of the R_N that we used are tabulated in Table I.

When an atom escaped, the calculation was interrupted and a procedure was executed to redirect the escaping atom back toward the cluster. The calculation was then restarted from the new state of the cluster. The reinitialization procedure involved modification of the velocities of the atoms only -- the configuration of the cluster was not changed. The procedure consisted of the following steps:

(1). The component of the escaping atom's velocity perpendicular to the spherical boundary was reversed.

(2). The velocities of all the atoms were scaled by a factor slightly larger than the unity to return the internal kinetic energy of the cluster, the kinetic energy in the center-of-mass coordinate system, to its value before the execution of Step 1. This compensates for the small amount of kinetic energy that is transferred from the internal

degrees of freedom to translational motion of the cluster when the escaping atom is reversed.

When the calculations are reinitialized in this way, the microscopic state of the cluster, defined by the center-of-mass coordinates of the atoms, was changed only slightly; and the kinetic and total energies and the angular momentum of the cluster were not changed at all. It is, therefore, reasonable to assume that the cluster is not driven into a "nonequilibrium" state by the reinitialization procedure.

The calculations yield a series of trajectory segments, each of which is terminated by the escape of an atom from the cluster. These data are exactly analogous to what would ideally be obtained from the actual observation of clusters in a real vapor since these clusters also change in size with time. Thermodynamic properties of clusters are obtained from averages over trajectory segments.

The choice of initial conditions for a calculation is arbitrary. It is desirable, however, that the initial configuration be close to that at equilibrium so that the cluster will not take long to reach equilibrium. In our calculations, 6000 time increments (6×10^{-11} sec.) were allowed for a cluster to equilibrate after its energy was modified. After a cluster was equilibrated, runs were made in which the coordinate data were saved for analysis. The lengths τ_N of these runs were proportional to $N^{-\frac{1}{2}}$, the relative magnitude of fluctuations in kinetic energy. The values of τ_N are tabulated in Table I.

IV. EVALUATION OF THE THERMODYNAMIC FUNCTIONS

The temperature of a cluster is computed from the time average internal kinetic energy and must be adjusted to account for the missing translational and rotational degrees of freedom,

$$T = \left(\frac{3N}{3N-6}\right) \frac{2}{3k} \left\langle \frac{1}{N} \sum_{i=1}^{N} \tfrac{1}{2} m v_i^2 \right\rangle, \tag{19}$$

where $\underline{v}_i$ is the velocity of the i^{th} atom and $\underline{m}$ is the mass of the atom.

In calculating the cluster thermodynamic properties, we assume the same separation of the cluster Hamiltonian as for the microcrystal model, Eq. (1), which enables us to compute the (quasi)-vibrational, rotational, and translational contributions to the free energy separately. The translational contribution is simply that determined in the perfect gas approximation. The rotational contribution is approximated using the time average of the rigid-rotator partition function,

$$q_{i,\,rot}(T) = \pi^{\frac{1}{2}} (8\pi^2 kT/h^2)^{3/2} \left\langle (I_A I_B I_C)^{\frac{1}{2}} \right\rangle, \tag{20}$$

where I_A, I_B and I_C are the time-dependent, principle-axis moments of inertia.

To calculate the vibrational contribution to the free energy of a cluster, we evaluate the vibrational energy and entropy and combine these to obtain the free energy. The thermodynamic energy is simply the internal total energy of the cluster, which is obtained from the

molecular dynamics calculations. The absolute entropy of a cluster was determined by extending the value of that function determined from the microcrystal model at 25°K, $S^{\circ}_{N}(25°K)$. The entropy at temperature T is

$$S_N(T) = S^{\circ}_N(25°K) + \int_{25°}^{T} \frac{C_N(T')}{T'} dT', \qquad (21)$$

where $C_N(T)$ is the heat capacity of the cluster determined from the molecular dynamics data.

As noted above the correct evaluation of the microcrystal model requires that all stable configurations of the cluster be included in the calculation. Such a calculation is not in general possible because of the extremely large number of stable configurations of a cluster. The best approximation that is feasible is based on a number of configurations that have low free energy at the temperature of interest.[4] Such a multiconfiguration approach was used in our calculation of the standard entropies $S^{\circ}_{N}(25°K)$. The number of configurations used for each cluster is indicated in Table 1.

V. RESULTS

A number of calculations were performed for each cluster. The total energies and temperatures that were obtained are shown in the plot of Fig. 2. Each point in the figure represents a calculation of length τ_N. The solid curves in Fig. 2 are quadratic polynomials obtained from least-square fits of the energy vs. temperature data. These polynomials were used in calculating the vibrational contributions to the cluster thermodynamic functions. The variation in the temperature of a cluster among runs with the same total energy is due to statistical error, which is discussed below.

Fluid motion inside the clusters can be characterized by the coefficient of self-diffusion $D_N(T)$. The coefficient was evaluated for the 2/3 of the atoms in a cluster that were closest to the center of mass at the beginning of a run. Contributions from surface atoms were thus excluded except where atoms initially in the interior of a cluster diffused to the surface during a run. The value of D_N was determined from the time-dependent mean-square-displacement function,

$$M(t) = \langle |\underset{\sim}{r}_k(t+t_o) - \underset{\sim}{r}_k(t)|^2 \rangle, \qquad (22)$$

where $\underset{\sim}{r}_k(t)$ is the position of the k^{th} atom in the center-of-mass coordinate system at time t. The average in Eq. (22) is over both atoms and values of t_o. In bulk fluids, M(t) becomes linear after an induction time τ_o of order 10^{-12} sec and the diffusion coefficient is related to the slope of the linear portion,[12]

$$D_N = \frac{1}{6} \, dM(t)/dt, \quad (t \gtrsim \tau_o). \qquad (22)$$

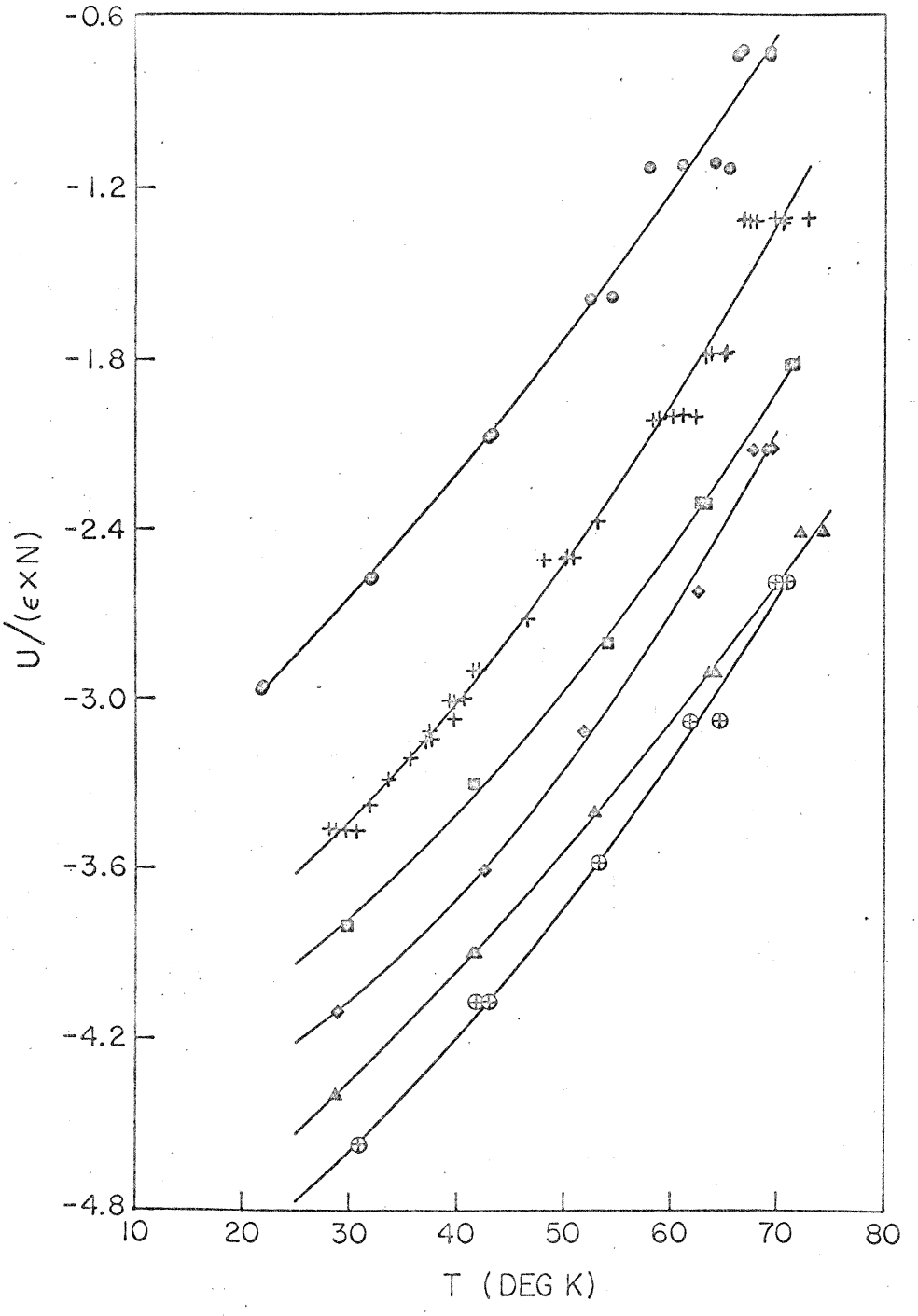

Fig. 2. The internal total energy per atom as a function of temperature. The solid lines are quadratic polynomial fits. Each point corresponds to a run of length τ_N: ●, 15-atom cluster; +, 30; ■, 45; ◆, 60; ▲, 80; ⊕, 100.

In a cluster an upper bound to the magnitude of M(t) is imposed by the finite size of the cluster and the slope of the function decreases to zero at long times. At intermediate times, however, the function is very nearly linear. We evaluated the diffusion coefficient from the slope in this region, using the interval from 3×10^{-12} to 10×10^{-12} sec for that purpose. Fig. 3 shows the temperature dependence of the diffusion coefficient for a 30-atom cluster. In the figure, $\log_{10} D_{30}$ is plotted as a function of 1/T. The line is a least-square fit of the data.

In Figs. 4 and 5 we have plotted the radial density function, the average number of atoms per unit volume at a given distance from the center of mass of the cluster. Each point in the plots represents the same amount of information. There are no points at small or large values of r because statistics are poor in these regions: the volume of the small radius region is small and the number of atoms in the large radius region is small. Fig. 5 shows the dependence of the function on cluster size at a temperature of ~70°K, and Fig. 4 shows the dependence of the density distribution of a 30-atom cluster on temperature. The horizontal lines in the figures indicate the density in the bulk phases. The upper line is the density of solid argon at 70°K and the lower one is the density of liquid argon at 84°K, the triple-point temperature.

The size of a cluster is not obviously defined by the radial distribution of its density. For the purpose of our later discussion of the thermal expansion of clusters, we shall regard the radius of a cluster as that of the spherical surface that contains, on the average, 90% of the cluster's mass. This radius is denoted $R_{90\%}$. Its value

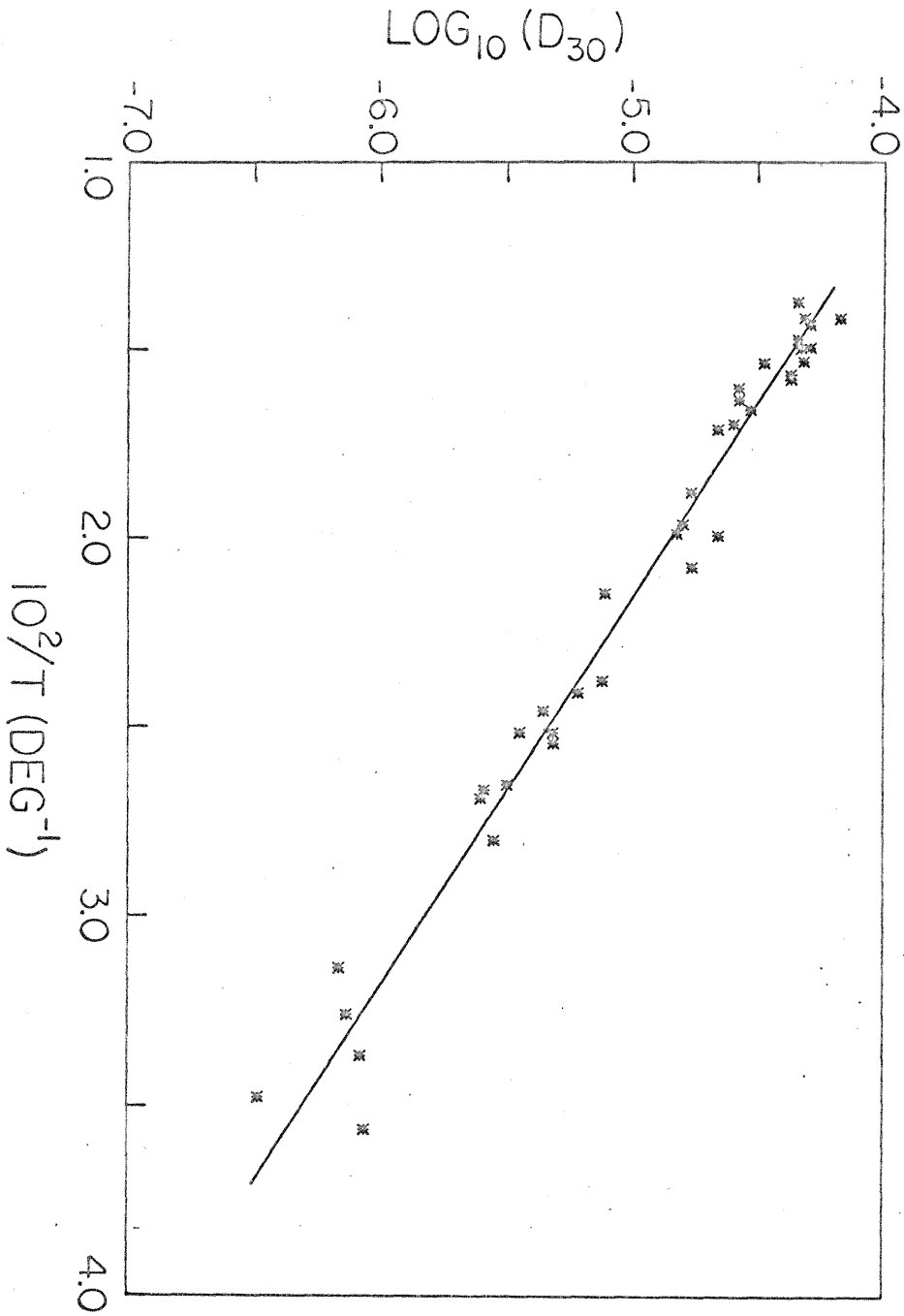

Fig. 3. The temperature dependence of the coefficient of self-diffusion for atoms inside a 30-atom cluster.

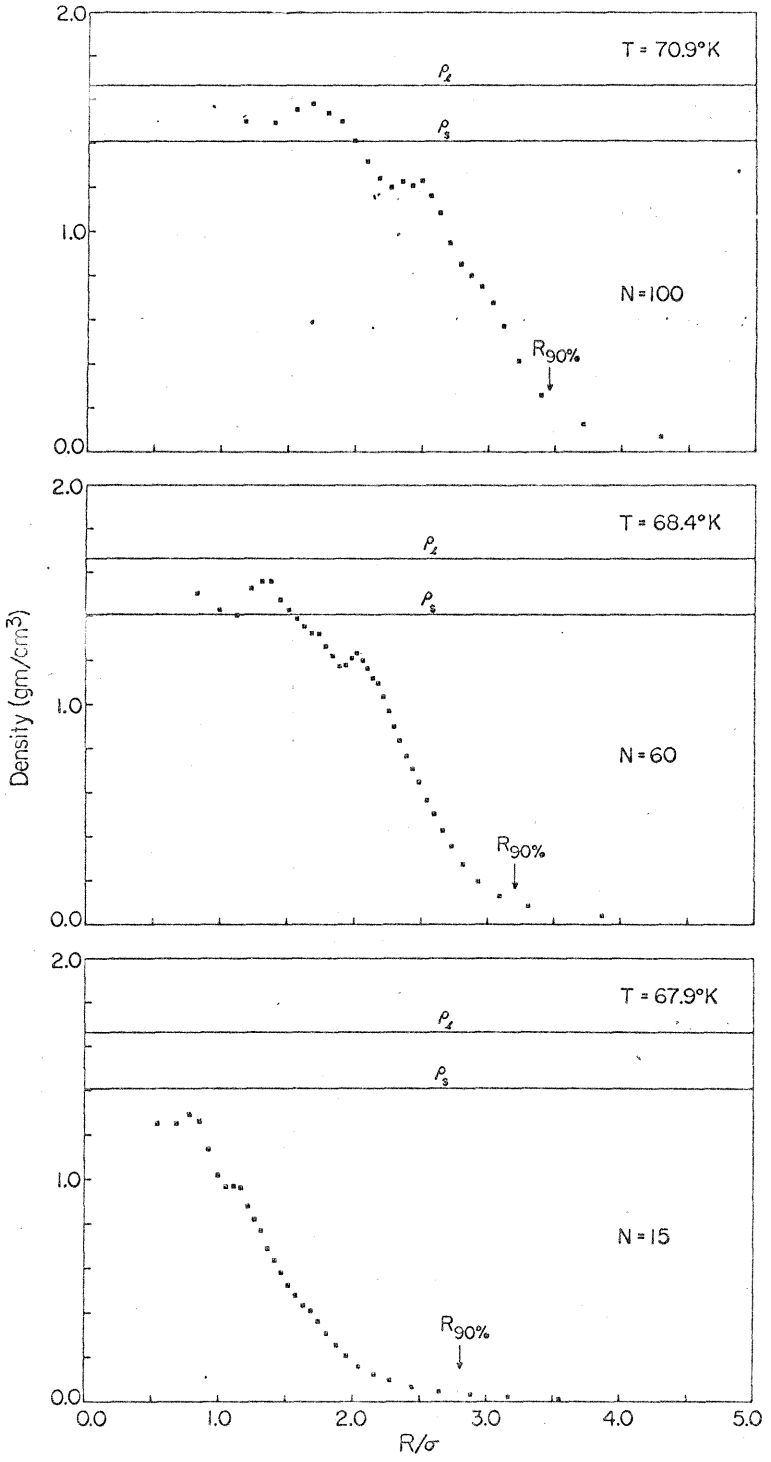

Fig. 4. The radial density function for three clusters each at about 70 °K. The horizontal lines mark bulk phase densities; ρ_s is the density of solid argon at 70 °K and ρ_l is that of liquid argon at 84 °K. Arrows mark the cluster radii.

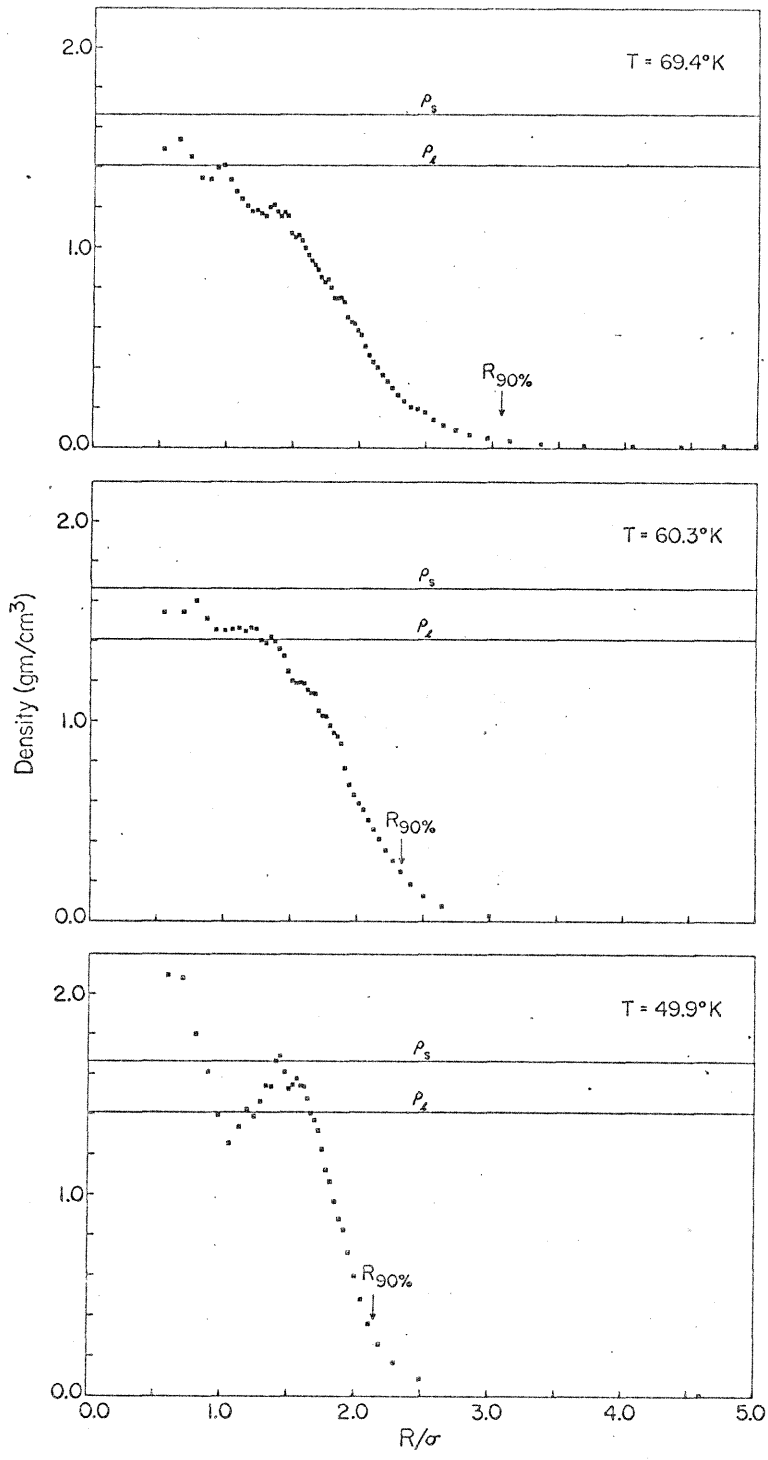

Fig. 5. The temperature dependence of the radial density function for a 30-atom cluster. The horizontal lines indicate bulk phase densities; ρ_s, density of solid argon at 70 °K; ρ_ℓ, density of liquid argon at 84 °K. Arrows mark the cluster radii.

for each of the clusters in Figs. 4 and 5 is indicated by an arrow and its temperature dependence for clusters of 30 and 100 atoms is shown in Fig. 6.

Fig. 7 shows the radial distribution of potential energy, the average potential energy of atoms at a given distance from the center of mass. The potential energy of an atom is $V_i = \frac{1}{2}\sum_{j\neq i} V_{LJ}(r_{ij})$, where $V_{LJ}(r_{ij})$ is the value of the Lennard-Jones pair potential. The curves refer to clusters at ~ 70°K.

In Fig. 8 we have plotted the rotational free energy as a function of temperature. Again each point represents one calculation and the solid curves are quadratic polynomials, obtained from least-square fits. The free energy was determined from the rotational partition function [Eq. (20)] by the usual relation, $G_{N,\,rot} = -\,kT\,\ln(q_{N,\,rot})$.

Figs. 9-11 show the temperature dependence of the total (all degrees of freedom) enthalpy, entropy, and Gibbs free energy for several different clusters, each at one atm partial pressure. In these plots the points indicate values obtained from the microcrystal model and the solid curves are from the molecular dynamics calculations.

Figs. 12 and 13 show the Gibbs free energy of formation from the monomer $\Delta G^{\dagger}_{N}(T, P)$ as a function of cluster size. It is this function that is used in Eq. 13 to compute the equilibrium cluster concentrations. The points in the figures are from the microcrystal model and the solid lines connect values obtained from the molecular dynamics data.

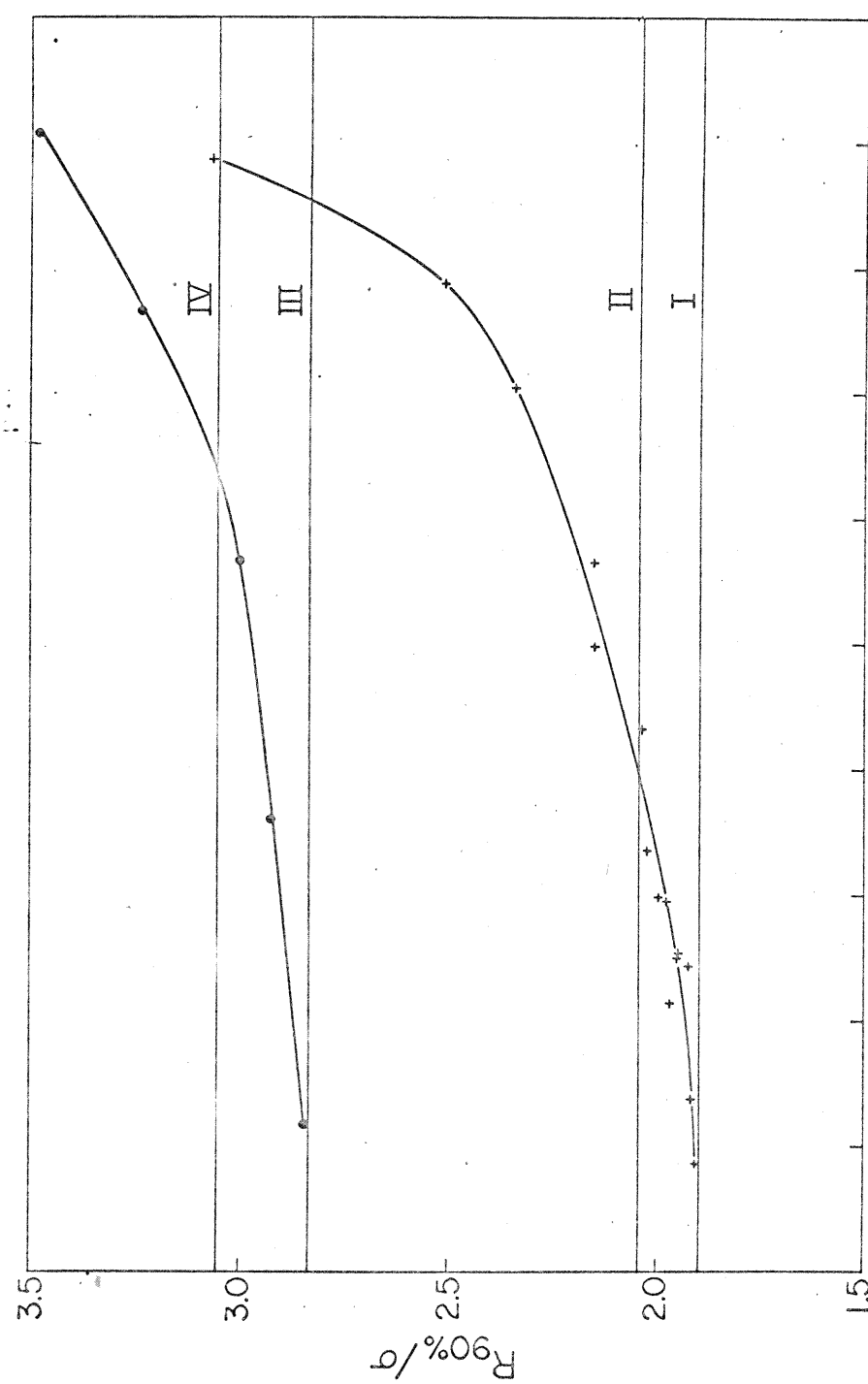

Fig. 6. Temperature dependence of the radii of clusters of 30 and 100 atoms. Points indicate computed values: +, N = 30; ●, N = 100. The curves were drawn by hand. The horizontal lines indicate values of R calculated from the equation $4\pi R^3/3 = Nv_b$. For lines I and III, v_b was the volume per atom in solid argon at 20 °K; for lines II and IV, v_b was the volume per atom in liquid argon at 84 °K.

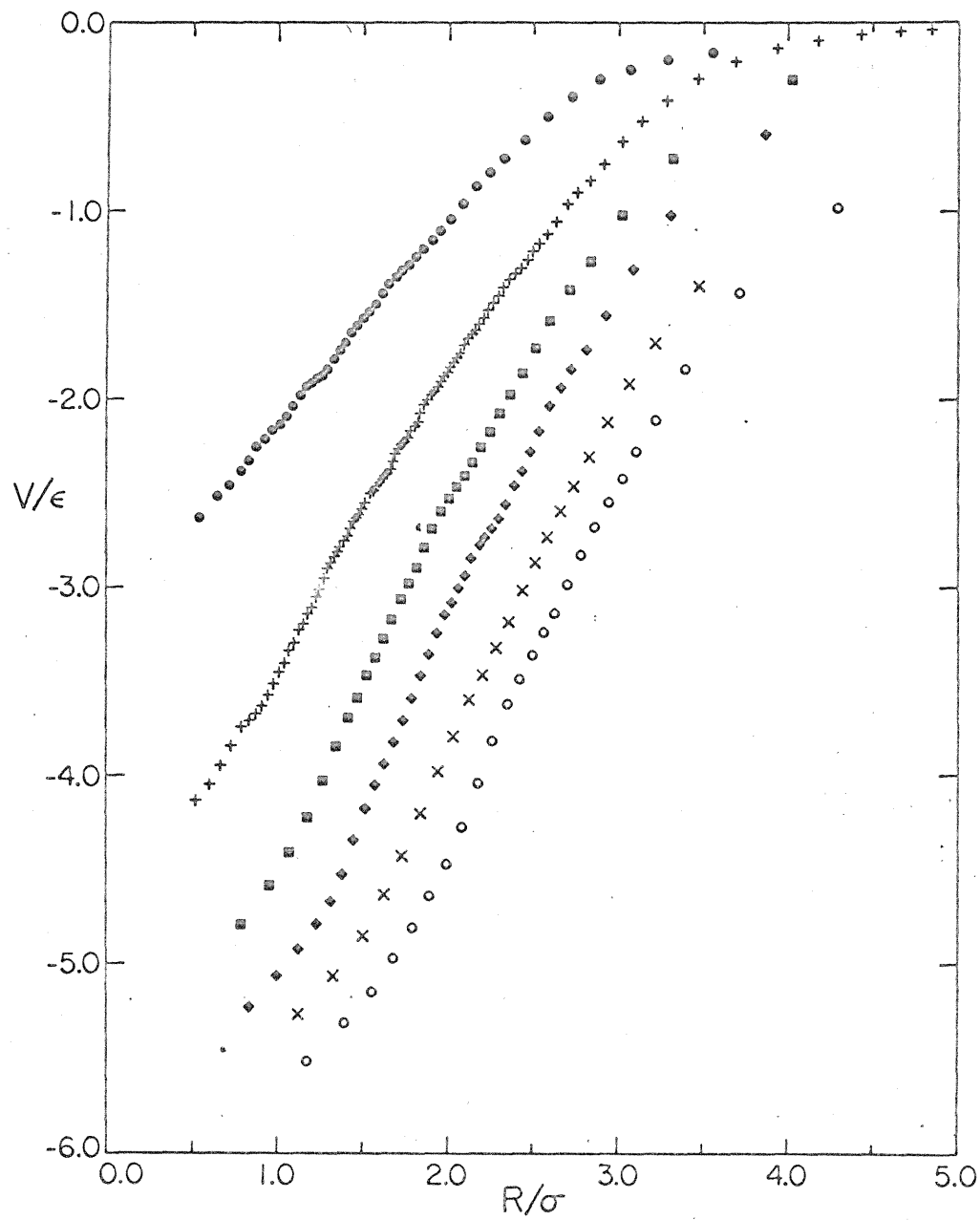

Fig. 7. The radial distribution of potential energy in clusters at about 70 °K: ●, 15-atom cluster; +, 30; ■, 45; ◆, 60; X, 80; ○, 100.

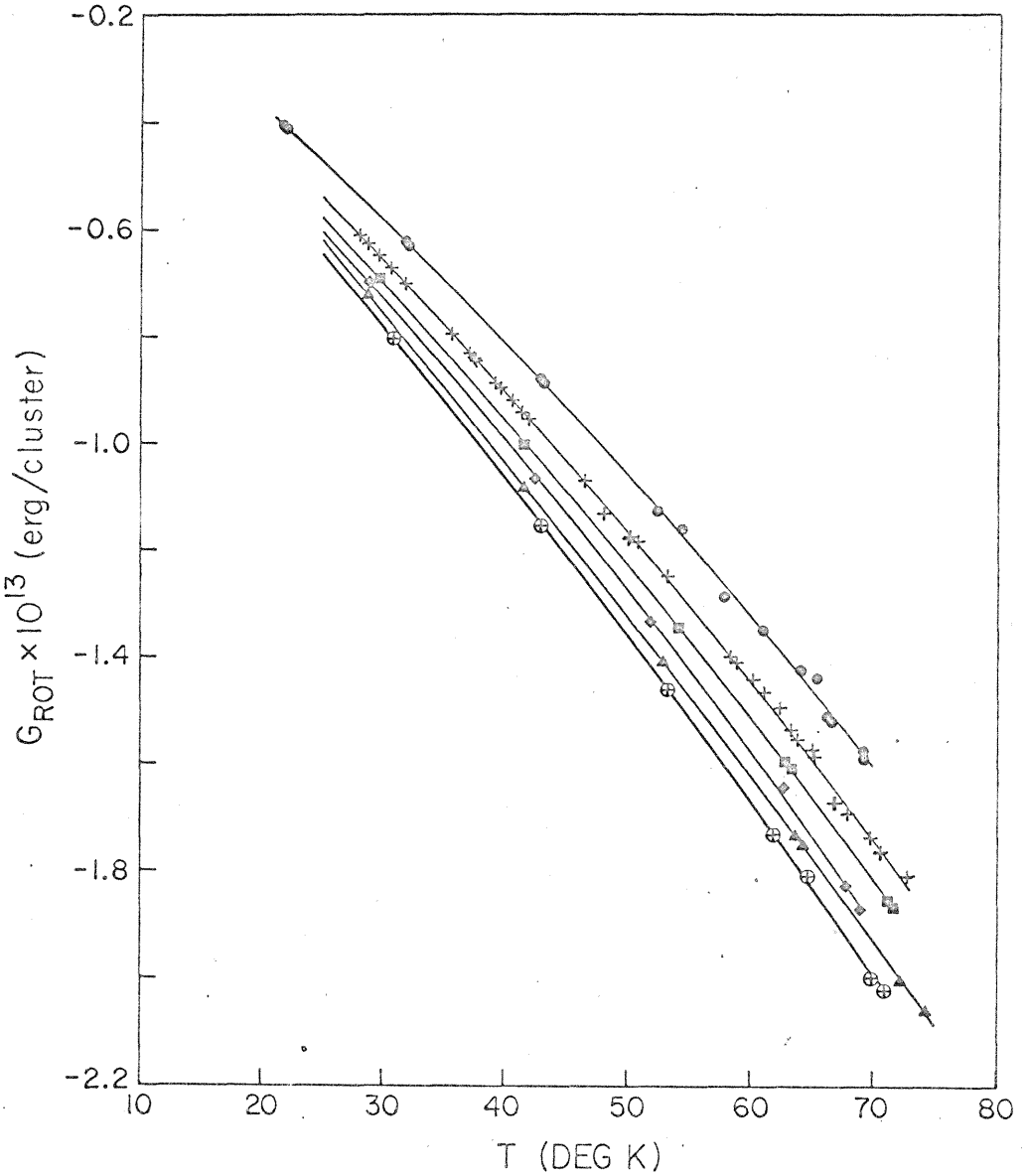

Fig. 8. The rotational free energy as a function of temperature. Each point was obtained from a run of length τ_N: ●, 15-atom cluster; +, 30; ■, 45; ◆, 60; ▲, 80; ⊕, 100. The solid lines are quadratic fits.

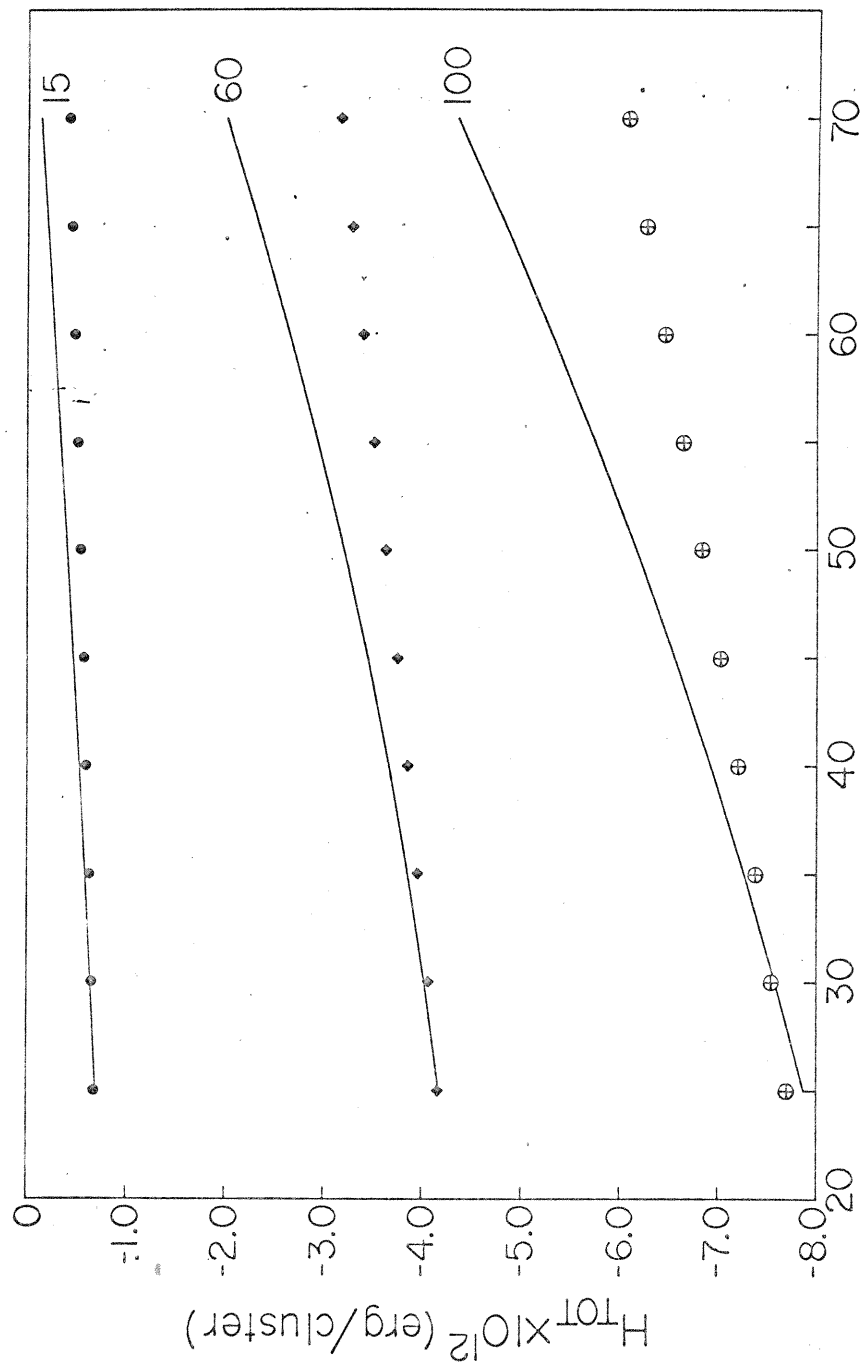

Fig. 9. Temperature dependence of the total enthalpy. Values from the molecular dynamics calculations are connected by solid curves: ——; and values from the microcrystal model are marked as follows: ●, 15-atom cluster; ◇, 60; ⊕, 100.

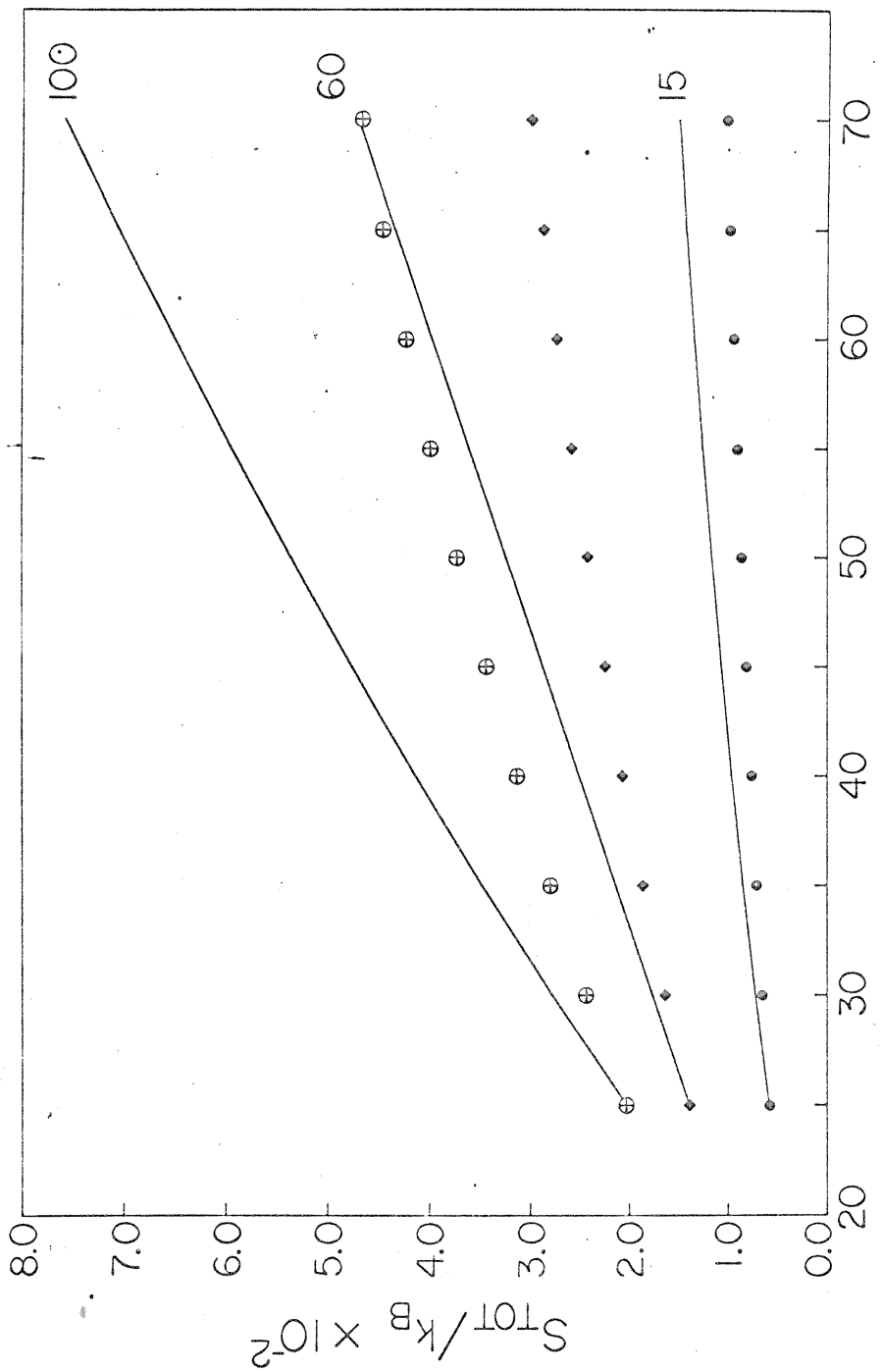

Fig. 10. Temperature dependence of the total entropy. Molecular dynamics values: ——; and microcrystal values: ●, 15-atom cluster; ◆, 60; ⊕, 100.

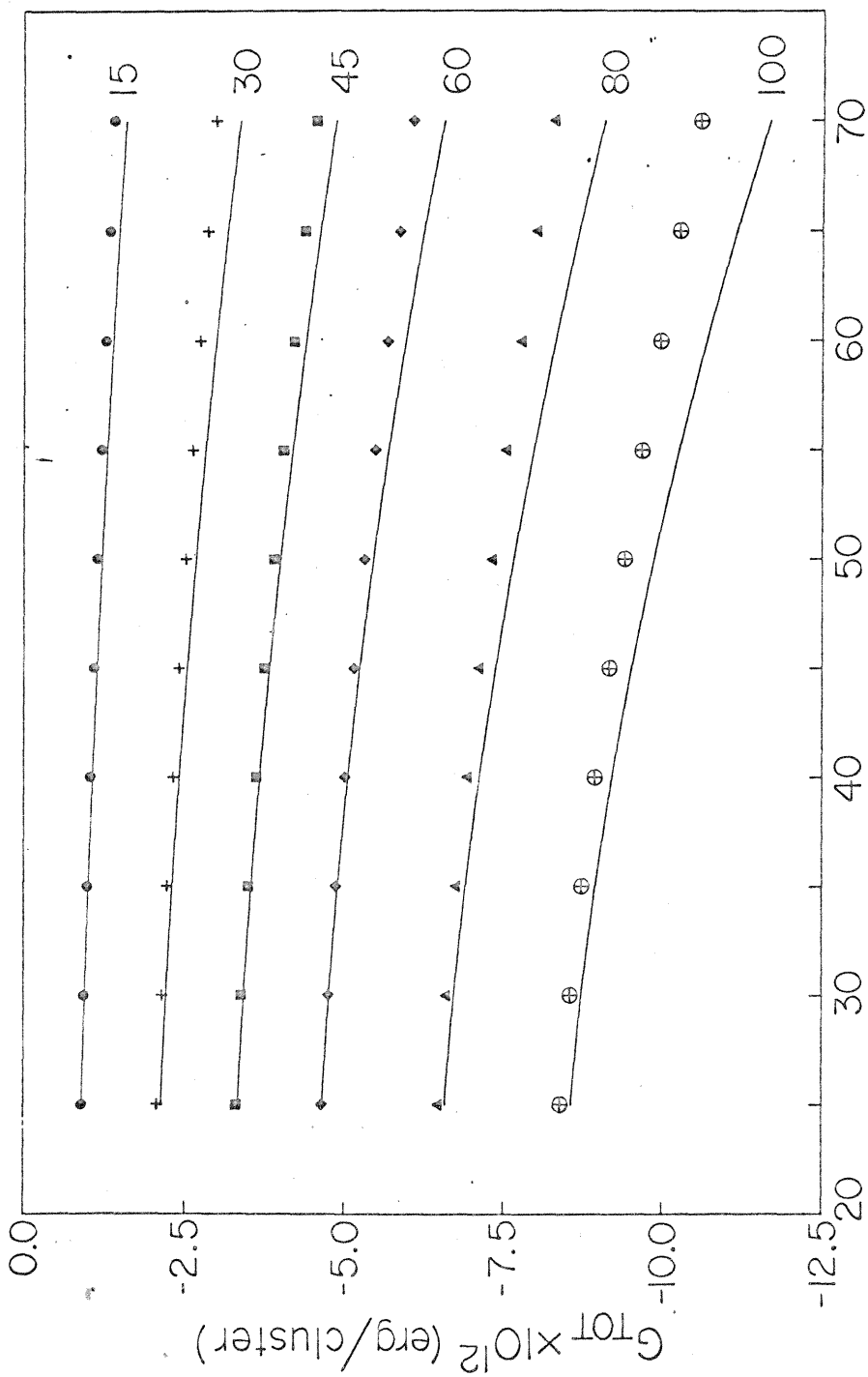

Fig. 11. Temperature dependence of the total Gibbs free energy. Molecular dynamics values; ——; and microcrystal values: ●, 15-atom cluster; +, 30; ■, 45; ◆, 60; ▲, 80; ⊕, 100.

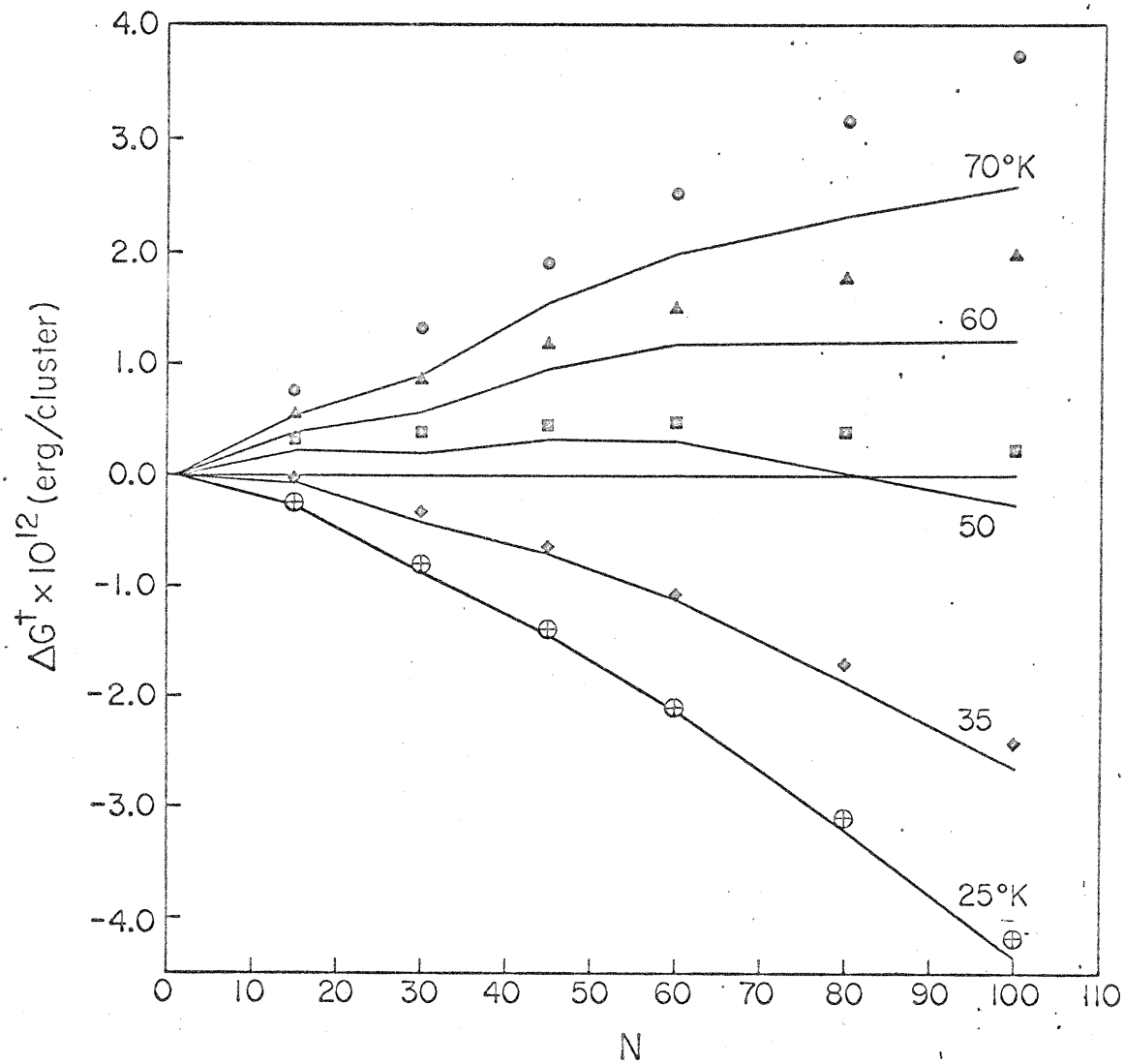

Fig. 12. The Gibbs free energy of formation, $\Delta G^{\dagger} = \Delta G^{\circ} + (1 - N)kT \ln P$, at 0.1 atm for clusters of N atoms. Molecular dynamics values; ——; and microcrystal values: ●, 70 °K; ▲, 60 °K; ■, 50 °K; ◆, 35 °K; ⊕, 25 °K.

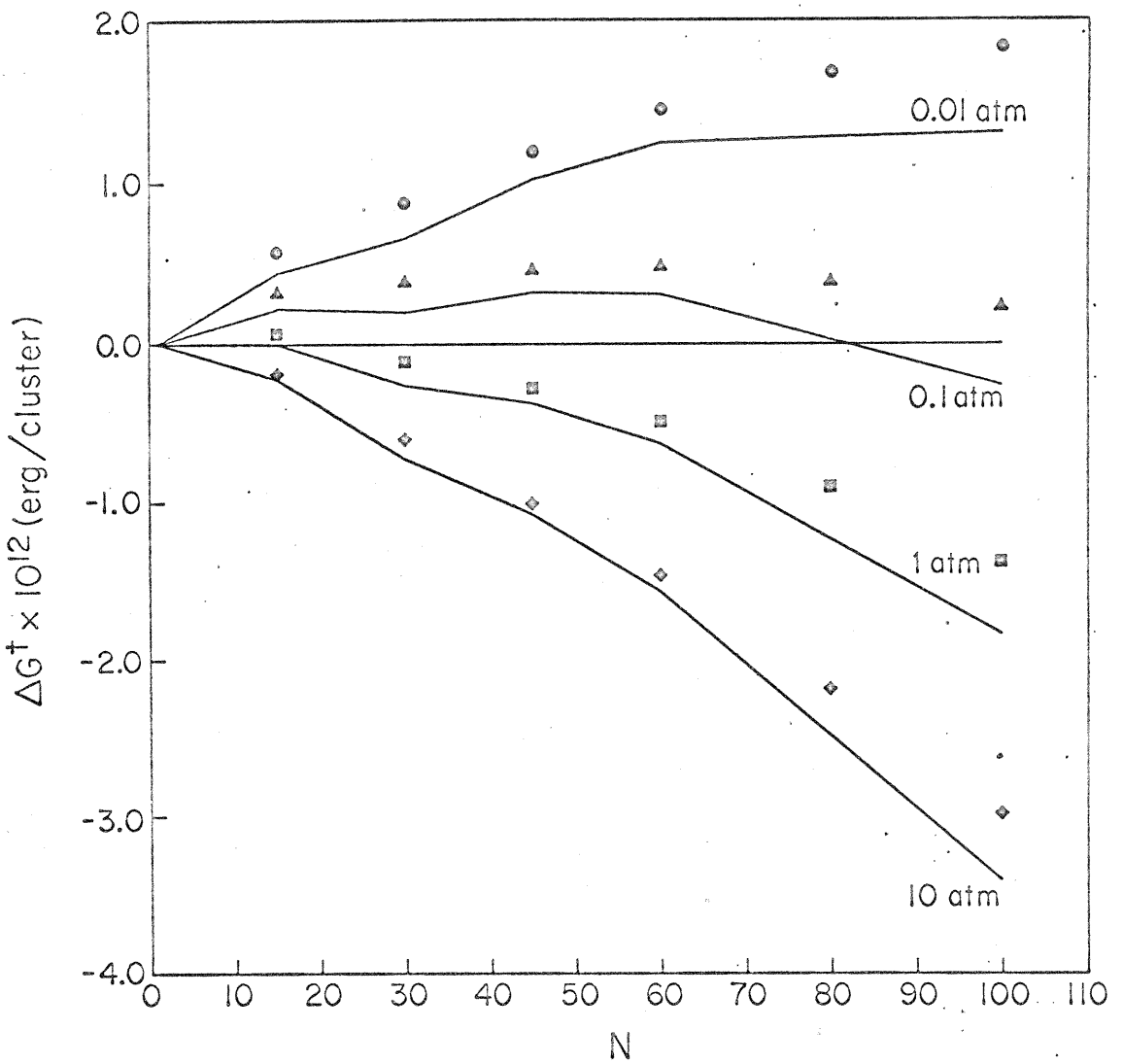

Fig. 13. The Gibbs free energy of formation at 50°K. Molecular dynamics values: ——; and microcrystal values: ●, 0.01 atm; ▲, 0.1 atm; ■, 1 atm; ◆, 10 atm.

VI. COMMENTS ON THE CALCULATIONS

A. Definition of the Clusters

The spherical boundary that we have used in our calculations effectively defines a cluster of N atoms by determining which configurations of the atoms will be identified with the cluster. This definition is simple and efficient to use in the molecular dynamics calculations. At the temperatures considered in our calculations, it is practically equivalent to the definition introduced earlier where a cluster is defined as a connected set of interacting pairs. That definition is particularly useful in the rigorous decomposition of the configuration integral of the vapor.

The definitions are nearly equivalent at reasonably low temperatures because the most probable configurations of the atoms are consistent with both definitions: configurations that are allowed by one of the definitions but not the other have low probability of occurring. Thus highly nonspherical configurations allowed by the "interacting-pairs" definition that might not "fit" inside the spherical boundary have high potential energy and are therefore improbable. Similarly, configurations allowed in the molecular dynamics calculations in which an atom is separated by more than $\sim 3\sigma$ from others in a cluster occurred infrequently. We expect, therefore, that the results of our calculations apply to the clusters defined in Section II. We also expect that our results for a cluster would not change significantly if the value of the cluster radius R_N were varied over a range of several atomic diameters

since the configurations that would be included or excluded by the variation would be those that occur with low probability.

B. Statistical Error in the Temperature

The temperature of a cluster is rigorously determined by the ensemble average of its kinetic energy, which according to the ergodic theory, is equivalent to the time average in the limit of infinite time. In molecular dynamic calculations the infinite average is approximated by a finite average. The error associated with the approximation is evidenced in Fig. 2 by the spread in temperature estimates from calculations at the same total energy. For the highest temperature state of the 30-atom cluster, for example, 8 calculations of length τ_{30} were performed; the standard deviation of the temperature estimates from these runs is 2°K and the standard deviation of their mean is 0.8°K.

This statistical error can be expressed quantitatively in terms of the autocovariance function for the kinetic energy,

$$C(t) = \langle E(t+s)\, E(s)\rangle - \langle E\rangle^2, \tag{24}$$

where E(t) is the kinetic energy at time t and the brackets indicate ensemble averages. Using a simple relationship from the theory of stochastic processes,[13] the variance of the temperature estimates for calculations of length τ_N is

$$\sigma_T^2 = \frac{4C(0)}{3k(N-2)\tau_N} \int_0^{\tau_N} (1-\frac{t}{\tau_N}) \left[C(t)/C(0)\right] dt. \tag{25}$$

We were unable to apply Eq. (25) directly to the calculation of σ_T^2 because of the large uncertainty that exists in our estimates of C(t)

from the molecular dynamics data.[14] The expression is, however, useful for understanding the origin of the statistical error. The factor of C(0) in front of the integral indicates that σ_T^2 is proportional to the average magnitude of the fluctuations; and the integral itself, which contains the normalized autocovariance function, indicates that σ_T^2 also depends on the time correlation of the fluctuations.

The error in our temperature estimates is somewhat larger than has been encountered in liquid state calculations where periodic boundary conditions are used and the density is uniform throughout the system. The fluctuations in kinetic energy of the clusters were relatively large because of the small size of the clusters and also because of the large variation in the potential energy of probably configurations of a cluster--both compact, low-potential-energy and diffuse, high-potential-energy configurations were frequently encountered. Variations in potential energy are, of course, accompanied by variations of equal magnitude in the kinetic energy. Another contribution to the error, we believe, is a tendency for the fluctuations to be correlated due perhaps to low frequency "breathing" motions of the clusters. The error in the temperature can be reduced by increasing the number or length of calculations at each total energy. To estimate the length that is necessary for a given degree of accuracy, knowledge of the decay properties of C(t)/C(0) is necessary. Hopefully such knowledge will be obtained from future calculations.

C. Errors in the Standard Entropy Values

Errors in the values of $S_N^0(25\,^\circ K)$ for a cluster are due primarily to the neglect of stable configurations of the cluster in evaluating its entropy. This error, which is discussed in some detail in Ref. 4, can be minimized by increasing the number of configurations actually used and selecting them in such a manner that they tend to have low free energy at 25 °K. The effect of anharmonicities in the potential energy function is not believed to be large at this low temperature.[3]

D. Vibration-Rotation Coupling

The neglect of vibration-rotation coupling in our calculations enabled us to consider only clusters with zero angular momentum and thereby saved considerable computer time. To include the coupling, it would have been necessary to vary the angular momentum as well as the total energy of a cluster. A molecular dynamics calculation that was actually performed with a spinning cluster, however, indicates that the effect of including the coupling would have been small compared to the statistical error in temperature.

A 30-atom cluster at ~ 50 °K with average rotational energy $\langle \frac{1}{2} I\omega^2 \rangle$ greater than 3kT/2 was considered. In Table II results of the calculations are compared with those from a calculation in which the same initial conditions were used except the angular momentum was zero. Both calculations were run for $2\tau_{30}$ or 1.2×10^{-10} sec. It will be noted in the table that the average of the vibrational total, kinetic, and potential energies from the two calculations are nearly equal even though their average rotational energies are quite different. If vibration-

rotation coupling were strong, one would expect the vibrational energy values to vary with rotational energy. The potential energy, for example, would increase with increasing rotational energy because of centrifugal distortion. This apparently does not occur for rotational energies that are comparable to the thermal average value, probably because the moments of inertia of the clusters are very large, causing their thermal rotational velocities to be small.

VII. DISCUSSION

A. Fluid Motion Inside The Clusters

To characterize the clusters according to the fluidity of the motion of their atoms, we compared the values of the coefficient of self diffusion D_N in the clusters to that in liquid argon at the triple point,[15] $D_\infty = 1.8 \times 10^{-5}$ cm^2/sec. Values of D_N larger than D_∞ are referred to as "fluid-like" and those smaller than D_∞ are referred to as "solid-like." According to this criterion, diffusion in each of the clusters is solid-like in its lowest temperature state: D_{15} at 22°K is 1.5×10^{-7} cm^2/sec and D_{100} at 31°K is 3.6×10^{-8} cm^2/sec. Similarly, each cluster is fluid-like in its highest temperature state: D_{15} at 68°K is 7.9×10^{-5} cm^2/sec and D_{100} at 71°K is 2.2×10^{-5} cm^2/sec.

A true phase transition is not expected in the clusters. A fairly sharp transition from solid-like to fluid-like diffusion would, however, be expected in the core region of large clusters. The transition would become more diffuse as the size of the cluster was decreased. We attempted to detect such a transition by examining the temperature dependence of the diffusion coefficient, but were not successful. The plot of $\log(D_{30})$ vs $1/T$ in Fig. 3 has the same linear behavior that has been determined for that function experimentally in liquid argon. We believe that a "melting zone" would be evidenced by a rather sharp change in the slope of the function as D_N increased from solid-like to fluid-like values. The other clusters exhibited similar behavior

although our data are not as extensive for these clusters making it more difficult to rule out a change in the slope of the function. The transition is too diffuse to be detected in our data.

B. Radial Dependence of the Density

The plots of density vs. distance from the center of mass in Figs. 4 and 5 are generally consistent with the classical drop model that pictures a solid or liquid core separated from the vapor by a transition region. It may be noted, however, that the volume of the core region is quite small even for the 100-atom cluster and that most of the atoms lie in the transition region -- the clusters are mostly "surface." The density inside the 15-atom cluster at 68 °K does not reach that of the bulk phases, which is not consistent with the drop model.

Very definite structure is evident in the plots of the radial density function. This structure, which was observed for each of the clusters at every temperature studied, is consistent with the spherical symmetry of the clusters and indicates a tendency for the atoms of a cluster to arrange themselves in shell-like layers about the center of mass. The plots in Fig. 5 show that the tendency is strongest at low temperatures where the free energy is dominated by the configurational energy of the cluster. The structure is especially pronounced in the 30-atom cluster at 50 °K even though diffusion in the cluster is still fluid-like at that temperature. Similar oscillatory character is predicted theoretically for the variation in density through a liquid-vapor interface.[16]

In Fig. 5, the radius of the 15-atom cluster at 70°K appears inordinately large compared to that of the 60 or the 100-atom cluster at the same temperature. The reason is that the small clusters expand much more rapidly with increasing temperature than do the larger ones -- the small clusters don't hold themselves together as well. The difference in rate of expansion for clusters of different size is shown quite clearly in Fig. 5. The curves in that figure not only indicate that the small clusters expand more rapidly than the larger ones but also that the difference between the rates of expansion becomes larger with increasing temperature. An interesting consequence of this expansion is that at some temperatures the cluster size (radius) will not be a monotonically increasing function of the number of atoms in the cluster: clusters containing fewer atoms will be larger than clusters containing more atoms.

The horizontal lines in Fig. 5 indicate values of the cluster radii calculated from the density of bulk solid and liquid argon using the equation $(4/3)\pi R^3 = Nv_b$, where v_b is the volume per atom in the bulk phase. The lower line for each cluster refers to the solid at 20°K and the upper one refers to the liquid at 84°K. These values for the radius, which are commonly used in the liquid drop model, are quite poor in general, especially for small clusters at high temperatures. The temperature dependence of v_b is much too small to enable the above equation to account for the rapid expansion of the clusters.

C. Radial Dependence of the Potential Energy

Even though the density in the core region of the clusters is nearly constant and roughly equal to that of the bulk phases, the environment in this region is quite different from that in the bulk phases. Because of the small size of the core region, the atoms in that region interact strongly with atoms in the transition region where the density is not constant. These interactions cause a gradient in the potential energy, shown in Fig. 6, that leads to an average radial force tending to hold the cluster together -- the surface tension effect. The gradient apparently exists right up to the center of the clusters. This means that the pressure is anisotropic throughout the cluster and that the thermodynamic energy is not constant even in the core region of the clusters. The clusters are not, therefore, consistent with the model on which Gibbs based his surface theory. In that model a surface is regarded as an interface separating phases in which the thermodynamic properties are homogeneous and isotropic.

The environment in the core region of the clusters does not in fact resemble that in either of the bulk phases and it is doubtful that valid theoretical calculations of cluster properties can be based on the properties of the bulk phases with corrections added for surface effects. This general approach, which is used in the liquid-drop model, is not consistent with our finding that the clusters are in fact almost entirely "surface."

D. The Cluster Thermodynamic Functions

The plot of enthalpy vs. temperature in Fig. 9 indicates that the molecular dynamics values are nearly equal to the microcrystal values at 25°K. As the temperature is increased past this value the molecular dynamics values increase much faster because of the rapid expansion of the clusters. This expansion, which is not allowed by the harmonic approximation used to evaluate the microcrystal model, causes a significant increase in the average potential energy of a cluster. A similar difference in the temperature dependence of the entropy may be noted in Fig. 10: the entropy of the "dynamic" clusters increases much faster than that of the microcrystal clusters. The reason is that the harmonic approximation severely constrains the motion of the atoms of a cluster and thus reduces its entropy. The difference is most pronounced at higher temperatures where the dynamic clusters are expanded and the motion of their atoms is fluid-like. The Gibbs free energy plotted in Fig. 11 indicates that there is somewhat less difference between the two sets of values for this function than for the enthalpy and the entropy. The higher enthalpy of the dynamic clusters tends to increase their free energy relative to that of the microcrystal clusters while their higher entropy tends to decrease it, and the two effects partially cancel. The result is that the microcrystal model apparently yields reasonable values of the cluster free energy even at temperatures where the model is unrealistic.

The plots of the Gibbs free energy of formation $\Delta G_N^\dagger$ vs. N in Figs. 12 and 13 show the behavior expected for that function. The nucleus in these curves is identified as the cluster for which $\Delta G_N^\dagger$ is maximum. It is noted that both the size and the free energy of formation of the nucleus decrease as the saturation level of the vapor is increased, i.e., as the temperature is decreased in Fig. 12 and the pressure is increased in Fig. 13. The small dip in the function at N = 30 is attributed to error in the standard entropy values $S_N^\circ(25^\circ K)$ and is not considered physically significant. It is interesting to note how close the microcrystal values of $\Delta G_N^\dagger$ are to the dynamic values. This suggests that the microcrystal model should be quite useful for estimating the equilibrium distribution of clusters and the rate of homogeneous nucleation.

E. Comment on the Liquid-Drop Model

The basic idea behind the liquid-drop approach is to use the Gibbs surface theory result for the free energy of formation of a drop to determine the Gibbs free energy of formation of a cluster, the quantity $\Delta G_i^\dagger(T, P)$ defined by Eqs. (15)-(19). There is, of course, a correspondence between drops and clusters; and the relation between them is apparent if one considers a system in which a drop exists in stable equilibrium with ambient vapor. Each instantaneous configuration of the system would appear as a large cluster surrounded by small clusters and monomers. In time the size of the large cluster would fluctuate. A drop, therefore, corresponds to a distribution of clusters; but it is reasonable to assume that the properties of the drop are nearly identical

to those of the most probable cluster of the distribution. Ideally, then, the free energy of formation of the drop could be used to evaluate $\Delta G^{\dagger}_{i^*}$, where i* is the size of that most probably cluster.

There is, however, no purely thermodynamic way to determine the value of i* for a drop. The problem is a consequence of the abstract manner in which Gibbs defines the fundamental variables in his surface theory.[17] In that theory the volume of a liquid-vapor system is divided by a geometrical dividing surface: for a volume V containing a liquid drop,

$$V = V_{\ell} + V_{v} \ , \tag{26}$$

where V_{ℓ} is the volume inside the surface and V_{v} is the remaining volume. Gibbs also divides the other extensive variables of the system using the dividing surface. The total number of molecules in the system, for example, becomes

$$N = N_{v} + N_{\ell} + N_{\sigma} \ . \tag{27}$$

Here N_{v} is the number of molecules that would be in V_{v} if the density of the vapor were constant up to the dividing surface; N_{ℓ} is the number of molecules that would be in V_{ℓ} if that volume contained homogeneous liquid at the temperatures and chemical potential of the vapor; and N_{σ} is essentially a correction factor to make the equation valid. The relation between N_{ℓ} and V_{ℓ} is simply stated by the relation $N_{\ell}v_{\ell} = V_{\ell}$, where v_{ℓ} is the volume per molecule in the bulk liquid. In the liquid-drop approach, N_{ℓ} is incorrectly identified with i*. The identification is invalid for two very fundamental reasons, which make N_{ℓ}, in a sense, doubly removed from physical significance. First, N_{ℓ} is unrelated to the number of molecules actually inside V_{ℓ}; and second, V_{ℓ} is

unrelated to the structure (density variation) of the drop. The first reason is obvious from the definition of N_ℓ, and the second will become apparent after further consideration of the surface theory.

According to Gibbs, the energy of the two-phase system is completely determined by the entropy S, the number of molecules N, the volumes V_v and V_ℓ, and the area $\mathcal{A}$ and principal curvatures c_1 and c_2 of the dividing surface: the fundamental equation of the system is $E(S, N, V_v, V_\ell, \mathcal{A}, c_1, c_2)$. Also, according to Gibbs, the dependence on c_1 and c_2 vanishes for a particular choice of the dividing surface, which we call the surface of tension. Gibbs argues that for surfaces of small curvature (large drops), the surface of tension will "sensibly coincide with the physical surface of discontinuity" (Ref. 17, p. 227). These arguments do not, however, apply to very small, microscopic drops that have high curvature and that do not have a homogeneous region in their interiors (Ref. 17, pp. 253-255). For these drops the position of the surface of tension with respect to the physical discontinuity is uncertain. A connection between V_ℓ and the structure of the small drops is not, therefore, established.

We conclude that considerable error exists in the index i* for values of $\Delta G^\dagger_{i*}$ determined using the liquid-drop approach. This means, for example, that the approach does not lead to an accurate determination of the number of molecules in the nucleus. It also makes it difficult to achieve a meaningful comparison between our values for $\Delta G^\dagger_i$ and those obtained from the liquid-drop model. A direct comparison could not, for example, be expected to establish preference for either the Reiss-Katz-Cohen[18] or the Lothe-Pound[19] solutions of the model. An

uncertainty of ± 1 in i* would be equivalent to ± 3 degrees of freedom, which is about the same as the difference between the two solutions. We have decided, therefore, to leave consideration of the liquid-drop model to another paper.

ACKNOWLEDGEMENTS

The author is indebted to Professor G. Wilse Robinson for continuing advice and support throughout the course of this work, to Dr. P. L. Fehder for suggesting the use of molecular dynamics to study clusters, and to Dr. R. P. Futrelle for many helpful discussions.

REFERENCES

1. R. Becker and W. Döring, Ann. Physik 24, 719 (1935); J. Frenkel, Kinetic Theory of Liquids (Dover Publications, New York, 1955), Cha. VII; W. J. Dunning, Nucleation, edited by A. C. Zettlemoyer (Dekker, New York, 1969), Chap. 1.
2. J. J. Burton, J. Chem. Phys. 52, 345 (1970) and Surface Sci. 26, 1 (1971).
3. D. J. McGinty, J. Chem. Phys. 55, 580 (1971).
4. D. J. McGinty, Chem. Phys. Lett. (in press).
5. F. F. Abraham and J. V. Dave, J. Chem. Phys. 55, 1587 (1971); K. Nishioka, R. Shawyer, A. Bienenstock, and G. M. Pound, J. Chem. Phys. 55, 5082 (1971).
6. A. Rahman, Phys. Rev. 136, 405A (1964); P. L. Fehder, J. Chem. Phys. 50, 2617 (1969).
7. L. Verlet, Phys. Rev. 159, 98 (1967).
8. J. Katz, J. Stat. Phys. 2, 137 (1970).
9. H. Reiss, J. Stat. Phys. 2, 83 (1970); F. H. Stillinger, Jr., J. Chem. Phys. 38, 1486 (1963).
10. J. O. Hirschfelder, C. F. Curtiss, and R. B. Bird, Molecular Theory of Gases and Liquids (Wiley, New York, 1954) p. 1110.
11. J. M. H. Levelt and E. G. D. Cohen. Studies in Statistical Mechanics, J. de Boer and G. E. Uhlenbeck, Eds. (North-Holland Publishing Co., Amsterdam, 1964), p. 114.

12. N. Wax, ed. Selected Papers on Noise and Stochastic Processes (Dover Publications, New York, 1954).

13. A. Papoulis, Probability, Random Variables and Stochastic Processes (McGraw-Hill, New York, 1965), p. 325.

14. R. Zwanzig and N. K. Ailawadi, Phys. Rev. 182, 280 (1969).

15. J. Naghizadeh and S. A. Rice, J. Chem. Phys. 36, 2710 (1962).

16. G. M. Nazarian, J. Chem. Phys. 56, 1408 (1972).

17. J. W. Gibbs, The Scientific Papers (Dover Publications, New Yoek, 1961), Vol. I.

18. H. Reiss, J. L. Katz, and R. E. Cohen, J. Chem. Phys. 48, 5553 (1968).

19. J. Lothe and G. M. Pound, J. Chem. Phys. 48, 1849 (1968).

Table I. Radii of the spherical boundaries, lengths of the calculations, and the number of stable configurations used in evaluating the standard entropies, $S_N^\circ(25\,^\circ K)$.

N	R_N/σ	$\tau_N/10^{-14}$ Sec	Number of Configurations
15	3.97	10000	19
30	5.00	6000	14
45	5.72	5000	7
60	6.30	4300	2
80	6.93	3700	2
100	7.47	3300	2

Table II: Comparison of the energies for rotating and a non-rotating clusters. A molecular dynamics calculation was first performed on the rotationless cluster. The cluster was then caused to rotate and another calculation performed. The average vibrational, total, potential, and kinetic energies are nearly the same for the two calculations.

	Rotationless	Rotating
$\langle E_{rot}/N\epsilon \rangle$	0.000036	0.03881
$\langle U_{vib}/N\epsilon \rangle$	-2.500	-2.494
$\langle V_{vib}/N\epsilon \rangle$	-3.084	-3.072
$\langle E_{vib}/N\epsilon \rangle$	0.5833	0.5785

C. Paper No. 4

CALCULATION OF SPECTRA AND CORRELATION FUNCTIONS FROM MOLECULAR DYNAMICS DATA USING THE FAST FOURIER TRANSFORM

Molecular dynamics[1-5] produces particle trajectories for atomic and molecular fluids and solids. Time-displaced autocorrelation functions calculated from these trajectories are used to study a host of transport, relaxation, and light scattering processes.[6,7] The autocorrelation functions C(t) of the dynamical variable $a[\underset{\sim}{R}^N(t), \underset{\sim}{P}^N(t)]$ for the N-particle system is approximated by a finite time average,

$$C(t) = \langle a(t)a(0)\rangle_{\text{ensemble}} \simeq \frac{1}{2T}\int_{-T}^{T} a(t+s)a(s)ds\,, \qquad (1)$$

and is generally calculated from particle trajectories by simple numerical integration. We have employed a computational technique that enables one to evaluate C(t) much more rapidly and with less round-off error.

It is well known that C(t) can be expressed in terms of the Fourier transform $\tilde{a}(\omega)$ of a(t),

$$C(t) = \frac{1}{2T}\int_{-\infty}^{\infty} |\tilde{a}(\omega)|^2 e^{i\omega t} d\omega\,. \qquad (2)$$

Our method uses Eq. (2) with very efficient Fourier transform algorithm, the "fast Fourier transform" (FFT),[8,9] to calculate $\tilde{a}(\omega)$ and thence C(t). Mathematically, the method is exactly identical to the "standard method" using Eq. (1).

Molecular dynamics produces a discrete time series of n values of a variable a(t). The efficiency of algorithms used to process these data can be measured by the number of multiplications or additions ("operations") they require to produce the same result. To compute C(t) using the "standard method" requires $[n^2 + 0(n)]$ operations. The FFT applied to Eq. (2) is computationally far more efficient, requiring

$3n[\log_2 n + 0(1)]$ operations.[8,9] For $n \gtrsim 30$, the FFT is superior to the "standard method," e.g., for n = 1000 the FFT is 25 times faster. Since the generation of the molecular dynamics data requires calculations $\propto n$, extensive calculations of correlation functions using the "standard method" ($\propto n^2$) could easily consume more time than the data generation. The FFT should be used in such cases.

As an example, in studying a liquid cluster of 30 atoms we have calculated the autocorrelation of the total kinetic energy for 6000 points. Using an IBM 360/75 computer (single precision), the data generation required 220 sec, the "standard method" for C(t) required 320 sec, and the FFT calculation of C(t) took only 8 sec. The values of C(t) for the two methods were the same to five significant figures. We estimate the time saving that could have been achieved using the FFT in past calculations of correlation functions to range between 4:1 and 25:1. Correlation functions have often been computed for a very limited number of time points but the efficiency of the FFT can allow calculation at all points for about the same effort.

If the FFT is simply applied to a block of data according to Eq. (2), it produces a periodic correlation function with an incorrect association of certain pairs of data points. This difficulty is easily circumvented by appending a block of n data points, all zero, to the original n points.[10] Also when two finite blocks of data are convoluted using the FFT, a different number of products contribute to each terms $C(t_k)$. To correct for this, each term is multiplied by a weighting factor; $C(t_k)$ becomes $C(t_k)/(n-k)$.

Some functions that are not normally thought of as autocorrelations can be cast into that form, allowing one to use the FFT procedure. The orientational function, $\langle P_2[\underset{\sim}{u}(0)\cdot\underset{\sim}{u}(t)]\rangle$, where P is the Legendre polynomial and $\underset{\sim}{u}$ is a unit vector along a molecular axis, can be written in terms of autocorrelations of $[u_x(t)]^2$, $u_x(t)u_y(t)$, etc. The mean-square displacement of a particle, $\langle|\underset{\sim}{r}(t) - \underset{\sim}{r}(0)|^2\rangle$ can be derived from the velocity autocorrelation function or expanded as, $2\langle|\underset{\sim}{r}(0)|^2\rangle - 2\langle\underset{\sim}{r}(t)\cdot\underset{\sim}{r}(0)\rangle$. Cross-correlations can also be calculated using $\tilde{a}_1^*(\omega)\tilde{a}(\omega)$ in place of $|\tilde{a}(\omega)|^2$ in Eq. (2). Other quantities of interest such as spectral moments can be calculated directly from power spectra obtained with the FFT.

It has recently been discovered using molecular dynamics data that the velocity autocorrelation function C(t) decays very slowly at long times.[11-14] This anomalous behavior can be studied directly via the power spectrum $\tilde{C}(\omega)$, avoiding the additional step of calculating C(t). In three dimensions $C(t) \propto t^{-3/2}$ for large t with spectrum[15] $\tilde{C}(\omega) \propto D + d_1\omega^{\frac{1}{2}} + 0(\omega)$ for small ω. D is the diffusion constant. In two dimensions $C(t) \propto t^{-\frac{1}{2}}$ so that $\tilde{C}(\omega) \propto \omega^{-\frac{1}{2}} + 0(1)$. Thus this power spectrum is divergent at zero frequency.

The FFT should be very useful in calculating space-time correlation functions $f(\underset{\sim}{r}, t)$ and their spectra $\tilde{f}(\underset{\sim}{k}, \omega)$, with special cases, e.g., $k_x = k_y = 0$, $k_z \neq 0$, being the easiest to compute. The radial distribution function g(r) is one case that can be computed more efficiently using a simple "standard method" in the radial variable r rather than a 3-d FFT in x, y, z with subsequent spherical averaging.

As a final application of Fourier transform techniques, consider the problem of determining the phonon spectrum of a solid. Two standard methods for this are (1) finding the eigenfrequencies from the force-constant matrix,[16] which can lead to a large matrix diagonalization problem, and (2) calculating the power spectrum of the velocity autocorrelation function $C_v(t)$ derived from molecular dynamics.[17] The second method is exact only if equipartition is obeyed and is therefore only an approximation in practice. The efficiency of the FFT suggests a third method in which the power spectrum of $C_v(t)$ is calculated directly from the particle velocities using a very fine frequency mesh. The spectrum will then be large only in the neighborhood of each of the eigenfrequencies, which can therefore be isolated (away from each eigenfrequency there will be a background contribution of Lorentzian or Breit-Wigner shape due to the finite frequency mesh spacing). This method would be particularly interesting if applied to the slightly anharmonic solid where any additional broadening will arise from anharmonicity.

Acknowledgment

This work was coauthored by Dr. Robert P. Futrelle, Joint Institute for Laboratory Astrophysics, Boulder, Colorado, 80302, and was supported in part by a grant (No. GP-12381) from the National Science Foundation.

REFERENCES

1. B. J. Alder and T. E. Wainwright, J. Chem. Phys. 31, 459 (1959); ibid. 33, 1439 (1960).
2. A. Rahman, Phys. Rev. 136, A405 (1964).
3. D. Levesque and L. Verlet, Phys. Rev. A2, 2514 (1970).
4. P. L. Fehder, J. Chem. Phys. 50, 2617 (1969).
5. B. J. Berne and G. D. Harp, Adv. Chem. Phys. 17, 63 (1970).
6. R. Zwanzig, Ann. Rev. Phys. Chem. 16, 67 (1965).
7. P. A. Egelstaff, An Introduction to the Liquid State (Academic Press, Inc., New York, 1967).
8. J. W. Cooley and J. W. Tukey, Math. Comput. 19, 297 (1965); W. T. Cochran et al., Proc. IEEE 55, 1664 (1967).
9. B. Gold and C. M. Rader, Digital Processing of Signals (McGraw-Hill Book Co., Inc., New York, 1969).
10. T. G. Stockham, Jr., Ref. 9, Chap. 7.
11. B. J. Alder and T. W. Wainwright, Phys. Rev. A1, 18 (1970).
12. P. L. Fehder, C. A. Emeis, and R. P. Futrelle, J. Chem. Phys. 54, 4921 (1971).
13. K. Kawaski, Phys. Letters A32, 379 (1970).
14. M. H. Ernst, E. H. Hauge, and J. M. J. van Leeuwen, Phys. Rev. Letters 25, 1254 (1970); J. R. Dorfman and E. G. D. Cohen, ibid. 25, 1257 (1970).
15. T. Gaskell and N. H. March, Phys. Letters A33, 460 (1970).
16. W. G. Hoover, M. Ross, K. W. Johnson, D. Henderson, J. A. Barker, and B. C. Brown, J. Chem. Phys. 52, 4931 (1970);

J. J. Burton, ibid. 52, 345 (1970); D. J. McGinty, ibid. 55, 580 (1971).

17. J. M. Dickey and A. Paskin, Phys. Rev. 188, 1407 (1969).